

THESIS

CONTINUOUS NAPL LOSS RATES USING SUBSURFACE TEMPERATURES

Submitted by

Emily Beth Stockwell

Department of Civil and Environmental Engineering

In partial fulfillment of the requirements

For the Degree of Master of Science

Colorado State University

Fort Collins, Colorado

Summer 2015

Master's Committee:

Advisor: Tom Sale

Jens Blotevogel

Jay Ham

Copyright by Emily Beth Stockwell 2015

All Rights Reserved

## ABSTRACT

### CONTINUOUS NAPL LOSS RATES USING SUBSURFACE TEMPERATURES

Petroleum hydrocarbons, in the form of Non-Aqueous Phase Liquids (NAPLs), are commonly encountered in soil and groundwater beneath petroleum facilities. These petroleum NAPLs are depleted via natural mechanisms in the subsurface through a process known as Natural Source Zone Depletion (NSZD). Recent studies have estimated NSZD rates at petroleum impacted sites that often rival loss rates associated with active remedies. Current methods for determining NSZD rates rely on measuring fluxes of gases in the vadose zone above NAPL releases, unfortunately, the mechanisms and measurement of gas fluxes are biased by temporally variable environmental factors and the NSZD rates are obtained over finite periods.

The primary objective of this thesis was to develop methods that yield estimates of NSZD rates that are more accurate and continuous through time using subsurface temperature data. To achieve this goal, a thermal NSZD rate model was developed based on the central hypothesis that NSZD rates can be calculated by dividing the rate of energy released during NAPL biodegradation by the change in enthalpy of the reaction.

The rate of energy released during NAPL biodegradation was determined by conducting an energy balance using subsurface temperatures at a NAPL impacted location and a representative unimpacted background location. The background temperatures were obtained by three methods: 1) measuring subsurface temperatures at an unimpacted location, 2) modeling using a simple analytical model, and 3) modeling using the program Hydrus. The background temperatures

were subtracted from the temperatures measured at the impacted location to determine the temperatures due to NAPL biodegradation. Background corrected temperatures were then used in the energy balance, which considered energy flows due to conduction, convection, and the change in storage of energy within the NAPL impacted area, to determine the rate of energy released during NAPL biodegradation.

The change in enthalpy of the biodegradation reaction was calculated as the change in enthalpy of formation of the products minus the reactants of the reaction. For this work, it was assumed that all reactions go to completion within the NAPL body, thus all NAPL was degraded to carbon dioxide and water. In addition, it was assumed that the change in enthalpy of the reaction was all released as heat to the surrounding environment.

The thermal NSZD rate model was applied to five petroleum impacted field sites across the United States. Subsurface temperatures were collected at NAPL impacted locations at all field sites over a period of approximately one year. The most robust data was collected for the field site in Kansas, which included: 1) subsurface temperatures at four NAPL impacted locations along a transect, 2) subsurface temperatures at one background location, and 3) daily water levels at four locations. Subsurface temperatures at the NAPL impacted locations at field sites in Kansas, Colorado, Wyoming, and Southern New Jersey were up to 4°C warmer than temperatures measured or modeled as background values. The field site in Northern New Jersey did not show this trend, likely because the LNAPL at this site is shallow and shallow subsurface temperatures are strongly influenced by short-term heating and cooling at the ground surface.

Average NSZD rates of up to 780 gal/acre/year were calculated by the thermal NSZD rate model. Calculated average NSZD rates for the sites in Kansas, Colorado, and New Jersey were

consistently lower than average NSZD rates obtained using CO<sub>2</sub> Traps at these field sites. In part, lower NSZD rates using the thermal method are due to poor constraint of the value used for the change in enthalpy of NAPL biodegradation, underestimates of the temperature gradient due to the placement of thermocouples below the methane oxidation front, and/or underestimates of the energy released during biodegradation due to an incomplete energy balance. In addition, the imperfections of the background correction may lead to large variability in the calculated NSZD rates. Uncertainties in critical data inputs indicate a need for a controlled lab study to better understand the thermodynamics of biodegradation.

A column study was conducted as a preliminary effort to evaluate the thermodynamics of biodegradation of a carbon substrate in soil. A column was filled with homogenous, well-sorted fine sand. Cold water was circulated through a copper coil at the bottom of the column to create a constant temperature boundary. Three subsequent molasses additions to the column led to increases in the temperature gradient, carbon dioxide, and methane production, verifying that molasses biodegradation occurred and heat was released due to biodegradation following each molasses injection. Application of the thermal NSZD rate model to the temperature data collected during the laboratory experiment indicated that the NSZD rate was highly dependent on the value used for the change in enthalpy of the reaction.

Overall, this work indicates that subsurface temperature measurements about a NAPL body can be used to resolve NSZD rates. However, the methods as used here would likely lead to underestimates of true NSZD rates. The imperfections of the background corrections, incomplete energy balances, and unknown composition and quantity of reactants and products limit the accuracy of NSZD rates calculated using the thermal NSZD rate model. In addition, a lack of

known NSZD rates to compare this method against makes it difficult to determine the accuracy of the thermal NSZD rate model. In summary, the thermal NSZD rate method shows great promise, but more work is needed to improve accuracy.

## ACKNOWLEDGEMENTS

The following people provided invaluable support for this work:

- Dr. Tom Sale provided the inspiration for this project as well as guidance and encouragement throughout the entire process
- Dr. Jens Blotevogel provided support with thermodynamic aspects of this project
- Dr. Jay Ham provided support with heat transfer aspects of this project
- Dr. Dave McWhorter assisted in the initial development of the model
- Greg Fletcher and Bob Sekich at Suncor Energy assisted with field work
- Keith Piontek, Brad Huxol, and Stephanie Deters at TRC assisted with field work
- Gary Dick and the rest of the Center for Contaminant Hydrology staff assisted with construction of field and lab equipment
- My friends and family provided support, encouragement, insight, and relief

Funding for this research was provided by Suncor Energy and TRC.

## TABLE OF CONTENTS

ABSTRACT.....	ii
ACKNOWLEDGEMENTS.....	vi
TABLE OF CONTENTS.....	vii
LIST OF TABLES.....	ix
LIST OF FIGURES.....	x
1. INTRODUCTION.....	1
1.1. Hypothesis and Objectives.....	2
1.2. Organization and Content.....	2
2. LITERATURE REVIEW.....	4
2.1. Significance of NSZD.....	4
2.2. Quantification of NSZD Rates.....	6
2.3. Heat Transfer in the Subsurface.....	7
2.3.1. Energy Balance at Grade.....	8
2.3.2. Soil Heat Flux.....	8
2.3.3. Soil Thermal Properties.....	10
2.4. Thermodynamics of NAPL Biodegradation.....	12
2.5. Microbial Yield Predictions Using Thermodynamics.....	14
2.6. Studies Regarding Heat Release in Landfills, Compost Piles, and Subsurface Waste Rock/Coal Piles.....	16
3. THERMAL NSZD RATE MODEL BASED ON SUBSURFACE TEMPERATURES.....	19
3.1. Objectives.....	19
3.2. Methods.....	19
3.2.1. Energy Balance.....	21
3.2.2. Energy Sources/Sinks.....	25
3.2.3. Background Correction.....	28
3.2.4. NSZD Rate.....	29
3.3. Model Inputs.....	30
3.3.1. Impacted Location Temperatures and Water Levels.....	30
3.3.2. Representative Background Temperatures.....	31
3.3.3. Soil and Contaminant Characteristics.....	31
3.4. Model Outputs.....	33
4. FIELD-SCALE APPLICATION OF THE THERMAL NSZD RATE MODEL.....	34
4.1. Objectives.....	34
4.2. Methods.....	34
4.2.1. Data Collection.....	35
4.2.1.1. Kansas.....	35
4.2.1.2. Colorado.....	41
4.2.1.3. Wyoming, Northern New Jersey, and Southern New Jersey.....	41

4.2.2.	Background Correction.....	43
4.2.3.	Model Inputs.....	45
4.2.4.	Parameter Sensitivity Analysis.....	49
4.3.	Results and Discussion.....	50
4.3.1.	Kansas.....	51
4.3.2.	Colorado.....	59
4.3.3.	Wyoming.....	63
4.3.4.	Northern New Jersey.....	68
4.3.5.	Southern New Jersey.....	72
4.3.6.	Parameter Sensitivity Analysis.....	77
4.4.	Limitations.....	79
5.	LABORATORY STUDY OF THERMODYNAMICS OF BIODEGRADATION.....	83
5.1.	Objectives.....	83
5.2.	Methods.....	83
5.2.1.	Column Setup.....	84
5.2.2.	Molasses Addition.....	86
5.2.3.	Sampling Procedure and Analytical Technique.....	86
5.2.4.	Loss Rate Modeling.....	87
5.3.	Results and Discussion.....	89
5.3.1.	Gas Sampling.....	89
5.3.2.	Loss Rate Modeling.....	93
6.	SUMMARY AND CONCLUSIONS.....	96
6.1.	Main Ideas and Themes.....	96
6.2.	Results of Field and Lab Studies.....	98
6.2.1.	Field Scale Application of the Thermal NSZD Rate Model.....	98
6.2.2.	Laboratory Study of Thermodynamics of Biodegradation.....	100
6.3.	Future Work.....	101
6.3.1.	Characterization of Biodegradation Reactants and Products.....	102
6.3.2.	Characterization of Microbial Use of Energy.....	102
6.3.3.	Numerical Modeling.....	103
7.	REFERENCES.....	104
8.	APPENDIX A.....	108
8.1.	Thermal NSZD Rate Model Using Background Location Correction.....	108
8.2.	Thermal NSZD Rate Model Using Simple Analytical Model.....	120
8.3.	Thermal NSZD Rate Model Using Hydrus.....	134
8.4.	Thermal NSZD Rate Model As Applied to the Laboratory Experiment.....	146
9.	APPENDIX B.....	151
9.1.	Soil Core Thermal Properties.....	151
9.2.	Values Used in Thermodynamics Calculations.....	152
9.3.	Gas Chromatography Calibration Curves.....	153

## LIST OF TABLES

Table 1. Decane redox reactions and standard free energy released per mole decane (calculated using values tabulated in Appendix B, following Wiedemeier et al. 1996) .....	13
Table 2. Fixed input parameters and their values .....	32
Table 3. Site-specific characteristics needed .....	32
Table 4. Decane characteristics and their values .....	33
Table 5. Thermocouple depths in meters below ground surface at each field site .....	38
Table 6. Background correction methods used for each field site .....	45
Table 7. Site-specific characteristics used in the thermal NSZD rate model.....	46
Table 8. Change in free energy ( $\Delta G_r$ ) and enthalpy ( $\Delta H_r$ ) for redox reactions of aqueous phase decane (calculated using values tabulated in Appendix B following Wiedemeier et al. 1996)....	47
Table 9. Site specific values used in the simple analytical model to calculate background temperatures .....	48
Table 10. Parameter values used in the sensitivity analysis .....	50
Table 11. Average NSZD rate and cumulative NAPL losses for field site in Kansas.....	54
Table 12. Proportion of each energy flow term to total rate of energy released by NAPL biodegradation.....	58
Table 13. Average NSZD rate and cumulative NAPL losses for the field site in Colorado .....	61
Table 14. Average NSZD rate and cumulative NAPL losses for the field site in Wyoming .....	66
Table 15. Average NSZD rate and cumulative NAPL losses for the field site in Northern New Jersey.....	70
Table 16. Average NSZD rate and cumulative NAPL losses for the field site in Southern New Jersey.....	75
Table 17. Results of the parameter sensitivity analysis for the site in Kansas using the background location background correction method.....	78
Table 18. Soil characteristics used in the thermal NSZD rate model for the laboratory experiment .....	88
Table 19. Standard change in free energy ( $\Delta G_r^o$ ) and enthalpy ( $\Delta H_r^o$ ) for redox reactions of standard phase glucose per mole glucose (calculated using values tabulated in Appendix B) ....	89
Table 20. Average loss rate and cumulative glucose losses for each molasses injection .....	94
Table 21. Measured thermal properties of soil core from Kansas .....	151
Table 22. Free energy and enthalpy of formation for species used in coupled oxidation-reduction reactions .....	152

## LIST OF FIGURES

Figure 1. Conceptual model of carbon fluxes associated with NSZD at a site with a stable or shrinking LNAPL plume..... 5

Figure 2. Energy balance volume consisting of the NAPL impacted area ..... 21

Figure 3. Energy balance conceptual model indicating heat sources and sinks in the subsurface 26

Figure 4. Temperature monitoring sticks in the impacted locations (N1, N2, N3, and N4) and background location (B1) and soil gas monitoring stick (G1) installed at petroleum terminal in Kansas ..... 36

Figure 5. Main components of each temperature monitoring stick installed in Kansas and Colorado..... 37

Figure 6. Above ground components of the temperature monitoring sticks. Left: datalogger, battery, charge regulator, and cell phone inside the enclosure. Right: Solar panel and enclosure as installed in Kansas ..... 39

Figure 7. Multi-level gas monitoring stick installed in Kansas ..... 40

Figure 8. Subsurface temperatures measured at N2 and B1 and calculated as background using the simple analytical model and Hydrus for the field site in Kansas..... 52

Figure 9. Cumulative NAPL losses at the field site in Kansas ..... 55

Figure 10. NAPL loss rate versus subsurface temperature at 5.79m bgs at the field site in Kansas ..... 56

Figure 11. Soil gas profiles for the site in Kansas. Note x-axis scales are set to the range of data ..... 57

Figure 12. Subsurface temperatures measured at impacted location and calculated as background using the simple analytical model and Hydrus for field site in Colorado..... 60

Figure 13. Cumulative NAPL losses at the field site in Colorado..... 62

Figure 14. NAPL loss rate versus subsurface temperature at 6.71m bgs at the field site in Colorado..... 63

Figure 15. Subsurface temperatures measured and calculated as background using the simple analytical model and Hydrus for the field site in Wyoming ..... 65

Figure 16. Cumulative NAPL losses at the field site in Wyoming..... 67

Figure 17. NAPL loss rate versus subsurface temperature at 2.44m bgs at the field site in Wyoming..... 68

Figure 18. Subsurface temperatures measured at impacted location and calculated as background using the simple analytical model and Hydrus for the field site in Northern New Jersey..... 69

Figure 19. Cumulative NAPL losses at the field site in Northern New Jersey..... 71

Figure 20. NAPL loss rate versus subsurface temperature at 2.13m bgs at the field site in Northern New Jersey..... 72

Figure 21. Subsurface temperatures measured at impacted location and calculated as background using the simple analytical model and Hydrus for the field site in Southern New Jersey..... 74

Figure 22. Cumulative NAPL losses at field site in Southern New Jersey.....	76
Figure 23. NAPL loss rate versus subsurface temperature at 3.43m bgs at the field site in Southern New Jersey.....	77
Figure 24. Schematic of experimental column setup.....	84
Figure 25. Carbon dioxide concentrations in the column throughout the laboratory experiment	90
Figure 26. Methane concentrations in the column throughout the laboratory experiment.....	91
Figure 27. Column carbon dioxide profiles following each molasses injection .....	93
Figure 28. Cumulative glucose losses following each molasses injection .....	95
Figure 29. Calibration curve with equation used to determine methane percentage .....	153
Figure 30. Calibration curve with equation used to determine carbon dioxide percentage.....	153

## 1. INTRODUCTION

The modern world relies on petroleum liquids for fuels, lubricants, and manufactured products (Sale 2003). Unfortunately, the production, processing, transport, and use of petroleum liquids has led to releases of these products to the environment. Petroleum hydrocarbons, in the form of Non-Aqueous Phase Liquids (NAPLs), are commonly found in the soil and groundwater beneath petroleum facilities. Some constituents of the petroleum liquids, such as benzene, are toxic and known human carcinogens. Management of these petroleum liquid releases is needed to minimize the risk to human health and the environment.

Petroleum NAPL (hereafter referred to as NAPL) in impacted soil and groundwater is depleted via natural mechanisms in the subsurface; this process is known as Natural Source Zone Depletion (NSZD) (ITRC 2009). Natural loss mechanisms include aerobic and anaerobic biodegradation, sorption, volatilization, and dissolution, with biodegradation accounting for the majority of natural losses (Lundegard and Johnson 2006). NSZD rates are emerging as a critical factor in making management decisions at many NAPL impacted sites.

Current methods for determining NSZD rates rely on measuring fluxes of gases in the vadose zone above NAPL releases. The mechanisms and measurement of gas fluxes are affected by temporally variable environmental factors, and provide NSZD rates from data measured over short time periods. Optimally, methods for resolving NSZD rates are needed that are less sensitive to environmental factors and provide continuous loss rates through time. Herein, an alternative is explored through the development of a NSZD rate model based on subsurface temperatures about NAPL bodies, hereafter referred to as the thermal NSZD rate model.

## **1.1. Hypothesis and Objectives**

Prior field observations have suggested that subsurface temperatures in NAPL impacted areas are higher than subsurface temperatures in unimpacted areas (McCoy et al. 2014; Sweeney and Ririe 2014). Building on these observations, the hypothesis is advanced that subsurface temperatures measured about a NAPL body during biodegradation can be utilized to estimate NSZD rates.

The primary objective of this thesis was to develop methods that yield real-time continuous estimates of NSZD rates for NAPL impacted soil and groundwater using subsurface temperatures. Knowledge of the magnitude and timing of NSZD rates at field sites will help site managers advance sustainable remedies. Real-time monitoring of NSZD rates may also alert site managers to potential new or active subsurface releases of NAPL. Another objective of this thesis was to gain insight into the governing processes of heat release due to biodegradation of NAPL in the subsurface.

## **1.2. Organization and Content**

Chapter 2 provides a review of fundamental concepts. These topics include current methods for quantifying NSZD rates, heat transfer in the subsurface, the thermodynamics of NAPL biodegradation, the use of thermodynamics to estimate microbial growth on specific substrates, and studies regarding heat release in landfills, compost piles, and subsurface waste rock/coal piles. Chapter 3 describes the development of a thermal NSZD rate model. The methods utilized by the model, the required model inputs, and the model outputs are detailed. Chapter 4 presents the methods and results of application of the thermal NSZD rate model to field data from five

sites. This chapter also includes the methods and results of a sensitivity analysis on the model, as well as limitations of the model. Chapter 5 presents the methods and results of a preliminary laboratory study conducted to evaluate the thermodynamics of biodegradation of a carbon substrate in soil. Chapter 6 provides a summary of the main ideas, themes, and results, along with recommendations for future work. Supplementary work not included in the main chapters is included in the appendices.

## **2. LITERATURE REVIEW**

This chapter introduces key concepts that are foundational to this thesis. First, an overview of the significance of NSZD is presented. Second, the current methods employed to quantify NSZD rates are described. Third, fundamental concepts of heat transfer in the subsurface are detailed. Fourth, the thermodynamics of biodegradation of NAPL in the subsurface are explored. Fifth, the use of thermodynamics to estimate microbial growth on specific substrates is summarized. Lastly, studies regarding heat release in landfills, compost piles, and subsurface waste rock/coal piles are considered.

### **2.1. Significance of NSZD**

NSZD rates are emerging as a critical factor in making management decisions at NAPL impacted sites. Recent studies have estimated NSZD rates on the order of hundreds to thousands of gallons/acre/year (Lundegard and Johnson 2006; Sihota et al. 2011; McCoy et al. 2014). Natural losses of NAPL limit migration of NAPL bodies (Mahler et al. 2012), and natural loss rates often rival loss rates associated with active remedies (McCoy et al. 2014). These factors suggest that NSZD may provide an effective, lower cost, and more sustainable remedy at many NAPL impacted sites.

Figure 1 shows a conceptual model of carbon fluxes associated with NSZD at a site with a stable or shrinking LNAPL (Light Non-Aqueous Phase Liquid) plume. The orange zone about the water table represents LNAPL impacted media. LNAPL may be degraded to methane ( $\text{CH}_4$ ) and carbon dioxide ( $\text{CO}_2$ ) via methanogenesis, fully degraded to carbon dioxide and water via aerobic oxidation, or partially degraded to solid phase precipitates, volatile fatty acids, and

biomass via anaerobic oxidation. While the majority of the carbon leaves the system as vertical fluxes of carbon dioxide and methane (Amos et al. 2005), a portion of the carbon stays in the system as solid phase precipitates and residual biomass that cannot be degraded, and a portion leaves the system as fluxes of biomass and volatile fatty acids. Above the water table, the vertical methane flux meets inward diffusing oxygen and is presumably all oxidized to carbon dioxide (Amos et al. 2005, Molins et al. 2010). At the ground surface, carbon dioxide associated with modern soil respiration and hydrocarbon degradation moves out of the subsurface.

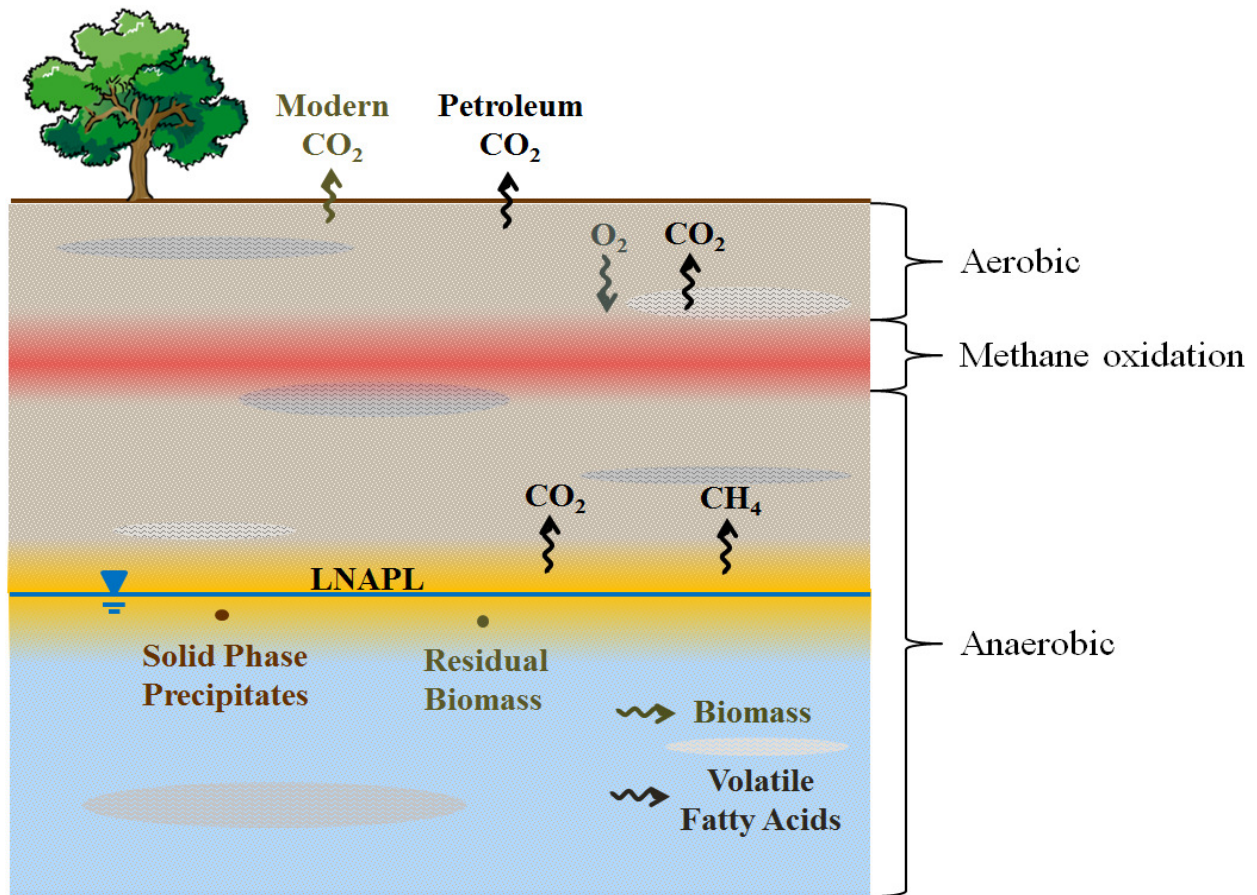


Figure 1. Conceptual model of carbon fluxes associated with NSZD at a site with a stable or shrinking LNAPL plume

## **2.2. Quantification of NSZD Rates**

Current methods for estimating NSZD rates rely on measuring the efflux of soil gases above subsurface NAPL. These methods include the concentration gradient method (Johnson et al. 2006), the dynamic closed chamber method (Sihota et al. 2011), and the CO<sub>2</sub> Trap method (McCoy et al. 2014). The following summary of these methods and their limitations follows Tracy (2015). The limitations of these methods provide the motivation for development of the novel thermal technique presented in this thesis.

The concentration gradient method utilizes vertical soil gas concentration profiles due to volatilization and biodegradation to calculate NSZD rates. Soil gas samples are collected at multiple locations along a vertical profile. The gradients of hydrocarbon gases, oxygen, and/or carbon dioxide are coupled with effective diffusion coefficients in Fick's First Law to determine a rate of subsurface NAPL depletion. Drawbacks of the gradient method include: the method is intrusive and requires subsurface sampling; results take several weeks to process; results are only valid for the period of measurement; a high level of effort is required to determine NSZD rates; the method only accounts for diffusive transport processes; and the results are subject to variations due to natural soil respiration, barometric pumping, surface wind, precipitation and/or soil moisture, artificial surfaces, and heterogeneities in the subsurface.

The dynamic closed chamber method utilizes a soil gas chamber placed on a PVC collar at grade. An infrared gas analyzer (IRGA) within the chamber measures total carbon dioxide efflux out of the soil, which is then converted into an equivalent NAPL biodegradation rate. Drawbacks of the chamber method include: results are only valid for the period of measurement; a moderate level of effort is required to determine NSZD rates; the method assumes all degraded NAPL is

converted to carbon dioxide; correction for natural soil respiration is required; and the results are subject to variations due to natural soil respiration, barometric pumping, surface wind, precipitation and/or soil moisture, artificial surfaces, and heterogeneities in the subsurface.

The CO<sub>2</sub> Trap method utilizes a PVC pipe at grade with two soda lime absorbent elements. The bottom absorbent element captures carbon dioxide efflux from the subsurface and converts it to solid phase carbonates, while the top absorbent element captures atmospheric carbon dioxide and prevents it from reaching the bottom absorbent element. The CO<sub>2</sub> Trap is placed in the field for approximately two weeks, and then the absorbent elements are analyzed to determine the carbon dioxide efflux from the subsurface. The carbon dioxide efflux is then converted into an equivalent NAPL biodegradation rate. Drawbacks of the CO<sub>2</sub> Trap method include: results take several weeks to process; results are only valid for the period of measurement; the method assumes all degraded NAPL is converted to carbon dioxide; correction for natural soil respiration is required; and the results are subject to variations due to barometric pumping, surface wind, precipitation and/or soil moisture, artificial surfaces, and heterogeneities in the subsurface.

### **2.3. Heat Transfer in the Subsurface**

The fundamentals of heat transfer in the subsurface are central to the ideas presented in this thesis. Following Hillel (1980), this section begins with a brief overview of a surface energy balance and then reviews the main modes of energy transfer within the subsurface. The majority of this section is devoted to an explanation of the governing equations of heat transfer in the subsurface via conduction and convection.

### **2.3.1. Energy Balance at Grade**

At the soil-atmosphere interface, no material volume exists, and correspondingly no capacity for energy storage exists. Thus, an energy balance can be written at the soil surface where the energy fluxes sum to zero. This surface energy balance is commonly written as:

$$R_n = G + H + LE \quad (1)$$

where  $R_n$  is the net radiation ( $\text{W}/\text{m}^2$ );  $G$  is the soil heat flux ( $\text{W}/\text{m}^2$ ), which describes the rate heat is transferred through the soil;  $H$  is the sensible heat flux ( $\text{W}/\text{m}^2$ ), which describes the rate heat is transferred from the ground surface to the atmosphere; and  $LE$  is the latent heat flux ( $\text{W}/\text{m}^2$ ), which describes the rate heat is transferred via evaporation to the atmosphere. This thesis is concerned with the soil heat flux within the subsurface, and the remainder of this section focuses on the soil heat flux.

### **2.3.2. Soil Heat Flux**

Heat transfers within the subsurface primarily by conduction and convection. Conduction is the transfer of energy by molecular collisions of particles within a body due to a temperature gradient, while convection is the transfer of energy via the movement of a heat-carrying mass. Heat can also be transferred through the subsurface by radiation, which is the transfer of energy via electromagnetic waves; however, heat transfer by radiation in the subsurface is usually minimal and is generally neglected.

Basic models of heat transfer in the subsurface focus on conduction. The first law of heat conduction, known as Fourier's law, states that heat flux is in the direction of and proportional to the negative temperature gradient:

$$q_c = -\kappa \nabla T \quad (2)$$

where  $q_c$  is the heat flux due to conduction ( $\text{W/m}^2$ ),  $\kappa$  is the thermal conductivity ( $\text{W/m K}$ ), and  $\nabla T$  is the temperature gradient ( $\text{K/m}$ ). In the vertical direction, Fourier's law in one dimension is:

$$q_{c_z} = -\kappa_z \frac{dT}{dz} \quad (3)$$

where  $q_{c_z}$  is the heat flux due to conduction in the vertical direction ( $\text{W/m}^2$ ),  $\kappa_z$  is the vertical thermal conductivity ( $\text{W/m K}$ ), and  $\frac{dT}{dz}$  is the change in temperature with respect to distance in the vertical direction ( $\text{K/m}$ ).

Heat is also transferred in the subsurface via convection of sensible heat by flowing water and/or vapor and via convection of latent heat by vapor flow. deVries (1958) proposed a heat flux equation that considers heat transfer in the subsurface via conduction and convection:

$$q = -\kappa \nabla T + C_w T q_w + C_v T q_v + L_0 q_v \quad (4)$$

where  $q$  is the total heat flux ( $\text{W/m}^2$ ),  $C_w$  is the volumetric heat capacity of liquid water ( $\text{J/m}^3 \text{ K}$ ),  $T$  is the temperature of the flowing water ( $\text{K}$ ),  $q_w$  is the total water mass flux ( $\text{m}^3/\text{m}^2 \text{ s}$ ),  $C_v$  is the volumetric heat capacity of water vapor ( $\text{J/m}^3 \text{ K}$ ),  $q_v$  is the total water vapor mass flux ( $\text{m}^3/\text{m}^2 \text{ s}$ ), and  $L_0$  is the volumetric latent heat of vaporization of liquid water ( $\text{J/m}^3$ ). Equation (4) indicates that the total heat flux is the sum of the conduction of sensible heat as described by Fourier's law (the first term on the right side), convection of sensible heat by water flow (the second term on the right side) and water vapor flow (the third term on the right side), and convection of latent heat by vapor flow (the fourth term on the right side).

Under transient conditions, the heat flux equation must be combined with the conservation of energy, which states that the change in fluxes of heat into or out of a system must be equal to the change in storage of that system:

$$\frac{\partial S_h}{\partial t} = -\frac{\partial q}{\partial z} - S(z, t) \quad (5)$$

where  $S_h$  is the storage of heat in the solid, liquid, and vapor fractions of the soil ( $\text{J}/\text{m}^3$ ),  $q$  is the total heat flux ( $\text{W}/\text{m}^2$ ), and  $S(z, t)$  represents sources and/or sinks that vary with space and/or time ( $\text{W}/\text{m}^2$ ). Storage of heat in the solid, liquid, and vapor fractions of the soil is given by:

$$S_h = C_m T + L_o \theta_v \quad (6)$$

where  $C_m$  is the bulk volumetric heat capacity of the porous media ( $\text{J}/\text{m}^3 \text{K}$ ), and  $\theta_v$  is the volumetric water vapor content ( $\text{m}^3/\text{m}^3$ ).

Combining Equations (4), (5), and (6) in the vertical direction yields the governing equation for heat transport in one dimension (e.g., Saito et al. 2006):

$$C_m \frac{\partial T}{\partial t} + L_o \frac{\partial \theta_v}{\partial t} = \frac{\partial}{\partial z} \left( \kappa \frac{\partial T}{\partial z} \right) - C_w \frac{\partial q_w T}{\partial z} - C_v \frac{\partial q_v T}{\partial z} - L_o \frac{\partial q_v}{\partial z} \pm S(z, t) \quad (7)$$

Equation (7) is utilized for heat transport with vapor transport. When vapor transport can be neglected, the terms relating to the vapor phase can be neglected, and the equation for heat transport is reduced to:

$$C_m \frac{\partial T}{\partial t} = \frac{\partial}{\partial z} \left( \kappa \frac{\partial T}{\partial z} \right) - C_w \frac{\partial q_w T}{\partial z} \pm S(z, t) \quad (8)$$

### 2.3.3. Soil Thermal Properties

Equations (7) and (8) show that heat transfer in the subsurface is dependent on two variables specific to the porous media: the volumetric heat capacity and the thermal conductivity. Volumetric heat capacity is defined as the change in heat content of a unit bulk volume of material per unit change in temperature. The volumetric heat capacity of a soil can be calculated

by adding the heat capacities of the soil constituents adjusted by their volume fraction, as given by deVries (1975):

$$C = \sum f_s C_s + f_w C_w + f_a C_a \quad (9)$$

where  $C$  is the volumetric heat capacity ( $\text{J/m}^3 \text{ K}$ ),  $f$  denotes the volume fraction of each phase, and subscripts  $s$ ,  $w$ , and  $a$  indicate solid (mineral and organic), water, and air, respectively. Volumetric heat capacity can also be measured using calorimetric techniques. Values for various soils and soil constituents have been tabulated by several authors, including Carslaw and Jaeger (1959) and Hillel (1980).

Thermal conductivity is defined as the amount of heat (Joules) transferred through a unit area in unit time under a unit temperature gradient. Thermal conductivity is based on the soil constituents, as well as the sizes, shapes, and spatial arrangement of soil particles. Thermal conductivity can vary with time, space, and temperature, and values for soils can range over one to two orders of magnitude based on the soil saturation. Because of the complex dependencies governing soil attributes, thermal conductivity cannot be readily calculated based on the fractionation of soil constituents but can be estimated using more complex equations. Bulk thermal conductivity can also be measured directly using a thermal conductivity probe. A thermal conductivity probe consists of a heating wire that emits heat at a continuous rate while the rate of temperature rise adjacent to the wire is measured. The thermal conductivity is calculated based on the solution of the equation for heat conduction in the radial direction from a line source. Thermal conductivity values for various soils and saturations have been tabulated by several authors (Carslaw and Jaeger 1959, Hillel 1980).

## 2.4. Thermodynamics of NAPL Biodegradation

NAPL in the subsurface degrades via microbially mediated biodegradation reactions (Wiedemeier et al. 1999). This section provides an overview of the reaction pathways of NAPL biodegradation and the energy released by these reactions.

NAPL is degraded via reduction-oxidation (redox) reactions. The NAPL donates electrons and is oxidized, while the respective electron acceptor is reduced. In the process, usable energy is released in the form of free energy. The electron acceptor used in the redox reaction depends on what is available in the environment and the energy yield of the reaction. Simplifying, reactions that yield the most energy will occur first, followed by reactions that yield less energy (Christensen et al. 2000). In aerobic environments, oxygen is used as the electron acceptor because it yields the greatest amount of energy. When all available oxygen has been consumed, denitrification is the predominant biodegradation pathway, followed by manganese reduction, iron reduction, and then sulfate reduction. Lastly, when all other electron acceptors have been reduced, methanogenesis occurs (Wiedemeier et al. 1996). Table 1 shows the standard free energy change ( $\Delta G_r^0$ ) during decane biodegradation via these pathways, illustrating the sequence of redox reactions that occur during decane biodegradation.

Table 1. Decane redox reactions and standard free energy released per mole decane (calculated using values tabulated in Appendix B, following Wiedemeier et al. 1996)

<b>Decane Redox Reaction</b>	<b><math>\Delta G_r^\circ</math> (kJ/mole)</b>
$15.5O_2 + C_{10}H_{22} \rightarrow 10CO_2 + 11H_2O$ Aerobic Respiration	-6570.2
$12.4NO_3^- + 12.4H^+ + C_{10}H_{22} \rightarrow 10CO_2 + 17.2H_2O + 12.4N_{2,g}$ Denitrification	-6660.1
$62H^+ + 31MnO_2 + C_{10}H_{22} \rightarrow 10CO_2 + 31Mn^{2+} + 42H_2O$ Manganese Reduction	-6571.1
$124H^+ + 62Fe(OH)_3 + C_{10}H_{22} \rightarrow 10CO_2 + 62Fe^{2+} + 166H_2O$ Iron Reduction	-4793.7
$15.5H^+ + 7.75SO_4^{2-} + C_{10}H_{22} \rightarrow 10CO_2 + 7.75H_2S + 11H_2O$ Sulfate Reduction	-1015.3
$4.5H_2O + C_{10}H_{22} \rightarrow 2.25CO_2 + 7.75CH_4$ Methanogenesis	-214.0

Free energy is defined as a combination of the enthalpy and entropy of a reaction:

$$G = H - TS \quad (10)$$

where G is the free energy, H is the enthalpy, T is the temperature in Kelvin, and S is the entropy. At constant temperature and pressure, the change in free energy is:

$$\Delta G = \Delta H - T\Delta S \quad (11)$$

The change in free energy of a reaction ( $\Delta G_r$ ) is a measure of the free energy change in the system as the reaction progresses. When all species are present in their standard state, the standard change in free energy of a reaction ( $\Delta G_r^\circ$ ) is used. The change in enthalpy of system is defined as the quantity of heat absorbed by a system at constant temperature and pressure. When the change in enthalpy is positive, the system absorbs heat, and the reaction is endothermic. When the change in enthalpy is negative, the system emits heat, and the reaction is exothermic. The change in entropy of a system considers the orientation, configuration and translation of the

molecules involved, and is defined by whether the system is moving from a more ordered state to a more random state or vice versa. Energy must be expended to confine or organize molecules, leading to a loss in entropy. Conversely, energy is gained when molecules are given more freedom, leading to a gain in entropy. The change in free energy, enthalpy, and entropy of a reaction can be calculated from the change in free energy, enthalpy, and entropy of the formation of the reactants and products as follows:

$$\Delta G_r = \Delta G_f(\text{products}) - \Delta G_f(\text{reactants}) \quad (12)$$

$$\Delta H_r = \Delta H_f(\text{products}) - \Delta H_f(\text{reactants}) \quad (13)$$

$$\Delta S_r = \Delta S_f(\text{products}) - \Delta S_f(\text{reactants}) \quad (14)$$

where subscript  $r$  represents the overall reaction, and subscript  $f$  represents the formation. Values of the change in free energy, enthalpy, and entropy of formation of most compounds can be found in standard references, such as the *CRC Handbook of Chemistry and Physics* (2014) and the *NIST Chemistry WebBook* (<http://webbook.nist.gov/chemistry/>).

## 2.5. Microbial Yield Predictions Using Thermodynamics

Thermodynamic methods based on the change in free energy of reactions are used to predict biomass yields of microorganisms grown on known substrates. The following section outlines the process of energy transfer between microorganisms and their surroundings during growth, as well as the methods of biomass yield prediction.

Microorganisms carry out most chemical reactions to create new cell material. This process requires nutrients to build macromolecules and synthesize enzymes, electrons to generate free energy to drive synthesis reactions, and electrons to oxidize carbon and nitrogen as necessary for incorporation into cell structures (VanBriesen 2002). Microorganisms may acquire both nutrients

and electrons from a single primary electron donor substrate. Electrons are removed from the primary electron donor and transferred by intracellular electron carriers to the terminal electron acceptor. Energy is captured by the microorganism through the transfer of energy from intermediate electron carriers to energy carriers, such as adenosine triphosphate (ATP). However, only a portion of the free energy generated by the redox reaction can be directly utilized by microorganisms; the rest is used to form higher entropy products or is lost as heat (VanBriesen 2002). Thus, during a redox reaction, a portion of the free energy is dissipated, a portion is used in the catabolic reaction oxidizing the electron donor, and a portion is used in the anabolic reaction synthesizing new biomass.

As outlined by Liu et al. (2007), initial approaches for biomass yield prediction correlated biomass yields in terms of ATP yields or energetic efficiencies. Rittmann and McCarty (2001) proposed a method based on electron and energy balances that relied on an energy transfer efficiency, which describes the fraction of free energy from the redox reaction that is used to synthesize biomass. VanBriesen (2001), Yuan and VanBriesen (2002), and Xiao and VanBriesen (2006) expanded on Rittmann and McCarty's method by also incorporating carbon and nitrogen balances to address oxygenases. Oxygenases are used by aerobic microorganisms to convert hydrocarbons, aromatic compounds, and ammonia to forms that can be used for energy and require an initial input of energy. An alternative method that does not rely on an energy transfer efficiency was proposed by Heijnen and van Dijken (1992). Heijnen and van Dijken noted that methods utilizing an energy transfer efficiency "are plagued with internal inconsistencies mainly due to the fact that the definition of an efficiency requires defining an energetic reference state and that changing the reference state modifies all efficiency values" (Liu et al. 2007). Instead,

Heijnen and van Dijken proposed a method to predict biomass yield based on free energy dissipation per amount of biomass grown.

These methods for estimating bacterial yields assume that during oxidation, a portion of the energy from the electron donor is dissipated, and the rest is converted into new biomass. However, when the biomass decays, almost all of this energy is released except for a small portion that is associated with residual biomass material that cannot be degraded (Rittmann and McCarty 2001). For older NAPL plumes that have established microorganism communities, the populations are likely at steady state and it is assumed that any energy used by the microorganisms to synthesize new biomass is released when those microorganisms decay. Thus, it can be assumed that the energy released as heat to the surrounding environment at these sites can be calculated as the total change in enthalpy of the oxidation reaction. However, at early stage sites where the microbial population is growing, a portion of the energy released during oxidation is used to build the microorganism population. At these sites, only a portion of the total change in enthalpy of the oxidation reaction is released as heat to the surrounding environment.

## **2.6. Studies Regarding Heat Release in Landfills, Compost Piles, and Subsurface Waste Rock/Coal Piles**

Temperature measurements have been used to monitor subsurface processes in several applications that are similar to heat release during NAPL biodegradation. In this section, the use of temperature as a tool for monitoring and analyzing landfills, compost piles, and subsurface mining waste rock/coal piles are explored.

Significant heat generation has been observed in landfills due to decomposition of wastes. Hanson et al. (2010) used thermocouples to monitor landfill temperatures over large spatial and

temporal ranges at multiple locations. From these observations, they concluded that: temperatures were highest in the middle third of the landfill; temperatures in the top third of the landfill followed similar trends as seasonal air temperatures; temperatures in the bottom third were lower than the middle third, but were sustained higher than mean annual air temperature; the highest heat generation and fastest heat gain were observed due to enhanced microbial activity associated with high precipitation rates and wet landfill wastes; and higher temperatures and heat gain were observed to occur during anaerobic decomposition than under aerobic conditions. In addition, lab and field studies (DeWalle et al. 1978; Rees 1980a, b; Hartz et al. 1982; Mata-Alvarez and Martinez-Viturtia 1986) have indicated that optimum temperatures for gas production are between 34°C and 45°C, while significantly reduced gas production rates occur below 20°C and above 75°C (Tchobanoglous et al. 1993).

Composting takes advantage of warm temperatures to facilitate the breakdown of organic matter, and is widely used to treat wastewater sludge and municipal wastes. Kumar (2011) provides an overview of the composting process and findings of several studies regarding the effects of temperature on the composting process. Composting can occur aerobically or anaerobically, but aerobic methods are generally preferred as it takes only one to two months for organic matter to be converted into compost, whereas anaerobic methods require four to six months for organic matter to be converted into compost. Compost is usually aerated with blowers, air diffusers, or by turning the compost piles. Temperatures of 45-55°C ensure the best degradation, and temperatures can reach up to 70°C during the initial stage of composting (Huang et al. 2006). At the lower temperatures, mesophilic microbial communities exist, but at higher temperatures, thermophilic microbial communities develop. The composting process concludes when

temperatures within the compost pile return to ambient temperatures, indicating that the microorganisms have consumed the majority of the degradable organic material.

Hollesen et al. (2011) use temperature measurements to model heat release in the subsurface by coal and mining waste rock piles. Oxidation of pyrite and coal in the subsurface releases heat, and the temperature of the waste rock pile rises when the heat release rate is greater than the heat loss rate. Hollesen et al. developed a model to study the generation and movement of heat within these waste rock piles. Heat flow is modeled by considering both conduction and convection through the waste rock pile. Heat release rates used in the model are based on laboratory measurements of daily heat release rates of the coal and waste rock. The model was validated using temperatures measured at several depths in the subsurface, and showed a good correlation for shallow depths (less than six meters), but a poor correlation for depths greater than six meters. The authors hypothesize that this poor correlation is due to the age of the waste rock material. Because the deeper waste rock is older, it likely has a smaller decay coefficient, and therefore less heat release, than the shallower material.

The use of subsurface temperatures to determine NSZD rates is relatively novel. Sweeney and Ririe (2014) present a theory for using temperature measurements to estimate aerobic biodegradation in hydrocarbon contaminated soils; however, they do not apply their method to their field data or report loss rates. Building on the concepts described in this literature review, this thesis proposes a novel method for estimating continuous NSZD rates based on subsurface temperature measurements.

### **3. THERMAL NSZD RATE MODEL BASED ON SUBSURFACE TEMPERATURES**

Based on the concepts presented in the literature review, a model to predict NSZD rates based on subsurface temperatures was created. This chapter details the development of that model. First, the objectives of the modeling effort are defined. Second, the methods utilized by the model are described. Third, the inputs required for the model are explained. Finally, the model outputs are described.

#### **3.1. Objectives**

This modeling effort was driven by the need for reliable, continuous estimates of NSZD rates of subsurface NAPL. Based on this need, two main objectives were defined. The first objective of this model was to provide reliable NSZD rate estimates of subsurface NAPL. As discussed in Chapter 2, current methods for estimating NSZD rates rely on the efflux of carbon dioxide from the subsurface, and the efflux of carbon dioxide at one location may be influenced by several factors. Therefore, a main objective of this model was to provide reliable NSZD rate estimates that are less sensitive to environmental factors. The second objective of this model was to provide continuous NSZD rate estimates of subsurface NAPL. Current methods for estimating NSZD rates provide values based on samples taken over short time periods, therefore, another main objective of this model was to provide continuous NSZD rate estimates to determine whether a seasonality of losses exists at each site.

#### **3.2. Methods**

This section details the mathematical techniques utilized to develop the model for estimating NSZD rates. First, a general energy balance for a NAPL release is developed. Second, the energy

flows, sources, and sinks considered in the energy balance are discussed. Third, the method utilized to correct the energy flows for background conditions is detailed and the derivation of the final energy balance equations is presented. Finally, the method employed to calculate the NSZD rate is presented.

Primary assumptions of this model include:

- Vertically, the energy balance volume extends from the base of the NAPL body to the top of the methane oxidation front in the vadose zone
- The energy flows are adequately represented in a two dimensional slice (x and z)
- Only the energy flow associated with flowing water is relevant in the x dimension
- The thermal conductivity, heat capacity, and water saturation of the unsaturated zone is constant and uniform
- The thermal conductivity, heat capacity, and water saturation of the saturated zone is constant and uniform
- The porosity and hydraulic conductivity of the media are constant and uniform
- Soil properties are the same at the impacted and background locations
- Energy sources and sinks other than the energy released during NAPL biodegradation are the same at the impacted and background locations
- Decane is used as an analog to represent all constituents of the NAPL
- The end products of all biodegradation reactions are carbon dioxide and water
- The microbial population is at steady-state and all enthalpy released during biodegradation is released as heat to the surrounding environment

### 3.2.1. Energy Balance

Figure 2 shows the energy balance volume upon which the model is based, as well as the energy flows considered in the energy balance. The energy balance volume consists of the NAPL impacted area both above and below the water table. All energy flows in the z direction are considered. Only the energy flow due to convection of sensible heat by water is considered in the x direction. All other energy flows in the x direction and all energy flows in the y direction are assumed to be negligible.

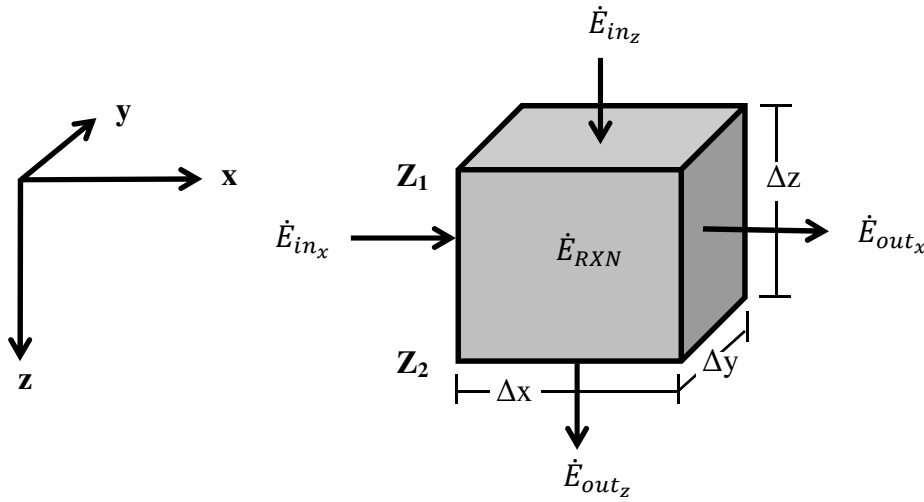


Figure 2. Energy balance volume consisting of the NAPL impacted area

Equation 15 is the energy balance applied to the energy balance volume:

$$\dot{E}_{in_z} - \dot{E}_{out_z} + \dot{E}_{in_x} - \dot{E}_{out_x} + \dot{E}_{RXN} \pm S = \frac{dE}{dt} \quad (15)$$

where  $\dot{E}_{in_z}$  is the rate of conductive and convective energy input in the z direction,  $\dot{E}_{out_z}$  is the rate of conductive and convective energy output in the z direction,  $\dot{E}_{in_x}$  is the rate of convective energy input due to groundwater flow in the x direction,  $\dot{E}_{out_x}$  is the rate of convective energy output due to groundwater flow in the x direction,  $\dot{E}_{RXN}$  is the rate of energy released by NAPL

biodegradation,  $S$  is a term that represents additional energy sources and/or sinks within the energy balance volume, and  $\frac{dE}{dt}$  is the rate of change of energy with time within the energy balance volume. All terms have units of watts (W).

The energy flow in the  $z$  direction is due to conduction, convection of sensible heat by water and vapor, and convection of latent heat by vapor and is represented by the following equation:

$$\dot{E}_{in_z} - \dot{E}_{out_z} = \dot{E}_{in_{z_{cond}}} - \dot{E}_{out_{z_{cond}}} + \dot{E}_{in_{z_{conv_w}}} - \dot{E}_{out_{z_{conv_w}}} + \dot{E}_{in_{z_{conv_v}}} - \dot{E}_{out_{z_{conv_v}}} - \dot{E}_{z_{conv_v_{latent}}} \quad (16)$$

where  $\dot{E}_{in_{z_{cond}}} - \dot{E}_{out_{z_{cond}}}$  is the energy flow due to conduction,  $\dot{E}_{in_{z_{conv_w}}} - \dot{E}_{out_{z_{conv_w}}}$  is the energy flow due to convection of sensible heat by water,  $\dot{E}_{in_{z_{conv_v}}} - \dot{E}_{out_{z_{conv_v}}}$  is the energy flow due to convection of sensible heat by vapor, and  $\dot{E}_{z_{conv_v_{latent}}}$  is the energy flow due to convection of latent heat by vapor. Again, all terms have units of watts (W). The energy inflow and outflow due to conduction are described by the following equations:

$$\dot{E}_{in_{z_{cond}}} = -\kappa_{unsat} \nabla T_{unsat} \Delta x \Delta y = -\kappa_{unsat} \left. \frac{dT}{dz} \right|_{z_1} \Delta x \Delta y \quad (17)$$

$$\dot{E}_{out_{z_{cond}}} = -\kappa_{sat} \nabla T_{sat} \Delta x \Delta y = -\kappa_{sat} \left. \frac{dT}{dz} \right|_{z_2} \Delta x \Delta y \quad (18)$$

where  $\dot{E}_{in_{z_{cond}}}$  is the energy flow into the energy balance volume in the  $z$  direction due to conduction (W),  $\dot{E}_{out_{z_{cond}}}$  is the energy flow out of the energy balance volume in the  $z$  direction due to conduction (W),  $\kappa_{unsat}$  is the thermal conductivity of the unsaturated zone (W/m K),  $\kappa_{sat}$  is the thermal conductivity of the saturated zone (W/m K),  $\nabla T_{unsat}$  is the temperature gradient in the unsaturated zone above the energy balance volume (K/m),  $\nabla T_{sat}$  is the temperature gradient in the saturated zone below the energy balance volume (K/m),  $\frac{dT}{dz}$  is the change in temperature

with respect to depth (K/m),  $z1$  and  $z2$  represent depths  $Z_1$  and  $Z_2$  in Figure 2 (m), and  $\Delta x \Delta y$  is the cross-sectional area of the energy balance volume perpendicular to the  $z$  direction ( $m^2$ ). The energy inflow and outflow due to convection of sensible heat by water in the  $z$  direction are described by the following equations:

$$\dot{E}_{in_{zconv_w}} = \dot{m}_{win} c_w T_{win} = n \frac{dh}{dt} C_w T_{win} \Delta x \Delta y \quad (19)$$

$$\dot{E}_{out_{zconv_w}} = \dot{m}_{wout} c_w T_{wout} = n \frac{dh}{dt} C_w T_{wout} \Delta x \Delta y \quad (20)$$

where  $\dot{E}_{in_{zconv_w}}$  is the energy flow into the energy balance volume in the  $z$  direction due to convection of sensible heat by water (W),  $\dot{E}_{out_{zconv_w}}$  is the energy flow out of the energy balance volume in the  $z$  direction due to convection of sensible heat by water (W),  $\dot{m}_w$  is the mass flow rate of water into/out of the energy balance volume (kg/s),  $c_w$  is the specific heat of water (J/kg K),  $T_w$  is the temperature of the water (K), subscripts *in* and *out* represent the inflowing and outflowing water,  $n$  is the porosity (dimensionless),  $\frac{dh}{dt}$  is the change in water level with respect to time (m/s), and  $C_w$  is the volumetric heat capacity of water ( $J/m^3 K$ ,  $C = \rho c$ , where  $\rho$  is density). Assuming a homogeneous body, Equations (19) and (20) are combined to give the energy flow due to convection of sensible heat by water in the  $z$  direction:

$$\dot{E}_{zconv_w} = n \frac{dh}{dt} C_w (T_{win} - T_{wout}) \Delta x \Delta y \quad (21)$$

The energy inflow and outflow due to convection of sensible heat by vapor in the  $z$  direction are described by the following equations:

$$\dot{E}_{in_{zconv_v}} = \dot{m}_{vin} c_v T_{vin} = n \frac{dh}{dt} C_v T_{vin} \Delta x \Delta y \quad (22)$$

$$\dot{E}_{out_{zconv_v}} = \dot{m}_{vout} c_v T_{vout} = n \frac{dh}{dt} C_v T_{vout} \Delta x \Delta y \quad (23)$$

where  $\dot{E}_{in_{zconv_v}}$  is the energy flow into the energy balance volume in the z direction due to convection of sensible heat by vapor (W),  $\dot{E}_{out_{zconv_v}}$  is the energy flow out of the energy balance volume in the z direction due to convection of sensible heat by vapor (W),  $\dot{m}_v$  is the mass flow rate of vapor into/out of the energy balance volume (kg/s),  $c_v$  is the specific heat of the vapor (J/kg K),  $T_v$  is the temperature of the vapor (K), and  $C_v$  is the volumetric heat capacity of the vapor (J/m<sup>3</sup> K). Again assuming a homogeneous body, Equations (22) and (23) are combined to give the energy flow due to convection of sensible heat by vapor in the z direction:

$$\dot{E}_{zconv_v} = -n \frac{dh}{dt} C_v (T_{vin} - T_{vout}) \Delta x \Delta y \quad (24)$$

The inflow due to convection of latent heat by vapor in the z direction is taken to be zero. The energy flow due to convection of latent heat by vapor in the z direction therefore is:

$$\dot{E}_{zconv_{vlatent}} = -L_w \rho_v q_v \Delta x \Delta y \quad (25)$$

where  $L_w$  is the latent heat of vaporization of liquid water (J/kg),  $\rho_v$  is the density of water vapor (kg/m<sup>3</sup>), and  $q_v$  is the volumetric water vapor flux (m<sup>3</sup>/m<sup>2</sup> s).

For this thesis, only the energy flow due to convection of sensible heat by water is considered in the x direction. Thus, the energy flow in the x direction is described by the following equation:

$$\dot{E}_{in_x} - \dot{E}_{out_x} = \dot{E}_{in_{xconv_w}} - \dot{E}_{out_{xconv_w}} \quad (26)$$

where  $\dot{E}_{in_{xconv_w}} - \dot{E}_{out_{xconv_w}}$  is the energy flow due to the convection of sensible heat by water in the x direction (W). Similar to the energy inflow and outflow due to convection of sensible heat by water in the z direction, the energy inflow and outflow due to convection of sensible heat by water in the x direction are described by the following equations:

$$\dot{E}_{in_{xconv_w}} = \dot{m}_{win} c_w T_{win} = q_w C_w T_{win} \Delta y \Delta z \quad (27)$$

$$\dot{E}_{out_{xconv_w}} = \dot{m}_{wout} c_w T_{wout} = q_w c_w T_{wout} \Delta y \Delta z \quad (28)$$

where  $\dot{E}_{in_{xconv_w}}$  is the energy flow into the energy balance volume in the x direction due to convection of sensible heat by water (W),  $\dot{E}_{out_{xconv_w}}$  is the energy flow out of the energy balance volume in the x direction due to convection of sensible heat by water (W),  $q_w$  is the water flux in the x direction ( $m^3/m^2 \text{ s}$ ), and  $\Delta y \Delta z$  is the cross-sectional area of the energy balance volume perpendicular to the x direction ( $m^2$ ). Equations (27) and (28) are combined to give the energy flow due to convection of sensible heat by water in the x direction:

$$\dot{E}_{xconv_w} = q_w c_w (T_{win} - T_{wout}) \Delta y \Delta z \quad (29)$$

The change in energy of the energy balance volume with respect to time is described by the following equation:

$$\frac{dE}{dt} = C_m \frac{dT}{dt} \Delta x \Delta y \Delta z \quad (30)$$

where  $\Delta x \Delta y \Delta z$  is the volume of the energy balance volume ( $m^3$ ) and  $C_m$  is the volumetric heat capacity of the energy balance volume ( $J/m^3 \text{ K}$ ). Plugging Equations (17), (18), (21), (24), (25), (29), and (30) into the overall energy balance (Equation (15)) yields:

$$\begin{aligned} & \left( -\kappa_{unsat} \frac{dT}{dz} \Big|_{z_1} \Delta x \Delta y \right) - \left( -\kappa_{sat} \frac{dT}{dz} \Big|_{z_2} \Delta x \Delta y \right) + \left( n \frac{dh}{dt} c_w (T_{win} - T_{wout}) \Delta x \Delta y \right) + \\ & \left( n \frac{dh}{dt} c_v (T_{vin} - T_{vout}) \Delta x \Delta y \right) + (-L_w \rho_v q_v \Delta x \Delta y) + (q_w c_w (T_{win} - T_{wout}) \Delta y \Delta z) + E_{RXN} \pm \\ S = & C_m \frac{dT}{dt} \Delta x \Delta y \Delta z \end{aligned} \quad (31)$$

### 3.2.2. Energy Sources/Sinks

Four primary energy sources and sinks considered in this energy balance influence subsurface temperatures: surface heating and cooling, the geothermal gradient, the heat released during

NAPL biodegradation, and other heat sources and sinks. Figure 3 shows the energy balance conceptual model, where the red arrows indicate the energy sources and sinks considered in this model, the arrow direction indicates the direction of the energy flow, and the arrow size represents the relative magnitude of the energy flow. This section describes these sources and sinks, as well as how they are considered in the model.

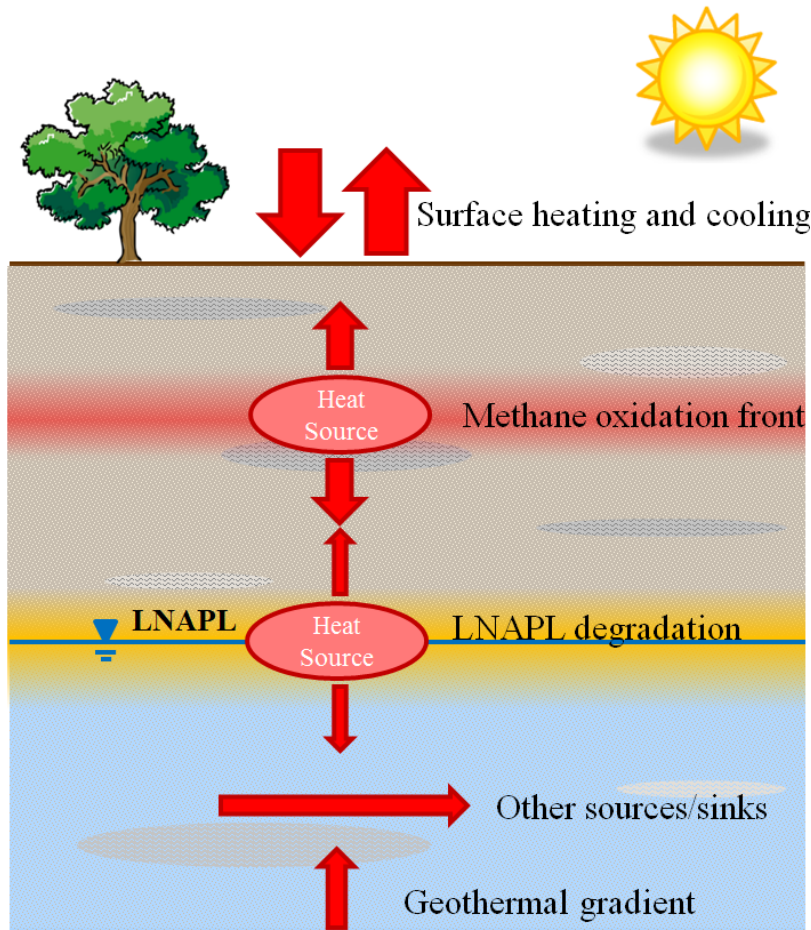


Figure 3. Energy balance conceptual model indicating heat sources and sinks in the subsurface

Heating and cooling of the subsurface is predominantly influenced by the net incoming radiation. Heat moves into the subsurface when the net radiation is greater than the losses due to the sensible and latent heat fluxes, and heat moves out of the subsurface when the losses due to the sensible and latent heat fluxes are greater than the net radiation. Near the ground surface,

subsurface temperatures closely resemble those of the air temperature. However, the influence of short-term air temperature changes are less pronounced with depth, and deeper subsurface temperatures follow dampened seasonal trends with a delay of the temperature peak. The dampening and delay effects are due to heat absorption by the soil along the path of propagation from the surface (Hillel 1980) and varies based on the soil composition. At considerable depth (greater than about 20 meters below ground surface (bgs)), the effects of temperature changes at the surface are not evident, and the subsurface temperature is equal to the average annual ground surface temperature.

The conceptual model includes a heat flow due to the geothermal gradient. Moving from the ground surface downward, temperatures increase due to heat released by the mantle and core of the Earth. Energy from the mantle and core is considered as a source that propagates heat upward from the Earth's core to the ground surface.

Additionally, the conceptual model includes the lateral translation of energy through the area of interest, representing energy brought in to the area of interest by flowing groundwater, as well as additional energy flows within the subsurface that are not accounted for previously. The movement of energy through the area of interest is considered as a source if energy is added to the area of interest and as a sink if energy is lost from the area of interest.

Lastly, the conceptual model includes energy sources due to NAPL biodegradation and methane oxidation. NAPL accumulates at the water table, and as the water table rises and falls, the NAPL is smeared vertically to create a zone of NAPL about the water table. As discussed in Chapter 2, dissolved NAPL constituents can be biodegraded by microorganisms in the subsurface, releasing energy. During biodegradation, a portion of the energy contained in the NAPL is dissipated as

heat to the surrounding environment. NAPL biodegradation commonly occurs under anaerobic conditions via methanogenesis (Amos et al. 2005). When the produced methane meets inward diffusing oxygen from the atmosphere, a portion of the energy contained in the methane is dissipated as heat during methane oxidation. This energy is considered as another source that propagates heat from the methane oxidation zone.

### 3.2.3. *Background Correction*

For this model, only the energy source due to NAPL biodegradation is of interest. To separate the heat released due to NAPL biodegradation from the heat flows due to surface heating and cooling, the geothermal gradient, and lateral translation of heat, a background subtraction method is utilized. The subsurface temperatures at an unimpacted background location, which is not influenced by an energy source due to NAPL biodegradation, are subtracted from the temperatures at the impacted location to give the temperature gradients due to NAPL biodegradation. The background temperatures may be obtained by modeling (described subsequently in Section 4.2.2) or measuring subsurface temperatures at an unimpacted location. These values are then used in the energy balance to determine the heat released from the NAPL biodegradation.

The method of this background correction is illustrated by first considering the simplified energy balance at the impacted location:

$$\dot{E}_{in_{Impact}} - \dot{E}_{out_{Impact}} + \dot{E}_{RXN} \pm S = \frac{dE}{dt}_{Impact} \quad (32)$$

where subscript *Impact* indicates the impacted area. At the background location, no energy source due to NAPL biodegradation exists, so the simplified energy balance is:

$$\dot{E}_{in_{Bkg}} - \dot{E}_{out_{Bkg}} \pm S = \frac{dE}{dt}_{Bkg} \quad (33)$$

where subscript *Bkg* indicates the background location. The term *S* represents sources and sinks due to surface heating and cooling, the geothermal gradient, and the lateral movement of energy into or out of the area of interest. Assuming that *S* is the same at both the impacted and background location, Equation (33) is solved for *S*, which is then used in Equation (32) and solved for  $E_{RXN}$  to obtain:

$$\dot{E}_{RXN} = -\left(\dot{E}_{in_{Impact}} - \dot{E}_{in_{Bkg}}\right) + \left(\dot{E}_{out_{Impact}} - \dot{E}_{out_{Bkg}}\right) + \left(\frac{dE}{dt}_{Impact} - \frac{dE}{dt}_{Bkg}\right) \quad (34)$$

Assuming that the soil properties are the same at the impacted and background locations, the energy flows in Equation (34) are due solely to the temperature difference between the impacted and background locations. By subtracting the temperatures at the background location from the temperatures at the impacted location, background corrected temperatures are obtained. The background corrected temperatures are then used in the overall energy balance (Equation (31)), which eliminates the unknown term *S*. The new energy balance becomes:

$$\begin{aligned} & \left(-\kappa_{unsat} \frac{dT_c}{dz}\Big|_{z1} \Delta x \Delta y\right) - \left(-\kappa_{sat} \frac{dT_c}{dz}\Big|_{z2} \Delta x \Delta y\right) + \left(n \frac{dh}{dt} C_w (T_{cwin} - T_{cwout}) \Delta x \Delta y\right) + \\ & \left(n \frac{dh}{dt} C_v (T_{cvin} - T_{cvout}) \Delta x \Delta y\right) + (-L_w \rho_v q_v \Delta x \Delta y) + (q_w C_w (T_{cwin} - T_{cwout}) \Delta y \Delta z) + \\ & E_{RXN} = C_m \frac{dT}{dt} \Delta x \Delta y \Delta z \end{aligned} \quad (35)$$

where  $T_c$  is the background corrected temperature (K).

#### 3.2.4. NSZD Rate

Equation (35) is solved for  $E_{RXN}$ , and once  $E_{RXN}$  is known, it is used to determine the NSZD rate using the following equation:

$$LossRate = \frac{-\dot{E}_{RXN}}{\Delta H_r} \quad (36)$$

where *LossRate* is the NSZD rate (mol/m<sup>2</sup> s) and  $\Delta H_r$  is the enthalpy released during oxidation of the NAPL (J/mol). Additionally, the NSZD rate can be calculated in units of [gal/acre/year] using the following equation:

$$LossRate = \frac{-\dot{E}_{RXN}}{\Delta H_r} \frac{MW_{LNAPL}}{\rho_{LNAPL}} \frac{264.17 \text{ gal}}{m^3} \frac{4046.86 \text{ m}^2}{\text{acre}} \frac{31556900 \text{ sec}}{\text{year}} \quad (37)$$

where  $MW_{LNAPL}$  is the molecular weight of the NAPL (kg/mol) and  $\rho_{LNAPL}$  is the density of the NAPL (kg/m<sup>3</sup>). For this model, following Johnson et al. (2006), decane is used as an analog to represent all constituents of the NAPL (decane molecular weight = 0.142 kg/mol, density = 730 kg/m<sup>3</sup>).

### 3.3. Model Inputs

This section describes the parameters needed to run the thermal NSZD rate model. Three main categories of inputs are needed: 1) subsurface temperatures and water levels measured at the impacted location; 2) subsurface temperatures measured at a representative background location; and 3) site soil and contaminant characteristics. The thermal NSZD rate model was built in Mathcad 15.0 (Parametric Technology Corporation, Needham, MA).

#### 3.3.1. Impacted Location Temperatures and Water Levels

Subsurface temperatures above, within, and below the NAPL zone at the impacted location are needed. Temperature measurements from at least two different locations above the methane oxidation front are needed to compute the temperature gradient above the NAPL impacted zone. Similarly, temperature measurements from at least two different locations below the NAPL zone are needed to compute the temperature gradient below the NAPL impacted zone. Additionally,

temperature measurements are needed from at least one location within the NAPL zone to calculate the change in energy with time of the NAPL zone.

To determine the energy flows due to the convection of water and vapor, water level measurements are needed. Water levels at the same location and time as the temperature measurements in the impacted location are needed to calculate the energy flows due to convection of sensible heat by water and vapor in the z direction, as well as the energy flow due to convection of latent heat by vapor in the z direction. Water levels taken from at least two additional nearby locations (a total of at least three locations) are needed to calculate the energy flow due to convection of sensible heat by water in the x direction.

### ***3.3.2. Representative Background Temperatures***

Subsurface temperatures are needed at a representative background location at the same depths and times as the temperature measurements taken in the impacted location. These temperatures may be obtained by modeling subsurface temperatures at the impacted location assuming that there is no heat released by NAPL biodegradation, or by measuring subsurface temperatures at a nearby location that is not impacted by NAPL. The representative background temperatures are used to correct the temperatures measured at the impacted location to determine the heat released due to NAPL biodegradation.

### ***3.3.3. Soil and Contaminant Characteristics***

Several fixed and site-specific input parameters are needed for the model. Fixed input parameters that are independent of site specific attributes are presented in Table 2. Necessary site-specific characteristics are presented in Table 3. Lastly, necessary contaminant specific parameters and

their values are summarized in Table 4. As stated previously, decane is used in this model to represent all constituents of the NAPL.

Table 2. Fixed input parameters and their values

Parameter	Symbol	Value	Units
Density of Solids	$\rho_s$	2650	kg/m <sup>3</sup>
Density of Water	$\rho_w$	1000	kg/m <sup>3</sup>
Density of Air	$\rho_a$	1.205	kg/m <sup>3</sup>
Density of Water Vapor	$\rho_{wv}$	0.023	kg/m <sup>3</sup>
Specific Heat of Solids	$c_s$	0.7391	kJ/kg
Specific Heat of Water	$c_w$	4.186	kJ/kg
Specific Heat of Air	$c_a$	1.005	kJ/kg
Latent Heat of Vaporization of Water	$L_w$	2257	kJ/kg

Table 3. Site-specific characteristics needed

Site Characteristics	Symbol	Units
<b>General</b>		
Porosity	$n$	-
Hydraulic Conductivity	$K_{sat}$	m/day
Length of Impacted Area	$L$	m
Width of Impacted Area	$w$	m
<b>Unsaturated Zone</b>		
Thermal Conductivity	$\kappa_{unsat}$	W/mK
Volumetric Heat Capacity	$C_{unsat}$	J/m <sup>3</sup> K
Water Saturation	$S_{wfc}$	-
<b>Saturated Zone</b>		
Thermal Conductivity	$\kappa_{sat}$	W/mK
Volumetric Heat Capacity	$C_{sat}$	J/m <sup>3</sup> K
Water Saturation	$S_w$	-

Table 4. Decane characteristics and their values

<b>Decane Characteristics</b>	<b>Symbol</b>	<b>Value</b>	<b>Units</b>
Free Energy of Degradation Reaction	$\Delta G_r$	-6779.2	kJ/mol
Enthalpy of Degradation Reaction	$\Delta H_r$	-6797.1	kJ/mol
Molecular Weight of LNAPL	$MW_{LNAPL}$	142.3	g/mol
Density of LNAPL	$\rho_{LNAPL}$	0.73	g/cm <sup>3</sup>

### 3.4. Model Outputs

The thermal NSZD rate model calculates the daily NSZD rate in gallons/acre as well as daily values of cumulative losses in gallons/acre. The model outputs this data in both graphical and tabular formats. The model also calculates the average annual NSZD rate for the period of record in gallons/acre/year. These units are used by professionals in groundwater remediation and are therefore used in this thesis to provide more meaningful results.

## **4. FIELD-SCALE APPLICATION OF THE THERMAL NSZD RATE MODEL**

This chapter presents the application of the thermal NSZD rate model to subsurface temperature data collected at five field sites across the United States. First, the objectives of applying the model to field data are discussed. Second, the methods used to collect the field data and background data are given. Third, the methods used for a sensitivity analysis on the parameters used in the model are described. Fourth, the results of application of the thermal NSZD rate model to the field sites are given. Fifth, the results of the sensitivity analysis are presented. Finally, limitations of the thermal NSZD rate model are discussed.

### **4.1. Objectives**

Three main objectives drove the field-scale application of the thermal NSZD rate model. The first objective was to determine the magnitude and timing of continuous NSZD rates at petroleum hydrocarbon impacted field sites. The second objective was to determine whether NSZD rates vary as a function of subsurface temperature. The last objective was to determine the sensitivity of the model to the input parameters.

### **4.2. Methods**

This section describes the methods used to apply the thermal NSZD rate model to field site data. First, the methods used to collect data at the various field sites are described. Next, the methods used to obtain a background correction estimate are discussed. Finally, the model inputs for each field site are presented.

#### **4.2.1. Data Collection**

Subsurface temperature data were collected at five field sites. Temperature monitoring systems were installed at an active petroleum terminal in Kansas and an active petroleum refinery in Colorado as a part of this work. Temperature monitoring systems were already in place at three additional locations: a former petroleum refinery in Wyoming (Kiaalhosseini 2014); a former petroleum refinery and now active petroleum terminal in Northern New Jersey; and an active chemical manufacturing facility in Southern New Jersey (Bezold 2015). This section details the data collection methods at each of these field sites.

##### *4.2.1.1. Kansas*

The petroleum terminal in Kansas is adjacent to a large river and is underlain by alluvium. The uppermost three to five meters are comprised of overbank silt, clay, and silty fine sand. Below this is a layer of point bar fine sand and silty fine sand approximately 1.5 meters thick. Underlying this layer are channel deposits that grade vertically from fine to medium sand. The water table at the site is strongly influenced by the river stage. The depth to groundwater ranges from less than 0.5 meters to over eight meters depending on the time of year (TRC 2012).

Figure 4 shows the locations of temperature monitoring systems (“sticks”) and soil gas monitoring sticks installed at the site. Four temperature monitoring systems (“sticks”) were installed along a petroleum impacted transect of the terminal (N1, N2, N3, and N4), roughly perpendicular to the Missouri River. An additional temperature monitoring stick was installed at an unimpacted location along the southern property boundary to serve as a background (B1). One multi-level soil gas monitoring stick was installed in the petroleum impacted area (G1).

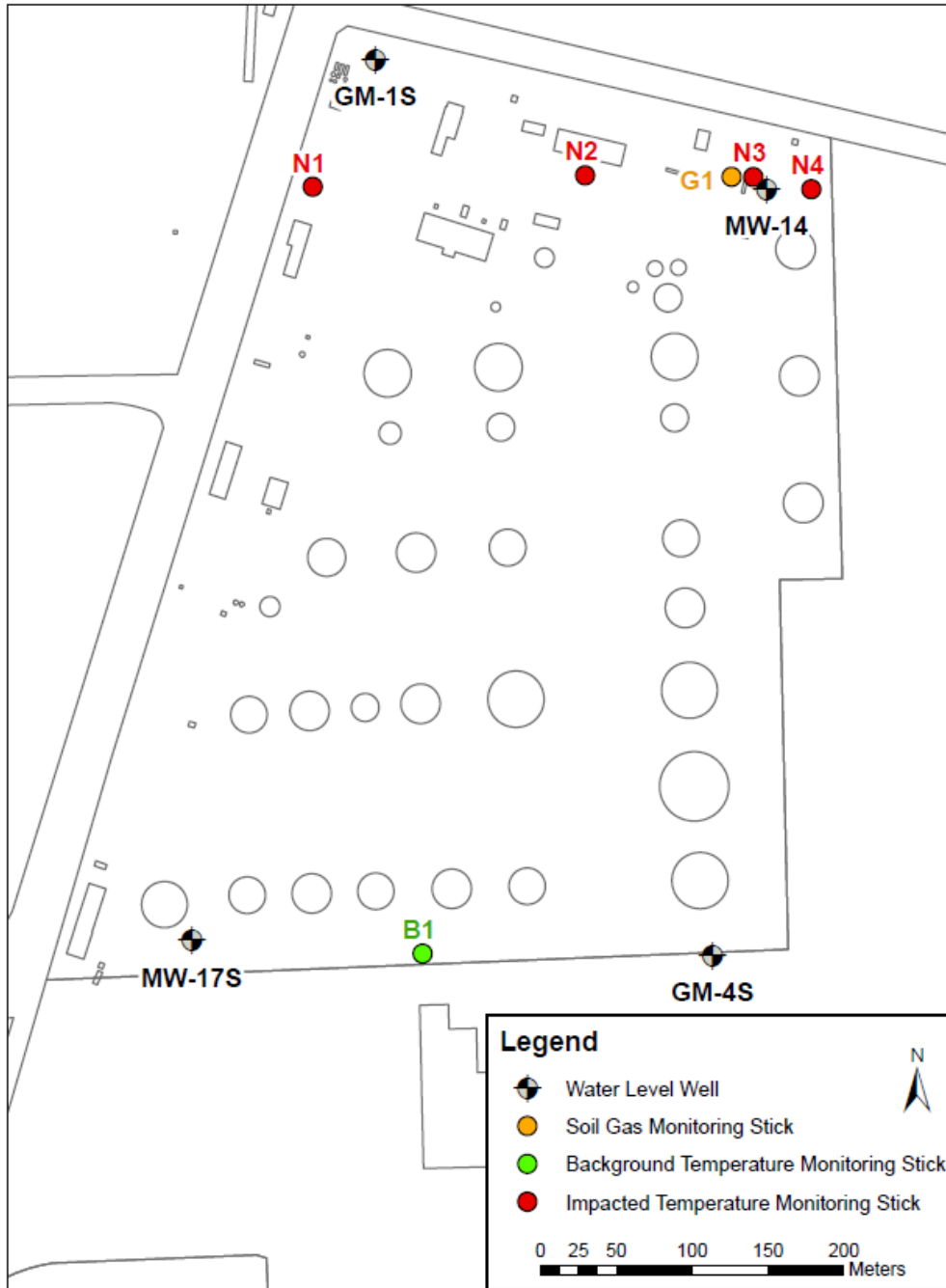


Figure 4. Temperature monitoring sticks in the impacted locations (N1, N2, N3, and N4) and background location (B1) and soil gas monitoring stick (G1) installed at petroleum terminal in Kansas

Figure 5 shows a schematic of each of the temperature monitoring sticks installed in Kansas. Each stick consists of eight type T (copper–constantan) thermocouples with two thermocouples located below the NAPL impacted area (10.67 m bgs and 11.28 m bgs), two thermocouples

located within the NAPL impacted area (5.79 m bgs and 8.23 m bgs), two thermocouples located above the NAPL impacted area (3.05 m bgs and 3.66 m bgs), and two thermocouples located just below the ground surface (0.15 m bgs and 0.30 m bgs). Table 5 summarizes the depth of each thermocouple as installed in Kansas, as well as at the thermocouple depths at the other field sites. The thermocouples were fabricated using type T PFA coated thermocouple wire (TC Direct, Hillside, IL) with the end enclosed in an epoxy-filled glass cap. The thermocouples were then attached to a 9.5 mm diameter PVC rod at the desired spacing. The thermocouples and PVC rod were installed using a direct-push drilling rig, and the annular space was filled with coarse sand (Quikrete All-Purpose Sand #1152, Denver, CO).

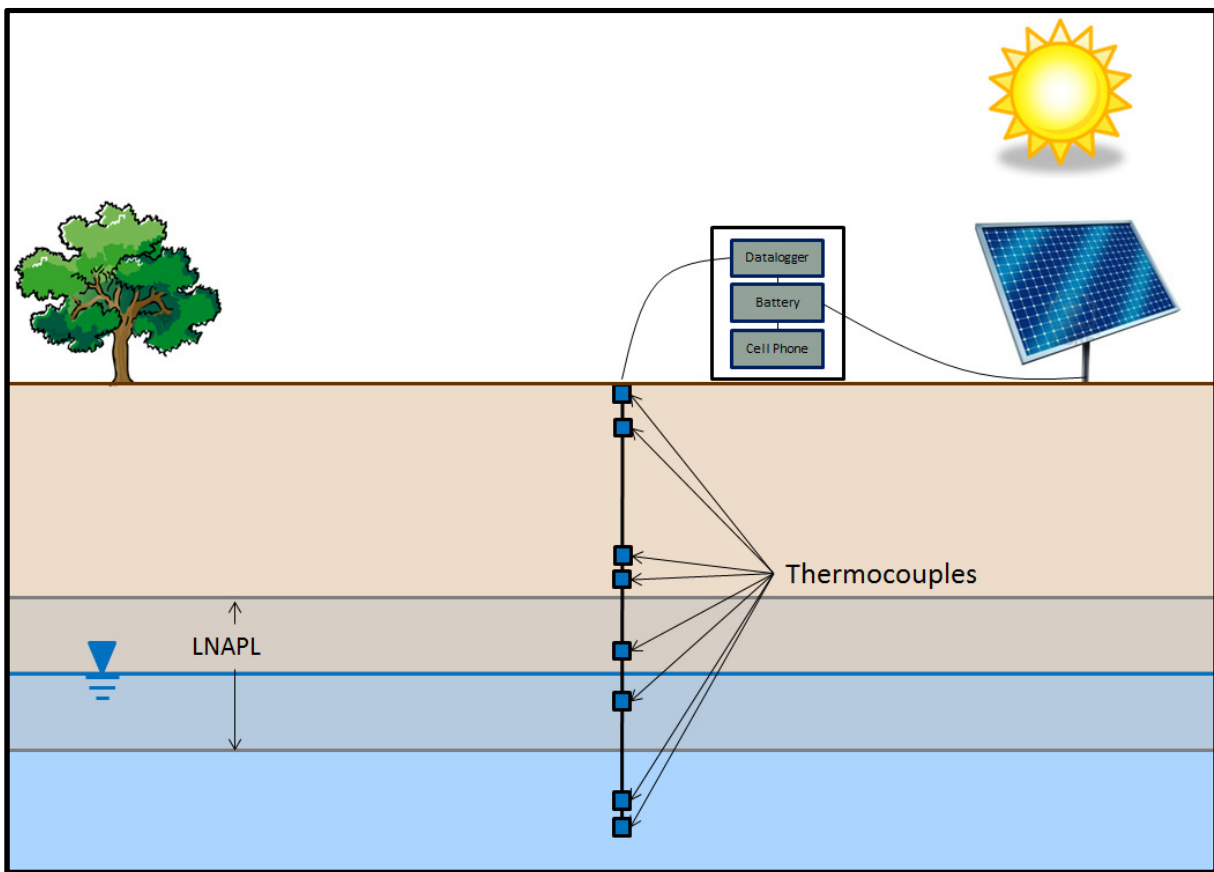


Figure 5. Main components of each temperature monitoring stick installed in Kansas and Colorado

Table 5. Thermocouple depths in meters below ground surface at each field site

Kansas					Colorado	Wyoming		Northern New Jersey		Southern New Jersey
N1	N2	N3	N4	B1	IW10MLS	Extinct	Background	SB1	SB2	
0.15	0.15	0.15	0.15	0.15	0.00	0.91	0.91	1.52	0.91	0.53
0.30	0.30	0.30	0.30	0.30	0.15	1.22	1.22	2.13	1.83	1.14
3.05	3.05	3.05	3.05	3.05	1.52	1.52	1.52	3.05	2.44	1.91
3.66	3.66	3.66	3.66	3.66	1.83	2.44	2.44	3.96	3.05	2.67
5.79	5.79	5.79	5.79	5.79	5.18	3.05	3.05	4.57	3.96	3.43
8.23	8.23	8.23	8.23	8.23	6.71	3.96	3.96	5.49	4.57	4.19
10.67	10.67	10.67	10.67	10.67	8.53	4.27	4.27	6.10	5.49	4.95
11.28	11.28	11.28	11.28	11.28	9.14	4.57	4.57			5.72
										6.48
										7.24

The above-ground components of each temperature monitoring stick consist of a datalogger, battery, power supply, and cellular digital modem, as shown in Figure 6. The thermocouples connect to the datalogger (CR1000, Campbell Scientific, Logan, UT). The datalogger is powered by a 12 Vdc, 24 Ah sealed rechargeable battery (BP24, Campbell Scientific, Logan, UT), which is charged by a 20 W solar panel (SP20, Campbell Scientific, Logan, UT). A 12 V charge regulator (CH100, Campbell Scientific, Logan, UT) regulates the current between the solar panel, battery, and datalogger. A cellular digital modem (Airlink Raven XT, Sierra Wireless, Richmond, British Columbia) connected to the datalogger transmits data over the Verizon cellular network. Subsurface temperatures are recorded by the datalogger every minute, and data are downloaded daily from the dataloggers via the wireless connection. The datalogger, battery, charge regulator, and cellular digital modem are housed in a protective weather-resistant enclosure (ENC14/16, Campbell Scientific, Logan, UT).

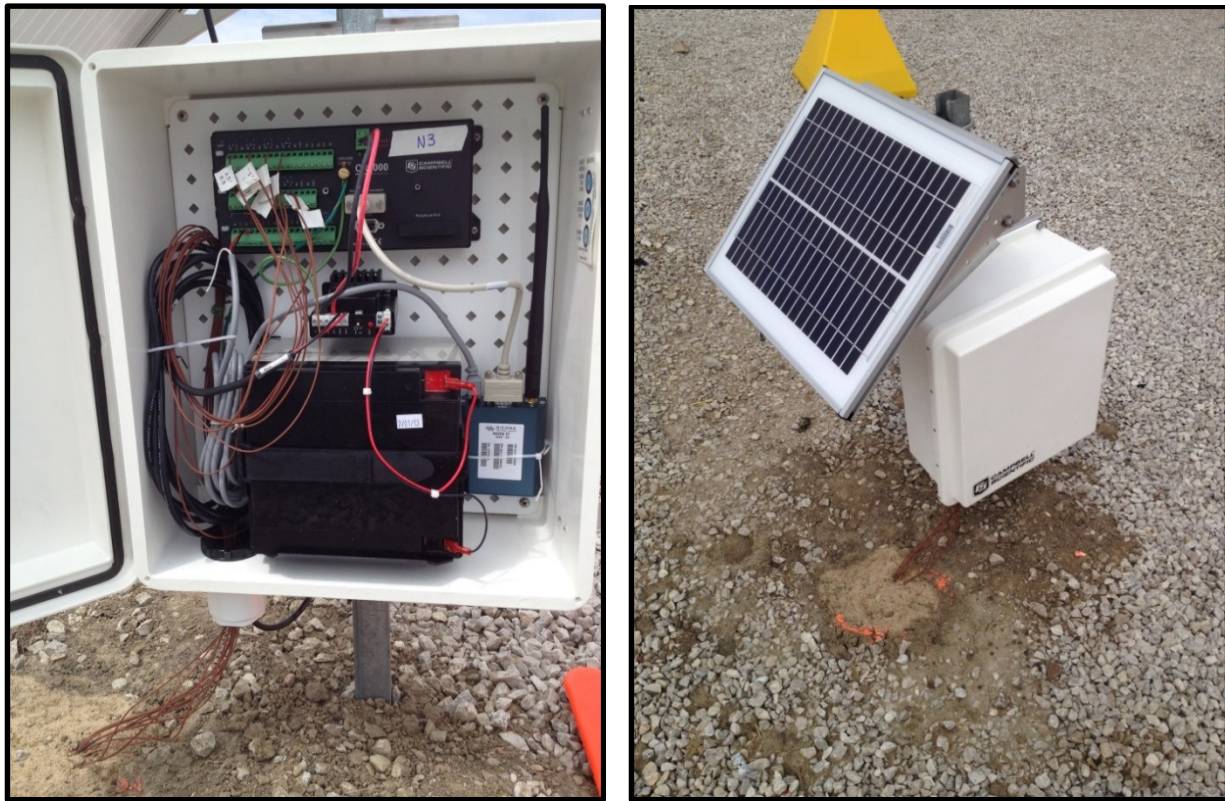


Figure 6. Above ground components of the temperature monitoring sticks. Left: datalogger, battery, charge regulator, and cell phone inside the enclosure. Right: Solar panel and enclosure as installed in Kansas

Figure 7 shows a schematic of the multi-level gas monitoring stick installed in Kansas. The gas monitoring stick consists of 15 gas sampling ports attached to a 1.27 cm ID PVC pipe and placed every 0.61 m from 0.61 m bgs to 9.14 m bgs. Sampling ports consist of 0.32 cm diameter PTFE tubing (Cole-Parmer, Vernon Hills, IL) wrapped with 5  $\mu$ m Nitex filter fabric (Wildco, Yulee, FL) to prevent the extraction of soil during sampling. Gas samples were collected by attaching a landfill gas meter to each sampling port to determine the percent oxygen, carbon dioxide, and methane plus other hydrocarbon gases at each depth. The gas monitoring stick was installed using a direct-push drilling rig, and the annular space was filled with fine sand topped with a 0.3 m bentonite plug to grade.

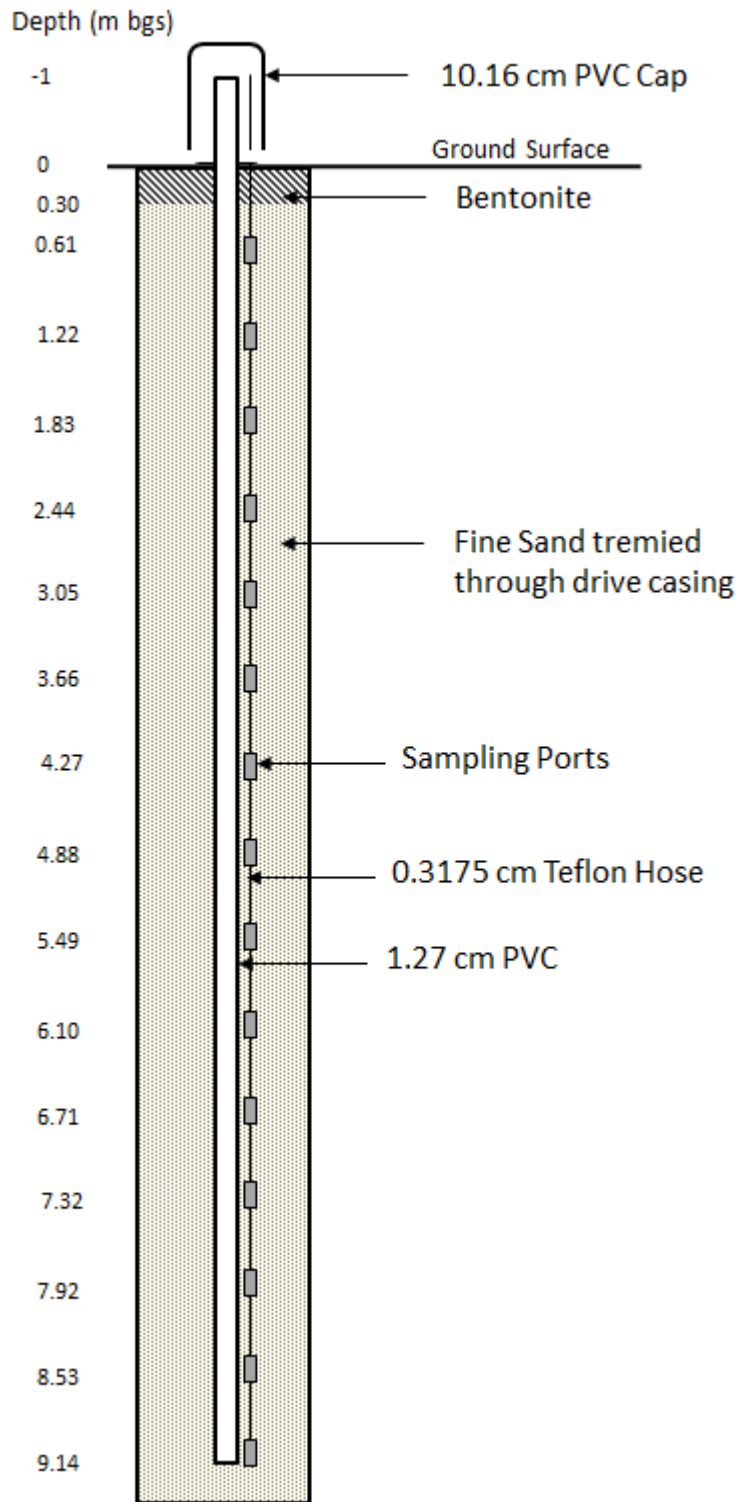


Figure 7. Multi-level gas monitoring stick installed in Kansas

#### 4.2.1.2. *Colorado*

The petroleum refinery in Colorado is adjacent to Sand Creek and is underlain by Sand Creek alluvium. This consists of overbank, point bar, and channel gravels that grade from fine to coarse with depth. Water levels at the site are controlled by vertical cutoff walls and hydraulic controls, and the depth to groundwater is relatively constant at about 7.6 meters (McCoy 2012).

A single temperature monitoring stick was installed in a petroleum impacted area of the refinery. The temperature monitoring stick consists of the same above- and below-ground components as those installed in Kansas. However, in Colorado, the thermocouples and PVC rod were placed in an existing 12.7 mm ID PVC multi-level sampler, and the annular space was filled with medium sand (Colorado Silica Sand, Premier Silica LLC, Colorado Springs, CO). Table 5 summarizes the depths of each thermocouple as installed in Colorado.

#### 4.2.1.3. *Wyoming, Northern New Jersey, and Southern New Jersey*

The temperature monitoring systems in Wyoming, Northern New Jersey, and Southern New Jersey were installed as part of multi-level monitoring systems that also include gas and water sampling ports. The specifics of the systems installed in Wyoming are outlined by Kiaalhosseini (2014). The specifics of the system installed in Southern New Jersey are outlined by Bezold (2015). Table 5 summarizes the depths of each thermocouple as installed in Wyoming, Northern New Jersey, and Southern New Jersey. The main differences between these systems and those installed in Kansas and Colorado are: these systems utilize type K (chromel–alumel) thermocouples, the thermocouples are attached to the outside of a hollow PVC pipe, the thermocouples are spaced evenly along the length of the PVC pipe, different dataloggers are

used, solar panels are not used to provide power, and the systems do not include cellular digital modems.

The former petroleum refinery in Wyoming is adjacent to the North Platte River and is underlain by North Platte alluvium. As with the Kansas and Colorado sites, soil includes overbank, point bar, and channel gravels that grade from fine to coarse with depth. As with the Colorado site, water levels are controlled by a cutoff wall and pumping systems, and the depth to groundwater is relatively constant at about 2.7 meters (McCoy 2012).

In Wyoming, three multi-level monitoring systems were installed. Subsurface temperatures are collected at two of these locations: one location that was formerly impacted by refined petroleum products but has since been remediated and is considered an expired zone and one background location that was never impacted by petroleum products. Subsurface temperatures are recorded using Omega thermocouple dataloggers (OM-CP-OCTTEMP-A, Omega Engineering, Stamford, CT).

The petroleum terminal in Northern New Jersey is adjacent to a large tidal river and is underlain by intermingled glacial and estuary deposits consisting of silt and sand deposits. Although near a tidal zone, water levels are largely stable, and the depth to groundwater is about 2.4 meters.

In Northern New Jersey, two multi-level monitoring systems were installed. Subsurface temperatures are collected at both locations, and both locations are in areas impacted with refined petroleum products. Subsurface temperatures are recorded using Lascar thermocouple dataloggers (EL-USB-TC, Lascar Electronics, Erie, PA).

Similar to the Northern New Jersey site, the chemical manufacturing facility in Southern New Jersey is also adjacent to a large tidal river and is underlain by intermingled glacial and estuary deposits consisting of silt and sand. Water levels are controlled by cutoff walls and pumping systems, and the depth to groundwater is relatively constant at about 1 meter (Bezold 2015).

In Southern New Jersey, one multi-level monitoring system was installed. Subsurface temperatures are collected at this location in an area impacted with nitroaromatic compounds. Subsurface temperatures are collected using Lascar thermocouple dataloggers.

#### **4.2.2. *Background Correction***

Subsurface temperatures used for the background correction were obtained by three different methods: 1) a temperature monitoring stick installed at a representative unimpacted background location, 2) modeling subsurface temperatures at the impacted location using a simple analytical model assuming no energy source due to biodegradation, and 3) modeling subsurface temperatures at the impacted location using the program Hydrus 1-D (PC-Progress, Prague, Czech Republic) assuming no energy source due to biodegradation. This section details these methods.

The first background correction method utilizes subsurface temperatures obtained from a temperature monitoring stick installed in an unimpacted background location. This method was possible for the field sites in Kansas and Wyoming. The background location was chosen based on prior site characterization that indicated no or minimal refined petroleum product impacts in these areas. The temperature monitoring sticks at these background locations collect subsurface temperatures at the same depths and times as those collected at the impacted locations.

The second background correction method calculates subsurface temperature as a function of depth and time, utilizing the equation for conduction of heat in a semi-infinite solid with a sinusoidal surface boundary condition (Carslaw and Jaeger 1959). The modified form of this equation written by Hillel (1980) is:

$$T(z, t) = T_{avg} + A_o \left[ \sin \left( \omega(t - t_o) - \frac{z}{d} - \frac{\pi}{2} \right) \right] / e^{\frac{z}{d}} \quad (38)$$

where  $T(z, t)$  is the temperature at a specified depth and time (K),  $T_{avg}$  is the average temperature of the ground surface (K),  $A_o$  is the amplitude of the ground surface temperature fluctuation (K),  $\omega$  is the radial frequency ( $\text{day}^{-1}$ ),  $t$  is the time of interest (day),  $t_o$  is the time lag from the start date to the occurrence of the minimum temperature (day),  $z$  is the depth (m), and  $d$  is the damping depth (the characteristic depth at which the temperature amplitude decreases to the fraction  $1/e$  of the amplitude at the soil surface) (m). The damping depth is calculated as:

$$d = \left( \frac{2\kappa}{C\omega} \right)^{\frac{1}{2}} \quad (39)$$

where  $\kappa$  is the thermal conductivity of the media (W/m K), and  $C$  is the volumetric heat capacity of the media ( $\text{J/m}^3 \text{K}$ ). Key assumptions for this model are:

- All heat is transferred via conduction
- The temperature at the soil surface follows a sinusoidal pattern
- At infinite depth, the soil temperature is constant
- The thermal conductivity and volumetric heat capacity of the soil are constant and uniform

The third background correction method utilizes the program Hydrus 1-D to model subsurface temperatures. Hydrus 1-D is used to simulate water flow, vapor flow, and heat transport in the subsurface in the vertical direction given user-specified initial conditions and boundary

conditions. For this application, water and vapor flow boundary conditions utilized were: an upper boundary condition of specified atmospheric conditions with surface runoff and a lower boundary condition of specified variable pressure head. Heat transport boundary conditions utilized were: an upper boundary condition of specified temperature and a lower boundary condition of specified heat flux.

**4.2.3. Model Inputs**

For each field site, the thermal NSZD rate model was run using the daily averaged subsurface temperatures measured at the impacted location(s) coupled with the daily averaged subsurface temperatures measured or calculated for each possible background correction method. Table 6 indicates the background correction methods applied to each field site. The Mathcad models for each background correction method as applied to the site in Kansas are included in Appendix A.

Table 6. Background correction methods used for each field site

Field Site	Background Location	Simple Model	Hydrus
Kansas	X	X	X
Colorado		X	X
Wyoming	X	X	X
Northern New Jersey		X	X
Southern New Jersey		X	X

Site specific characteristics needed for the thermal NSZD rate model and the values used for each site are listed in Table 7. These characteristics include the porosity ( $n$ ), which was assumed to be 0.25 for all sites; the water saturation in the unsaturated ( $S_{wfc}$ ) and saturated ( $S_w$ ) zones, which was assumed to be 0.1 and 1 for all sites, respectively; the hydraulic conductivity ( $K$ ), which was obtained from prior site investigations for the site in Kansas and was not used for all

other sites; the length (L) and width (w) of the impacted area, which was obtained from prior site characterizations for the site in Kansas and taken as 0.305 m for all other sites; the thermal conductivity in the unsaturated ( $\kappa_{\text{unsat}}$ ) and saturated ( $\kappa_{\text{sat}}$ ) zones; and the volumetric heat capacity in the unsaturated ( $C_{\text{unsat}}$ ) and saturated ( $C_{\text{sat}}$ ) zones. For the field site in Kansas, the thermal conductivity and volumetric heat capacity of the unsaturated and saturated zones were measured using a thermal properties analyzer (KD2 Pro, Decagon Devices, Pullman, WA) for soil core collected at the site. This data set is included in Appendix B. For the rest of the field sites, the thermal conductivity and volumetric heat capacity of the soil in the unsaturated and saturated zones was initially estimated using values tabulated by Carslaw and Jaeger (1959) and Hillel (1980). These values were then adjusted so that the temperatures modeled using the simple analytical model matched the temperatures measured at the shallowest depth.

Table 7. Site-specific characteristics used in the thermal NSZD rate model

Field Site	n	$S_{\text{wfc}}$	$S_{\text{w}}$	K (m/day)	L (m)	w (m)	$\kappa_{\text{unsat}}$ (W/mK)	$\kappa_{\text{sat}}$ (W/mK)	$C_{\text{unsat}}$ (kJ/m <sup>3</sup> K)	$C_{\text{sat}}$ (kJ/m <sup>3</sup> K)
Kansas	0.25	0.1	1	4.32	304.8	0.305	0.963	1.465	1573.6	2514.3
Colorado	0.25	0.1	1	-	0.305	0.305	0.419	1.549	1573.6	2514.3
Wyoming	0.25	0.1	1	-	0.305	0.305	0.419	1.005	1573.6	2514.3
Northern New Jersey	0.25	0.1	1	-	0.305	0.305	0.712	1.591	1573.6	2514.3
Southern New Jersey	0.25	0.1	1	-	0.305	0.305	0.837	2.931	1573.6	2514.3

In addition, daily water level data at four wells near the impacted location were available for the site in Kansas, and the groundwater flow direction and gradient were calculated as outlined in Appendix A. For the rest of the field sites, daily groundwater flow direction and gradient information was not available. Due to this lack of data, the energy flows due to convection of sensible heat and latent heat were not considered in the energy balances for these sites.

As stated in Chapter 3, this thesis uses decane as an analog to represent all constituents of the NAPL in the impacted locations. The change in free energy ( $\Delta G_r$ ) and enthalpy ( $\Delta H_r$ ) of biodegradation of aqueous phase decane under aerobic, denitrifying, manganese reducing, iron reducing, sulfate reducing, and methanogenic conditions, as well as methane oxidation, are listed in Table 8. These values were calculated, as described in Chapter 2, following Wiedemeier et al. (1996). For this thesis, it is assumed that all degraded NAPL is initially oxidized via methanogenesis, and all produced methane meets inward diffusing oxygen from the atmosphere and is oxidized into carbon dioxide. The values of the change in free energy and enthalpy of decane biodegradation used in the thermal NSZD rate model were therefore taken as the sum of the values for methanogenesis and methane oxidation listed in Table 8.

Table 8. Change in free energy ( $\Delta G_r$ ) and enthalpy ( $\Delta H_r$ ) for redox reactions of aqueous phase decane (calculated using values tabulated in Appendix B following Wiedemeier et al. 1996)

<b>Aqueous Phase Decane Redox Reaction</b>	<b><math>\Delta G_r</math> (kJ/mole)</b>	<b><math>\Delta H_r</math> (kJ/mole)</b>
$15.5O_2 + C_{10}H_{22} \rightarrow 10CO_2 + 11H_2O$ Aerobic Respiration	-6779.1	-6791.7
$12.4NO_3^- + 12.4H^+ + C_{10}H_{22} \rightarrow 10CO_2 + 17.2H_2O + 12.4N_2$ Denitrification	-6387.5	-6316.4
$62H^+ + 31MnO_2 + C_{10}H_{22} \rightarrow 10CO_2 + 31Mn^{2+} + 42H_2O$ Manganese Reduction	-6524.1	-6560.6
$124H^+ + 62Fe(OH)_3 + C_{10}H_{22} \rightarrow 10CO_2 + 62Fe^{2+} + 166H_2O$ Iron Reduction	-4459.5	-5161.6
$15.5H^+ + 7.75SO_4^{2-} + C_{10}H_{22} \rightarrow 10CO_2 + 7.75H_2S + 11H_2O$ Sulfate Reduction	-969.0	-231.5
$4.5H_2O + C_{10}H_{22} \rightarrow 2.25CO_2 + 7.75CH_4$ Methanogenesis	-120.1	-25.4
$7.75CH_4 + 15.5O_2 \rightarrow 7.75CO_2 + 15.5H_2O$ Methane Oxidation*	-6658.9	-6766.3

\* Values of  $\Delta G_r$  and  $\Delta H_r$  are based on 1 mole of decane oxidizing to 7.775 moles methane

Additional model inputs used by the simple analytical model to calculate background temperatures at each field site are listed in Table 9. Following Wu and Nofzinger (1999), the average temperature of the ground surface ( $T_{avg}$ ) was taken to be the annual average air temperature plus two degrees Celsius. The amplitude of the surface temperature fluctuation ( $A_o$ ) was taken to be the amplitude of the annual air temperature fluctuation. Both the average annual air temperature and the amplitude of the annual air temperature were obtained for nearby weather stations through NOAA's (National Oceanic and Atmospheric Administration) Online Weather Data (NOWData) system. The radial frequency ( $\omega$ ) was based on an annual cycle of ground surface temperatures. The time lag ( $t_o$ ) was calculated as the number of days between the model start date and the coldest day of the year. The simple analytical model was run for both the unsaturated and saturated zones using the appropriate respective thermal properties.

Table 9. Site specific values used in the simple analytical model to calculate background temperatures

Field Site	$T_{avg}$ (°C)	$A_o$ (°C)	$\omega$ (day <sup>-1</sup> )	$t_o$ (days)
Kansas	14.5	15.94	0.0172	263.5
Colorado	12.39	14.7	0.0172	92.5
Wyoming	9.72	15.5	0.0172	75
Northern New Jersey	15	14.89	0.0172	159.5
Southern New Jersey	14.67	14.58	0.0172	29

The model inputs used by Hydrus to calculate background temperatures varied for each field site. For all sites, the daily precipitation and potential evaporation rates were obtained from nearby weather station data. For the site in Kansas, the daily water table elevation was obtained from a transducer in a nearby monitoring well. For the rest of the sites, the daily water table was assumed constant and based on prior site investigations. The temperature at the top of the soil profile was input as the temperature measured at the shallowest depth of the temperature

monitoring stick. The temperature at the bottom of the soil profile was input as the annual average air temperature plus two degrees Celsius. The site in Kansas was modeled as a 15 meter deep profile with the upper half consisting of loamy sand and the lower half consisting of sand. The sites in Colorado, Wyoming, Northern New Jersey, and Southern New Jersey were modeled as 15 meter deep profiles consisting of loamy sand. Water flow parameters and heat transport parameters were chosen by Hydrus based on the specified soil types.

#### **4.2.4. *Parameter Sensitivity Analysis***

An analysis was performed on the model to determine the sensitivity of the thermal NSZD rate model to key input parameters. Because the field site in Kansas had the most robust data set, the sensitivity analysis was only conducted on the thermal NSZD rate models for the Kansas site. Eight primary model input parameters were identified that were not well constrained. These parameters describe both site and contaminant characteristics that influence how NSZD rates are calculated in the model. Three values of each parameter were defined: low, base, and high. The base values are defined as the best fit values based on the literature and knowledge of site characteristics. The low and high values were calculated as 20% less than and 20% greater than the base value, respectively. These parameters were then varied one at a time within each model run. These parameters, along with their values, are shown in Table 10.

The eight primary model input parameters considered in the sensitivity analysis were:

- Porosity –  $n$
- Hydraulic conductivity –  $K$  (m/day)
- Unsaturated zone water saturation –  $S_{wfc}$
- Unsaturated zone thermal conductivity –  $\kappa_{unsat}$  (W/m)

- Saturated zone thermal conductivity –  $\kappa_{\text{sat}}$  (W/m)
- Unsaturated zone volumetric heat capacity –  $C_{\text{unsat}}$  (kJ/m<sup>3</sup>)
- Saturated zone volumetric heat capacity –  $C_{\text{sat}}$  (kJ/m<sup>3</sup>)
- Change in enthalpy of the oxidation reaction –  $\Delta H_r$  (kJ/mol)

Table 10. Parameter values used in the sensitivity analysis

Parameter (units)	Level Value		
	Low	Base	High
n	0.2	0.25	0.3
K (m/day)	3.46	4.32	5.18
$S_{\text{wfc}}$	0.08	0.1	0.12
$\kappa_{\text{unsat}}$ (W/m)	0.77	0.963	1.156
$\kappa_{\text{sat}}$ (W/m)	1.172	1.465	1.758
$C_{\text{unsat}}$ (kJ/m <sup>3</sup> )	1258.9	1573.6	1888.3
$C_{\text{sat}}$ (kJ/m <sup>3</sup> )	2011.4	2514.3	3017.2
$\Delta H_r$ (kJ/mol)	-5433.4	-6791.7	-8150.0

The thermal NSZD rate model was run using the background stick correction method for the field site in Kansas with the base parameter values to provide a base case scenario. The sensitivity analysis was then conducted by varying one parameter at a time, while all other parameters were held at base values.

### 4.3. Results and Discussion

This section contains the results of the field-scale applications and sensitivity analysis of the thermal NSZD rate model. First, NSZD rates and cumulative NAPL losses at each of the five field sites are presented and discussed. Then, the results of the parameter sensitivity analysis are presented and discussed.

#### 4.3.1. *Kansas*

For the field site in Kansas, the daily average subsurface temperatures measured at location N2 (impacted location) and B1 (background location), as well as the subsurface temperatures calculated as background values using the simple analytical model and Hydrus, are plotted in Figure 8. The temperatures measured at locations N1 and N3 are very similar to those measured at location N2, and therefore are not shown. Subsurface temperatures at the impacted location and the calculated and measured background values are very similar at 0.15m bgs and 0.30m bgs. However, at 3.05m bgs, 3.66m bgs, 5.79m bgs, 8.23m bgs, 10.67m bgs, and 11.28m bgs, the temperatures at the impacted location are approximately two to four degrees Celsius warmer than the temperatures calculated and measured as background values, consistent with the elevated temperatures in NAPL impacted soils documented by Sweeney and Ririe (2014). This difference is attributed to heat released during NAPL biodegradation at the impacted location. Additionally, temperatures measured at the background stick are warmer than the temperatures calculated as background values using the simple analytical model and Hydrus. This could result from the background stick being in close enough proximity to the impacted area that it is warmed by the heat released during NAPL biodegradation, causing subsurface temperatures slightly elevated from true background temperatures. Figure 8 also indicates that temperatures measured at the impacted location at 3.05m bgs and 3.66m bgs show sudden spikes and dips throughout the year. The cause of these temperature anomalies is attributed to precipitation events where infiltrating rainwater preferentially flows along the temperature monitoring sticks. These anomalous values were removed from the data set prior to use in the thermal NSZD rate model.

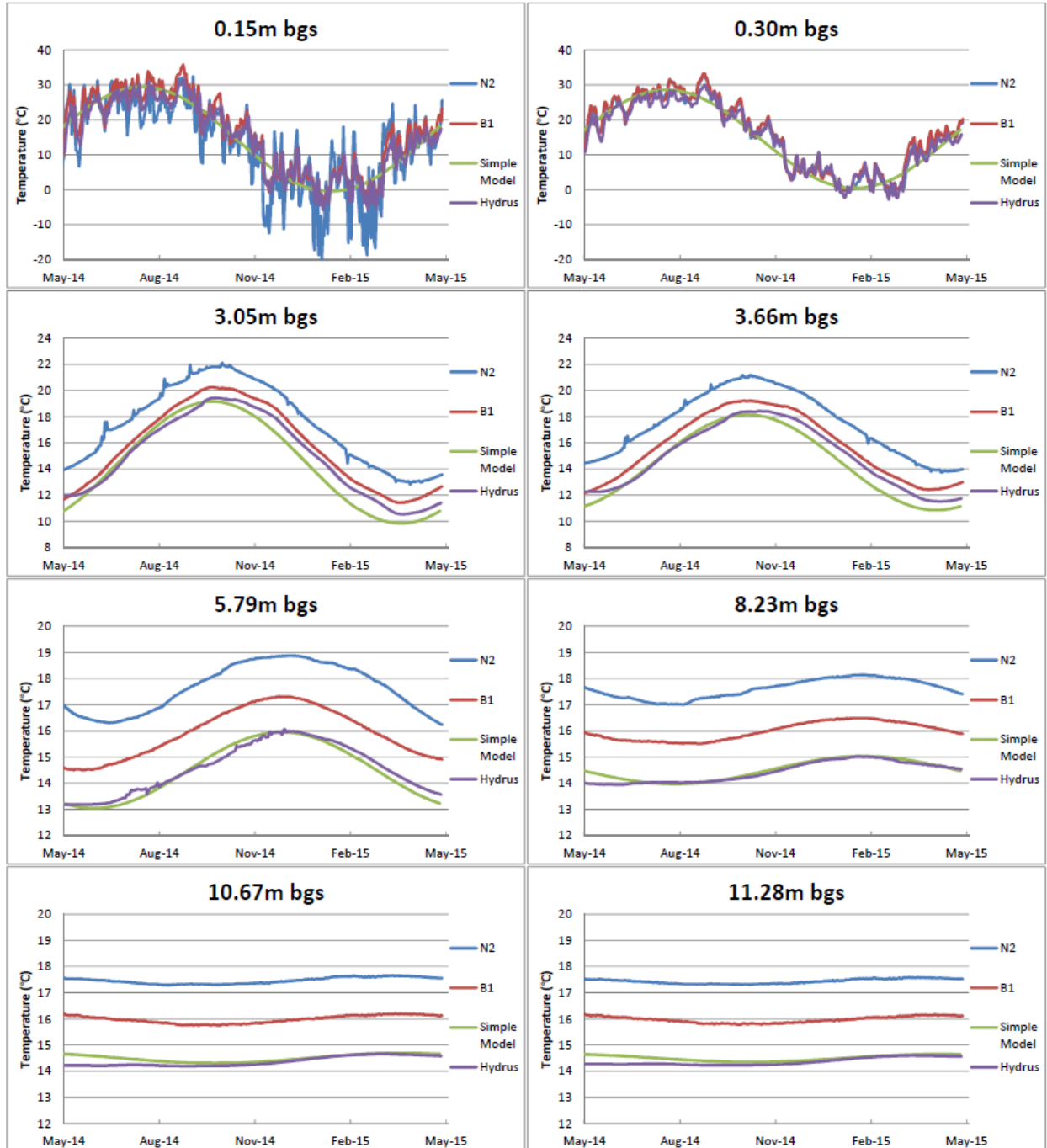


Figure 8. Subsurface temperatures measured at N2 and B1 and calculated as background using the simple analytical model and Hydrus for the field site in Kansas

The average NSZD rates and cumulative NAPL losses over one year for the field site in Kansas using all three of the background correction methods are shown in Table 11. These data indicate that the three background correction methods produce similar results. Average NSZD rates range

from 474 to 709 gal/acre/year, and cumulative NAPL losses range from 471 to 697 gal/acre. Prior characterization of NSZD rates at this site using CO<sub>2</sub> Traps at the same locations as the temperature monitoring sticks indicate average loss rates of approximately 4,700 gal/acre/year (unpublished field data). NSZD rates calculated using the thermal NSZD rate model are an order of magnitude less than loss rates determined using CO<sub>2</sub> Traps. This discrepancy is likely due to overestimation of the true change in enthalpy of the oxidation reactions occurring at the site and underestimation of the energy flow due to conduction. For this work, it is assumed that all NAPL is initially oxidized via methanogenesis, and all produced methane is oxidized into carbon dioxide; however, it is likely that other oxidation reactions occur, and a portion of the NAPL is not fully degraded to carbon dioxide and stays in the system as solid phase precipitates or leaves the system with flowing groundwater as volatile fatty acids or dissolved methane. This work also assumes that the microbial population is at steady-state, so all enthalpy released during oxidation is released as heat to the surrounding environment; however, some of the energy released during oxidation is used by the microorganisms to create biomass that is not degraded or leaves the system and therefore is not released as heat to the surrounding environment. Consideration of these factors would lead to smaller estimates of the change in enthalpy of the oxidation reaction. In addition, the methane oxidation front moves vertically throughout the year due to water level changes (Figure 11), and for portions of the year, the methane oxidation front is above the lower thermocouple used to measure the temperature gradient above the NAPL body. This seasonal phenomenon causes the measured temperature gradient to undercompensate for the heat released at the methane oxidation front. Better understanding of the reactants and products of biodegradation, the mass flows occurring in the system, and increasing the number of

thermocouples in the subsurface would likely lead to calculations of larger NSZD rates by the thermal NSZD rate model.

Table 11. Average NSZD rate and cumulative NAPL losses for field site in Kansas

<b>Background Correction</b>	<b>Average Loss Rate (gal/acre/year)</b>	<b>Cumulative NAPL Losses 1 year (gal/acre)</b>
Hydrus	474	471
Simple Model	709	697
Background Location	478	495

Cumulative NAPL losses calculated using daily NSZD rates are shown in Figure 9. This figure indicates that NSZD rates are slower in late spring/early summer and relatively constant the rest of the year. Lower NSZD rates in late spring/early summer could be due to the rising water table trapping methane and preventing it from being oxidized. When the water table falls, the methane is released and is oxidized to carbon dioxide, producing large energy flows. Figure 9 also indicates that daily NSZD rates are somewhat variable and occasionally negative. Calculation of negative NSZD rates by the model is likely due to imperfections of the background correction methods. Because of differences in ground cover, soil properties, and subsurface heterogeneities, heat transfer at the impacted location is somewhat different than heat transfer at the modeled and measured background locations. These differences create an imperfect background correction so that negative NSZD rates are occasionally calculated by the model, indicating incorrect estimates of background temperatures. The negative NSZD rates calculated using the Hydrus background correction method in July 2014 are attributed to poor estimates of background temperatures by Hydrus at this time, possibly due to improper initial conditions in the Hydrus model. The variability in the daily calculated NSZD rates is also likely due to imperfections of the background correction methods as well as variability of measured data. Further, variability in

data measurements can cause variability in the calculated energy flows. For example, because the volume used in the energy balance is large, small temperature changes within the energy balance volume cause a large change in the storage term, leading to large variations in NSZD rates. In addition, site activities may impact subsurface temperatures at the impacted location in ways that are not captured by the measured or calculated background temperatures.

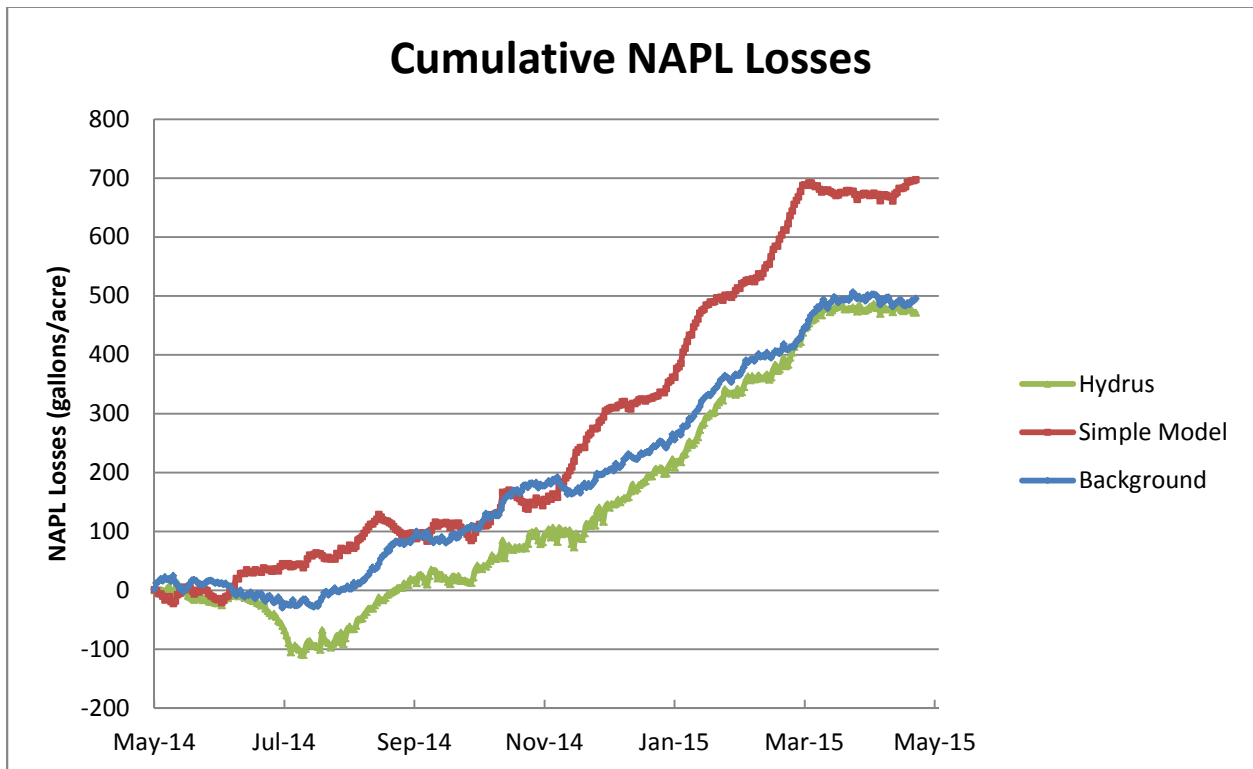


Figure 9. Cumulative NAPL losses at the field site in Kansas

Figure 10 shows the daily NAPL loss rate in gallons/acre versus the subsurface temperature at 5.79m bgs. This depth represents the approximate center of the vertical extent of the NAPL zone. These results indicate no correlation between subsurface temperature and increased NAPL loss rate at this site. This finding is consistent with Figure 9, which indicates that NSZD rates are relatively constant throughout the year. NSZD rates at this site do not appear to be influenced by seasonal changes in subsurface temperatures.

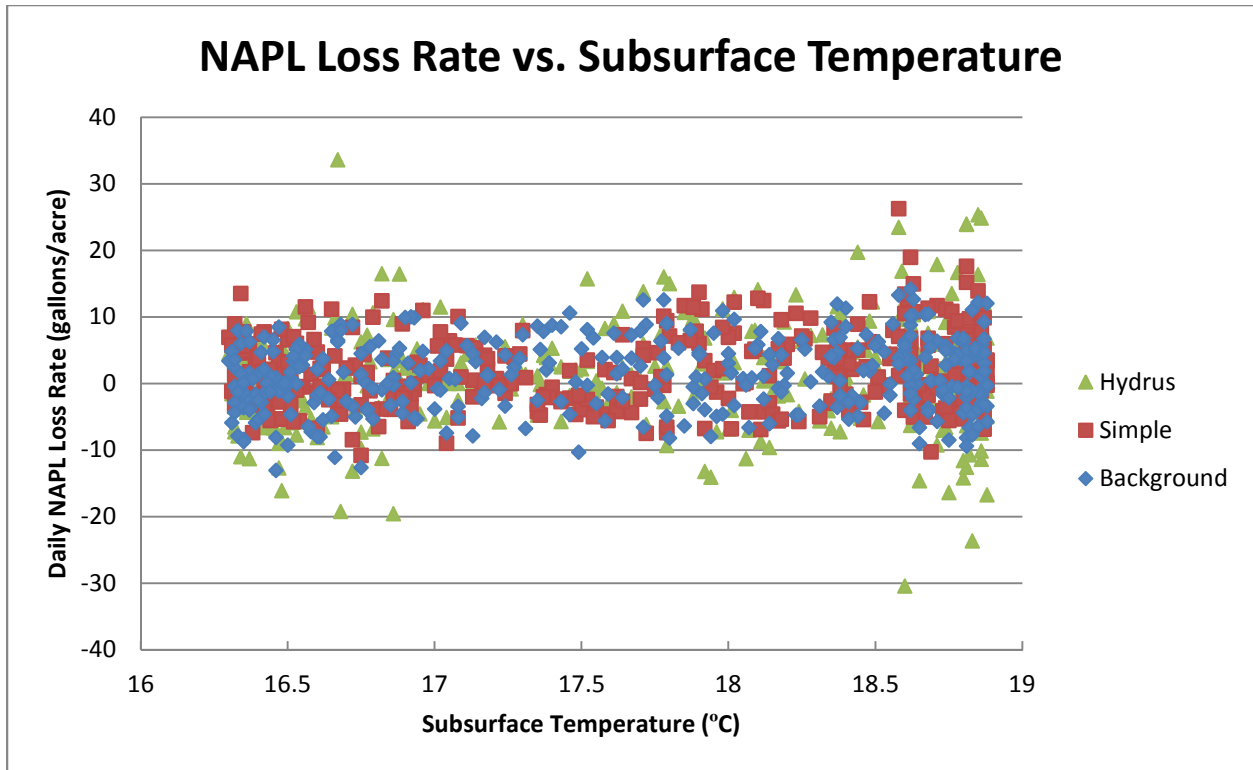


Figure 10. NAPL loss rate versus subsurface temperature at 5.79m bgs at the field site in Kansas

Figure 11 shows the soil gas profiles in the vadose zone in November 2014 and March 2015. In November, concentrations of more than 40% methane are seen at 2.4 m bgs and below, indicating methanogenic conditions, with methane concentrations sharply decreasing as the depth decreases. This decrease in methane concentration corresponds to an increase in oxygen concentration. Following Amos et al. (2005), this correlation is attributed to upward diffusing methane from the vadose zone meeting inward diffusing oxygen from the atmosphere causing a methane oxidation front where methane is oxidized into carbon dioxide. This same trend is seen for the soil gas profiles in March, although the methane oxidation front appears to be deeper, around 3.6m bgs. This lowering of the methane oxidation front is attributed to lowering of the water table. In November, the water table was 6.3m bgs, while in March, the water table was 8.0 m bgs. In both cases, the methane oxidation front is slightly above the halfway point between the

water table and ground surface. In addition, much lower concentrations of methane and carbon dioxide were observed in March as compared to November. The reason for these lower concentrations is not known at this time; possibly, the rising water table in spring may be limiting the release of carbon dioxide and methane from the NAPL body.

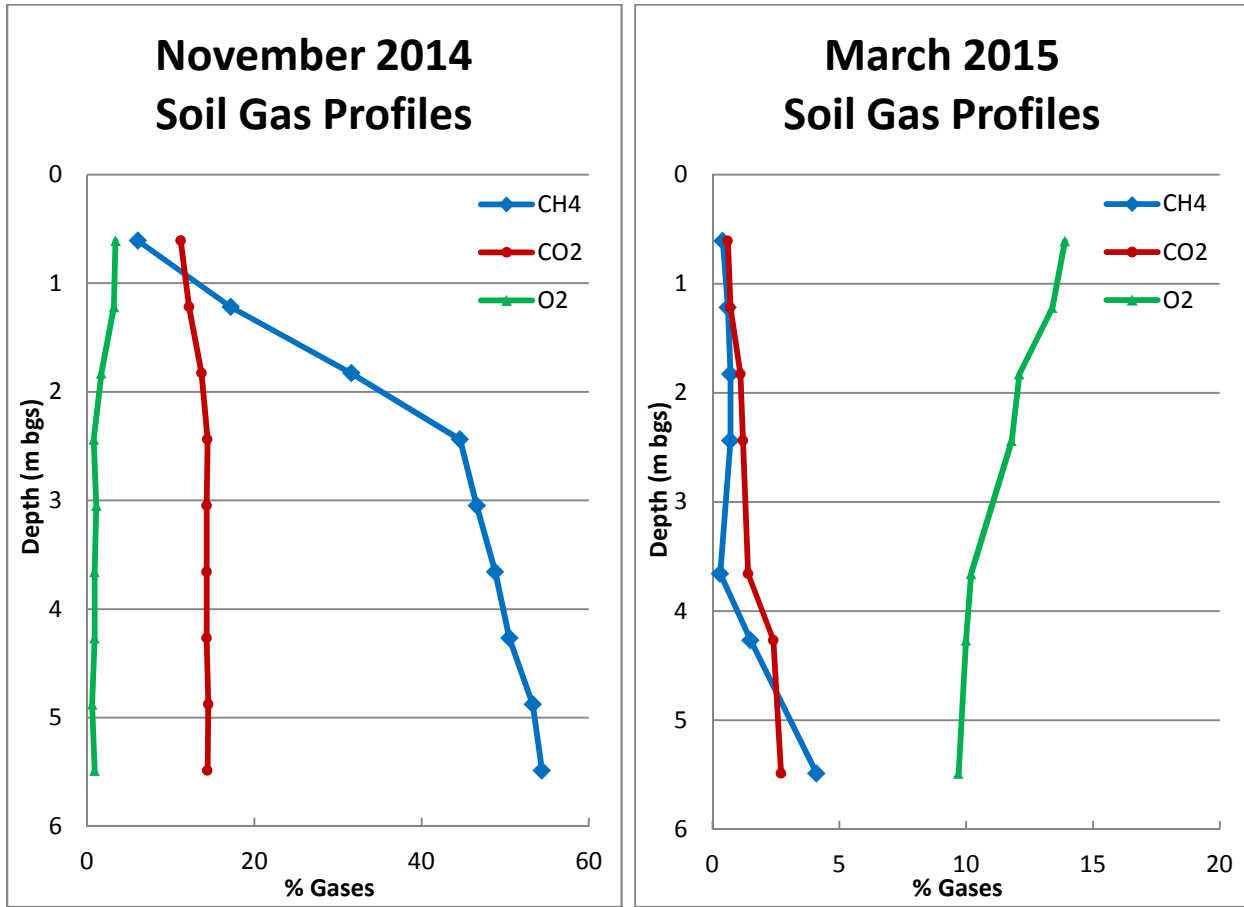


Figure 11. Soil gas profiles for the site in Kansas. Note x-axis scales are set to the range of data

Only the field site in Kansas had daily groundwater level data available, allowing all energy flow terms outlined in Chapter 3 to be considered in the energy balance. Following each thermal NSZD rate model run, each energy flow term in the energy balance was compared to the total rate of energy released by NAPL biodegradation to determine the significance of each term. The results of this comparison are listed in Table 12. These results suggest that for all three

background correction methods, the energy flows due to convection of sensible heat by water in the x direction, conduction out of the bottom of the NAPL body in the z direction, convection of sensible heat by vapor in the z direction, and convection of latent heat by vapor in the z direction are less than 0.02 times the total rate of energy released and are therefore relatively insignificant in determining the NSZD rate. The energy flows due to conduction out of the top of the NAPL body in the z direction, convection of sensible heat by water in the z direction, and the change in energy represent significant proportions of the total rate of energy released. The relative significance of each term depends on the background correction method utilized, as shown in Table 12. These results suggest that the energy flows due to convection of sensible heat by water in the x direction, conduction out of the bottom of the NAPL body, convection of sensible heat by vapor, and convection of latent heat by vapor could be neglected for the energy balance and thermal NSZD rate model. However, neglecting the energy flow due to convection of sensible heat by water in the z direction, as was done for the remainder of the field sites due to lack of groundwater level data, may cause the thermal NSZD rate model to underestimate the total rate of energy released by NAPL biodegradation, leading to underestimation of NSZD rates.

Table 12. Proportion of each energy flow term to total rate of energy released by NAPL biodegradation

Energy Flow Term	Proportion of $E_{RXN}$		
	Background	Simple Model	Hydrus
$E_{xconvw}$	0.01	0.01	0.02
$E_{inzcond}$	1.14	0.66	0.73
$E_{zconvw}$	0.35	0.49	0.77
$E_{outzcond}$	-0.03	0.01	-0.02
$E_{zconvv}$	0.00	0.00	0.00
$E_{zconvvlatent}$	0.00	0.00	0.00
$dE/dt$	-0.47	-0.18	-0.50

#### **4.3.2. Colorado**

For the field site in Colorado, the daily average subsurface temperatures measured at location IW10MLS (impacted location), as well as the subsurface temperatures calculated as background values using the simple analytical model and Hydrus are plotted in Figure 12. From mid-July to mid-September 2014, data were not collected due to technical difficulties with the datalogger. The magnitude of subsurface temperatures measured at the impacted location and calculated as background values are similar at 0.00m bgs and 0.15m bgs, but the timing of temperatures calculated using the simple model is incorrect. However, this inconsistency is not relevant, as subsurface temperatures at these depths are not used in the thermal NSZD rate model. At 1.52m bgs and 1.83m bgs, temperatures at the impacted location are slightly warmer than temperatures calculated using Hydrus and significantly warmer than temperatures calculated using the simple analytical model. This trend continues with depth, and at 8.53m bgs and 9.14m bgs, the temperatures at the impacted location are approximately three degrees Celsius warmer than the temperatures calculated as background values. Figure 12 also highlights the disparity between subsurface temperatures calculated using the simple analytical model and Hydrus, especially at shallower depths. These results suggest that temperatures calculated using the simple analytical model are a poor fit for this site, and temperatures calculated using Hydrus provide better representations of background temperatures.

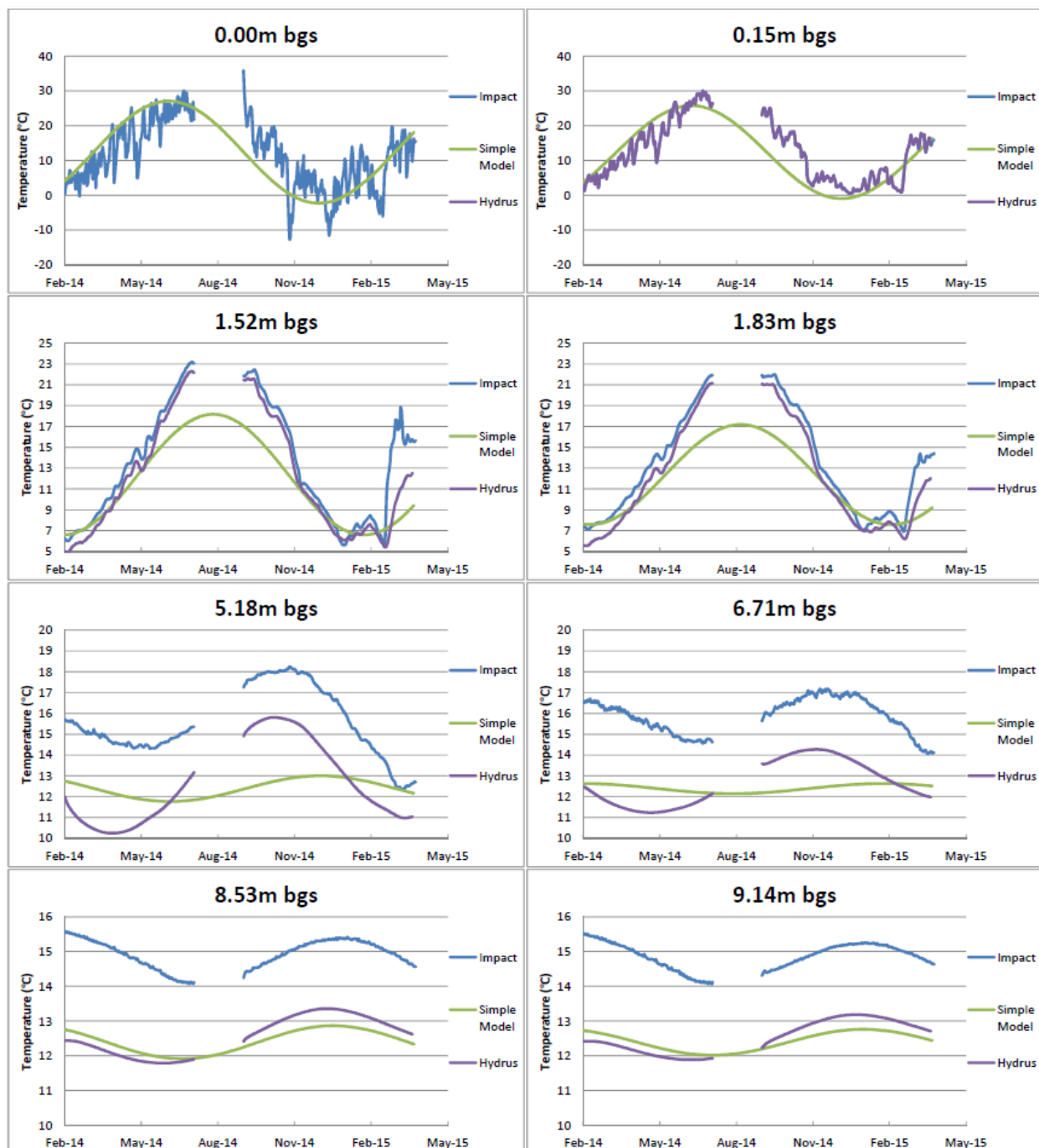


Figure 12. Subsurface temperatures measured at impacted location and calculated as background using the simple analytical model and Hydrus for field site in Colorado

Average NSZD rates and cumulative NAPL losses over one year for the field site in Colorado using both of the calculated background correction methods are shown in Table 13. This data set indicates negative results from the two background correction methods, with average NSZD

rates of -216 gal/acre/year using the simple analytical model and -427 gal/acre/year using Hydrus. Cumulative NAPL losses are -214 gal/acre using the simple analytical model, and -419 gal/acre using Hydrus. The negative values for average NSZD rate and cumulative NAPL losses are unreasonable and are likely due to inaccurate estimates of background temperatures using both background correction methods. Prior characterization of NSZD rates at this site using CO<sub>2</sub> Traps at the same locations as the temperature monitoring sticks indicate average loss rates of approximately 3,000 gal/acre/year (McCoy 2012). NSZD rates calculated using the thermal NSZD rate model do not agree with loss rates determined using the CO<sub>2</sub> Trap method. This discrepancy may be due to the incomplete energy balance at this site causing an underestimation of the energy released due to biodegradation. In addition, the discrepancy may be due to an overestimation of the true change in enthalpy of the oxidation reactions occurring at the site and/or underestimation of the energy flow due to convection, as discussed previously. Better understanding of these factors could lead to calculations of larger NSZD rates by the thermal NSZD rate model.

Table 13. Average NSZD rate and cumulative NAPL losses for the field site in Colorado

<b>Background Correction</b>	<b>Average Loss Rate (gal/acre/year)</b>	<b>Cumulative NAPL Losses 1 year (gal/acre)</b>
Hydrus	-427	-419
Simple Model	-216	-214

Cumulative NAPL losses calculated using daily NSZD rates are shown in Figure 13. Because daily NSZD rates could not be calculated from mid-July to mid-September 2014, the daily NSZD rate is assumed as zero for this time period. Figure 13 indicates that NSZD rates are not constant throughout the year. NSZD rates calculated using Hydrus suggest that the NSZD rate is essentially zero in the spring, negative in the summer, and positive in the fall and winter. NSZD

rates calculated using the simple analytical model suggest that the NSZD rate is positive in the spring and summer and negative in the fall and winter. Calculation of negative NSZD rates by the model is likely due to the incomplete energy balance at this site, as well as imperfections of the background correction methods leading to incorrect estimates of background temperatures. The variability in the daily calculated NSZD rates is also likely due to imperfections of the background correction methods as well as variability of measured data, as discussed previously.

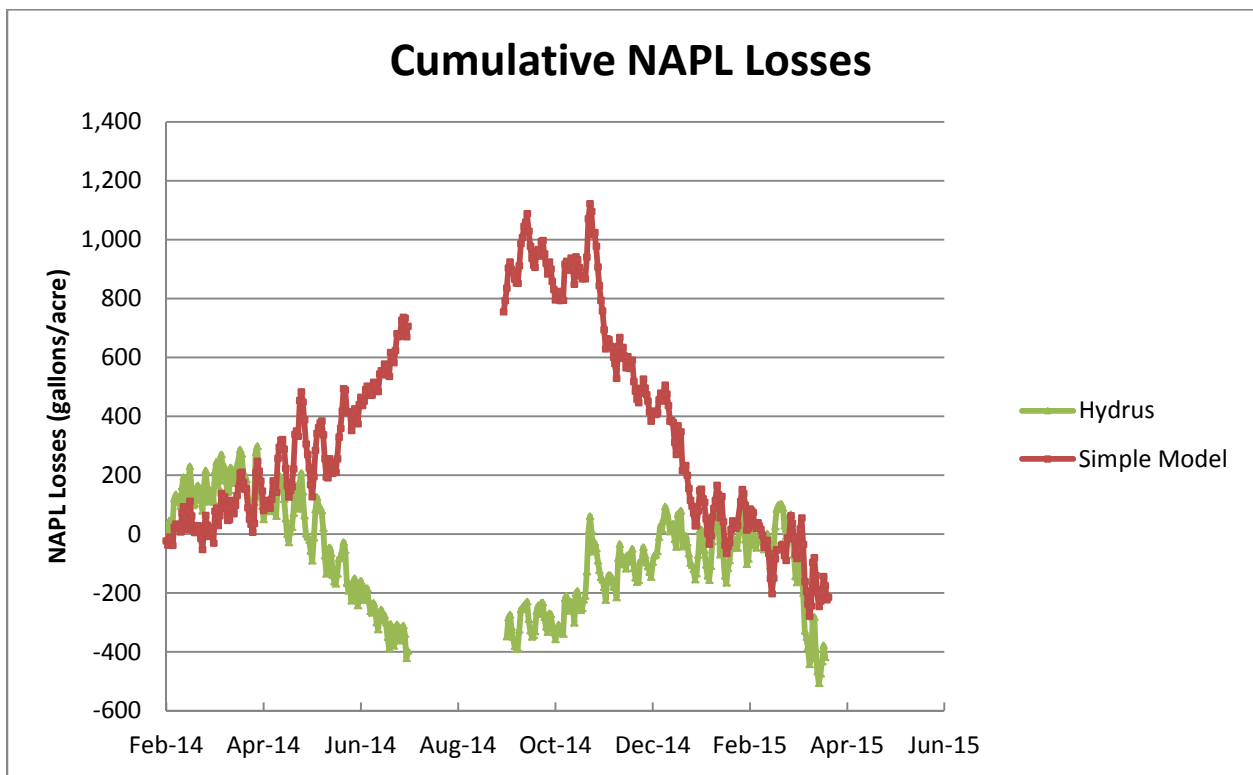


Figure 13. Cumulative NAPL losses at the field site in Colorado

Figure 14 shows the daily NAPL loss rate in gallons/acre versus the subsurface temperature at 6.71m bgs. This depth represents the approximate center of the vertical extent of the NAPL zone. These results indicate no correlation between subsurface temperature and increased NAPL loss rate at this site, a finding not consistent with Figure 13, which indicates variable NSZD rates

throughout the year. It is unclear whether NSZD rates at this site are influenced by seasonal changes in subsurface temperatures.

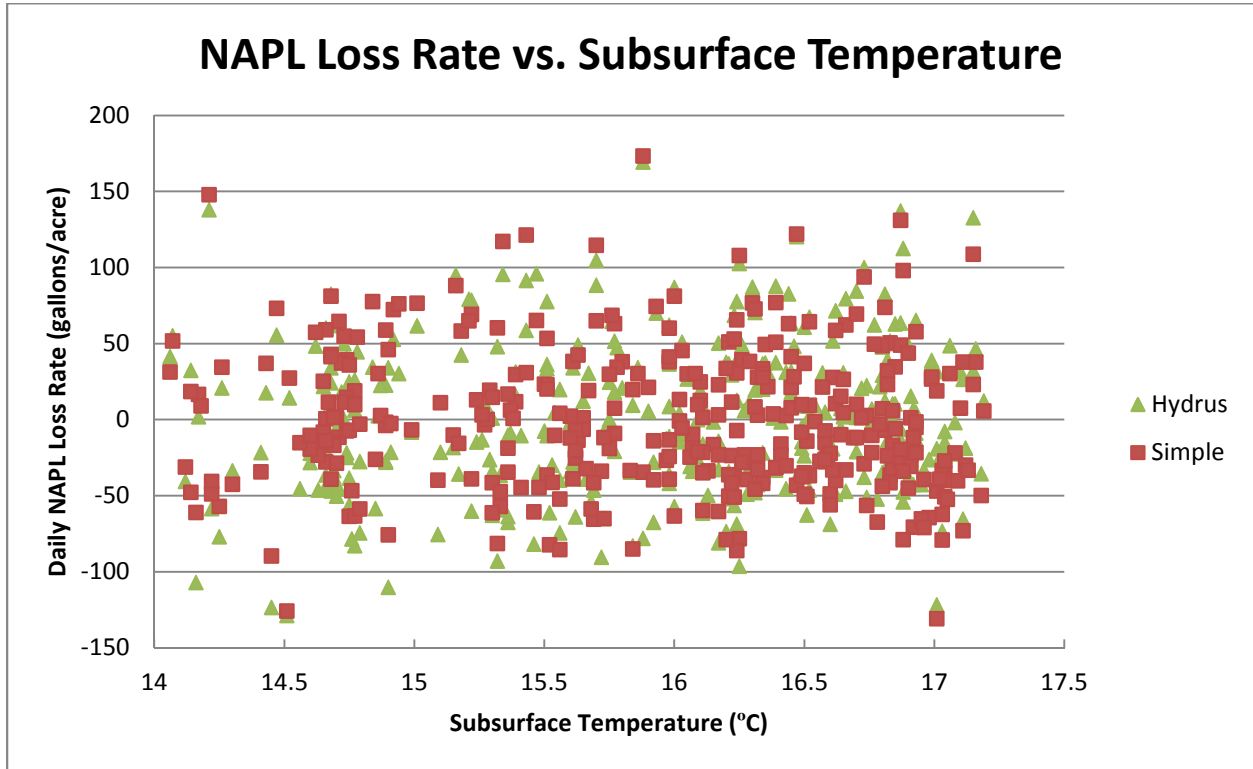


Figure 14. NAPL loss rate versus subsurface temperature at 6.71m bgs at the field site in Colorado

#### 4.3.3. Wyoming

For the field site in Wyoming, the daily average subsurface temperatures measured at the expired zone location and background location, as well as the subsurface temperatures calculated as background values using the simple analytical model and Hydrus, are plotted in Figure 15. Subsurface temperatures measured at the expired zone location and the calculated and measured background values are similar at 0.91m bgs, 1.22m bgs, 1.52m bgs, and 2.44m bgs from October 2013 through June 2014; however, from June to August 2014, temperatures at the expired zone location are warmer than temperatures calculated and measured as background values. At 3.05m

bgs, 3.96m bgs, 4.27m bgs, and 4.57m bgs, temperatures at the expired zone location are warmer than temperatures calculated and measured as background values throughout the year. Figure 15 also indicates that background temperatures calculated using Hydrus better mimic the magnitude of temperatures measured at the background stick than temperatures calculated using the simple analytical model, suggesting that temperatures calculated using Hydrus provide better representations of background temperatures for this site.

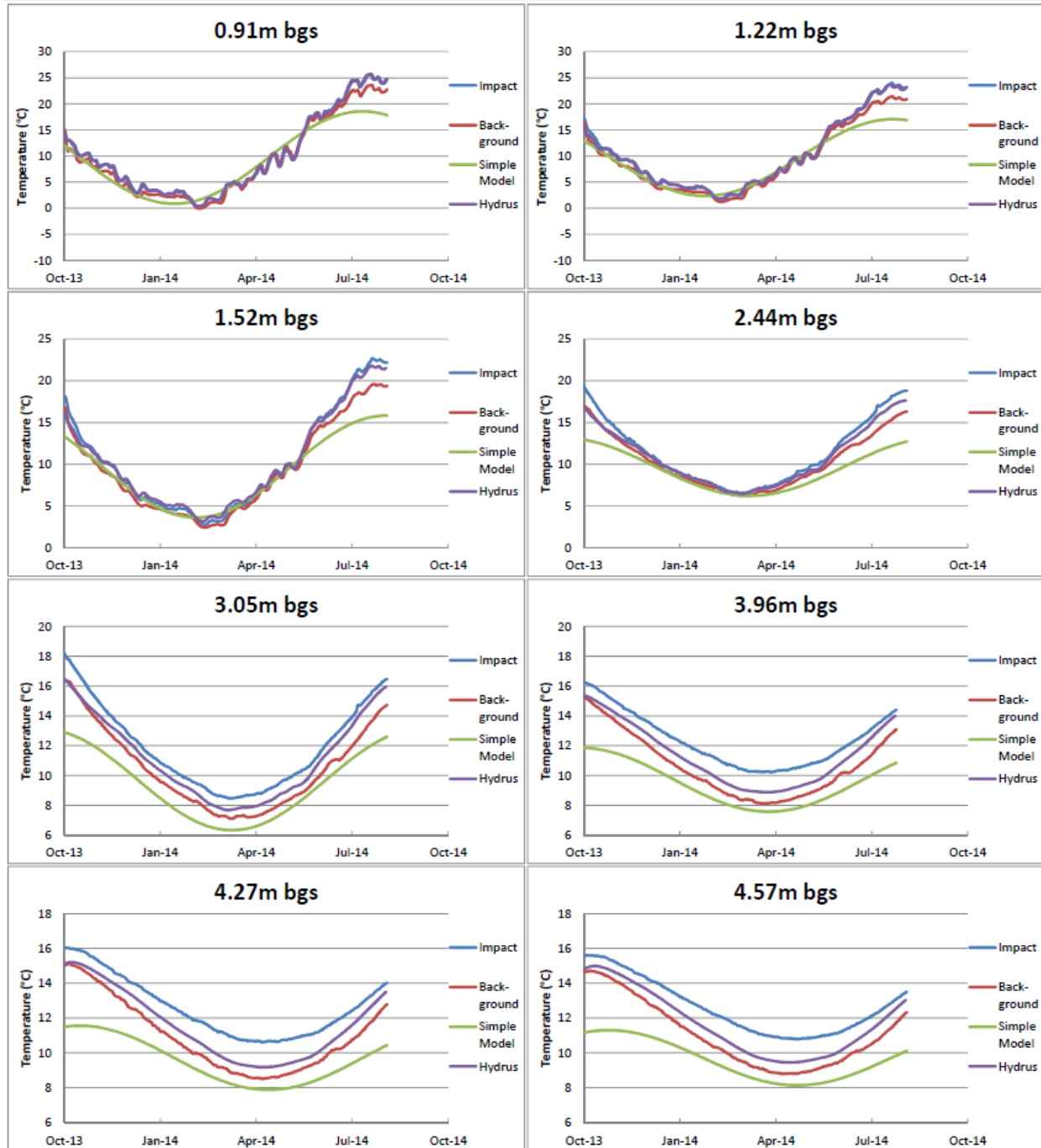


Figure 15. Subsurface temperatures measured and calculated as background using the simple analytical model and Hydrus for the field site in Wyoming

Average NSZD rates and cumulative NAPL losses over 10 months for the field site in Wyoming using all three of the background correction methods are shown in Table 14. This data set indicates a range of average NSZD rates from -165 gal/acre/year to 380 gal/acre/year.

Cumulative NAPL losses range from -144 gal/acre to 325 gal/acre. Prior characterization of NSZD rates at this site using CO<sub>2</sub> Traps at the same locations as the temperature monitoring sticks indicate that NAPL loss rates in the expired zone are not significantly different from loss rates in the background location, and therefore NSZD rates in the expired zone are not significant (McCoy 2012). NSZD rates calculated using the thermal NSZD rate model are low, consistent with the rates determined using the CO<sub>2</sub> Trap method.

Table 14. Average NSZD rate and cumulative NAPL losses for the field site in Wyoming

<b>Background Correction</b>	<b>Average Loss Rate (gal/acre/year)</b>	<b>Cumulative NAPL Losses 10 months (gal/acre)</b>
Hydrus	-165	-141
Simple Model	-23	-20
Background Location	380	325

Cumulative NAPL losses calculated using daily NSZD rates are shown in Figure 16. There is some agreement between the NSZD rates calculated using the background location and Hydrus background correction methods, with both methods indicating that NSZD rates are highest in the summer and then relatively constant the rest of the year. NSZD rates calculated using the simple analytical model are highly negative in the fall and winter, then positive in the spring and summer. Calculation of negative NSZD rates by the model using Hydrus and the simple analytical model background correction methods is likely due to the incomplete energy balance at this site, as well as imperfections of the background correction methods leading to incorrect estimates of background temperatures. In addition, the variability in NSZD rates calculated using the simple analytical model, their disagreement with NSZD rates calculated using Hydrus and the background location, and their large negative values indicate that the simple analytical model does not provide accurate estimates of background temperatures or NSZD rates at this site.

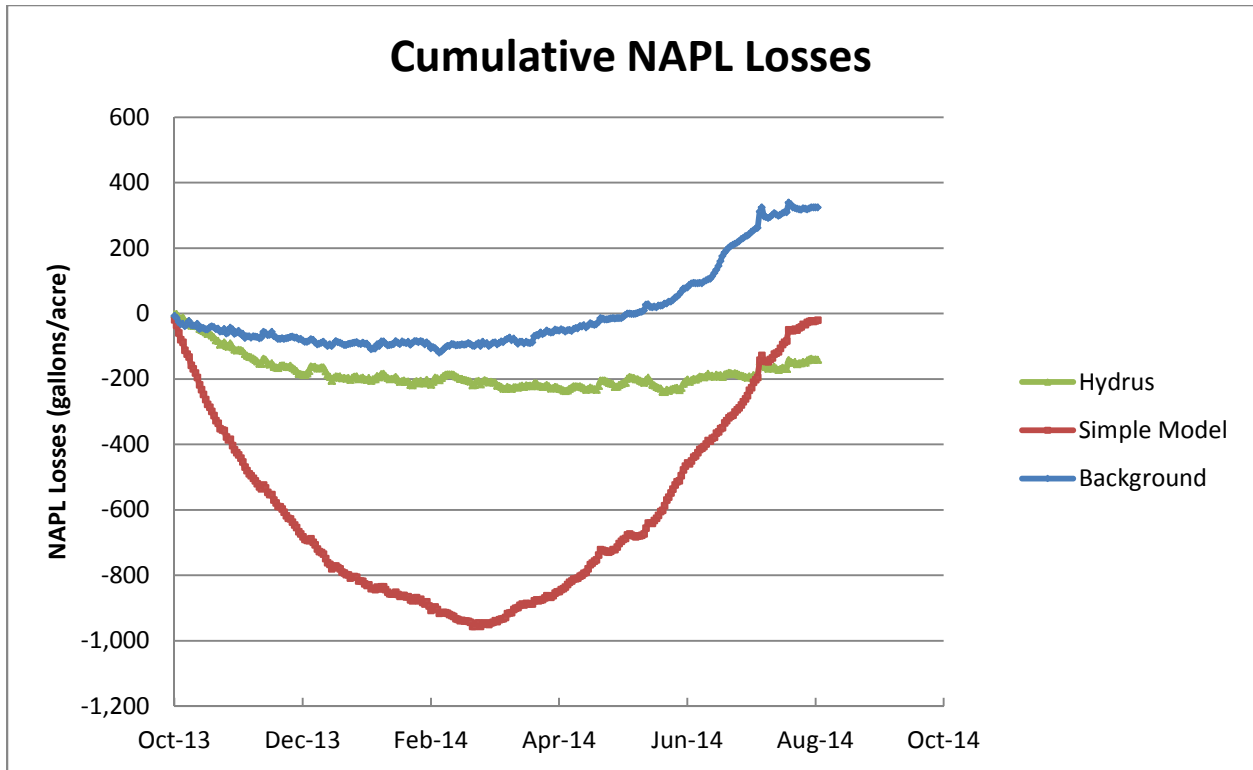


Figure 16. Cumulative NAPL losses at the field site in Wyoming

Figure 17 shows the daily NAPL loss rate in gallons/acre versus the subsurface temperature at 2.44m bgs. This depth represents the approximate center of the vertical extent of the NAPL zone. Figure 17 shows no correlation between subsurface temperatures and increased NAPL loss rates at this site. This finding is not consistent with Figure 16, which indicates largest NSZD rates in the summer. It is unclear whether NSZD rates at this site are influenced by seasonal changes in subsurface temperatures.

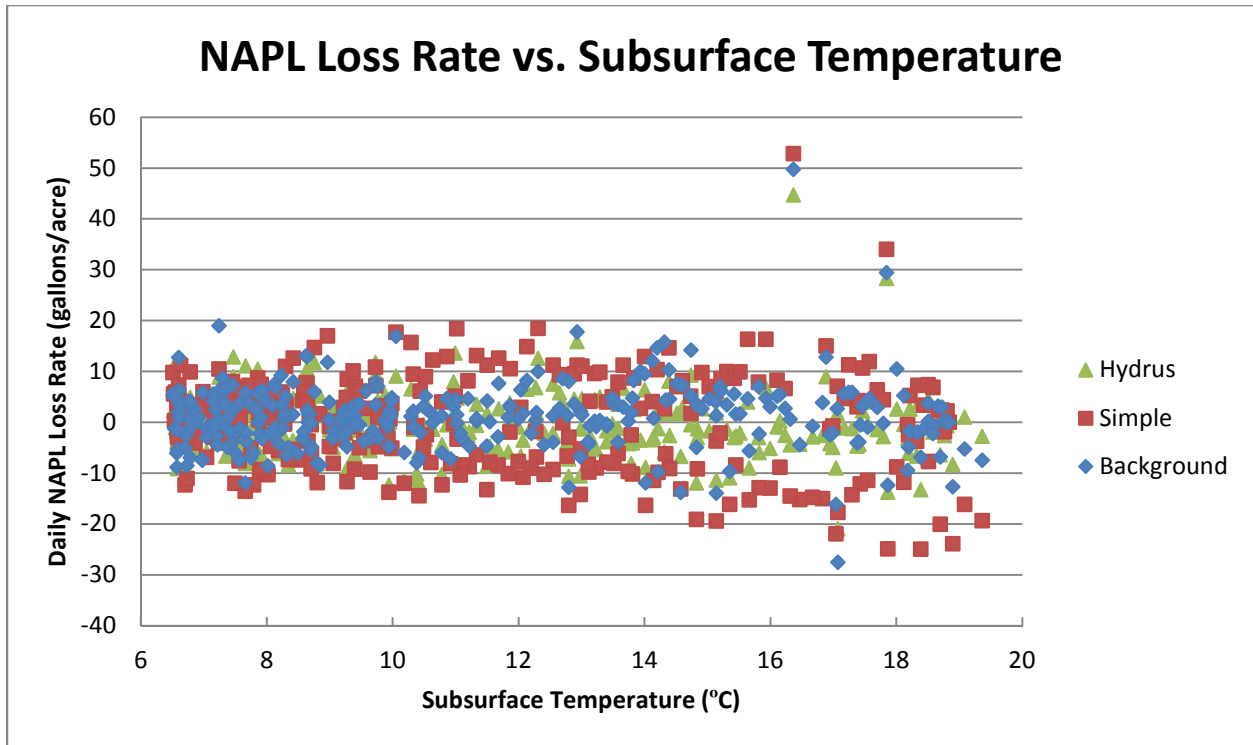


Figure 17. NAPL loss rate versus subsurface temperature at 2.44m bgs at the field site in Wyoming

#### 4.3.4. Northern New Jersey

For the field site in Northern New Jersey, the daily average subsurface temperatures measured at SB1 (impacted location) as well as subsurface temperatures calculated as background values using the simple analytical model and Hydrus are plotted in Figure 18. Since the subsurface temperatures measured at location SB2 are very similar to those measured at location SB1, SB2 data are not shown. Data were not collected from the end of February 2014 to the end of March 2014 while the datalogger was off site. At shallow depths, the amplitude of temperatures calculated using Hydrus is greater than temperatures measured at the impacted location. At depth, the timing of temperatures calculated using the simple analytical model is incorrect. Only at 5.49m bgs and 6.10m bgs are temperatures calculated as background values using both background correction methods slightly cooler than temperatures measured at the impacted

location. These results suggest that temperatures calculated as background values using both Hydrus and the simple analytical model provide poor representations of background temperatures for this site.

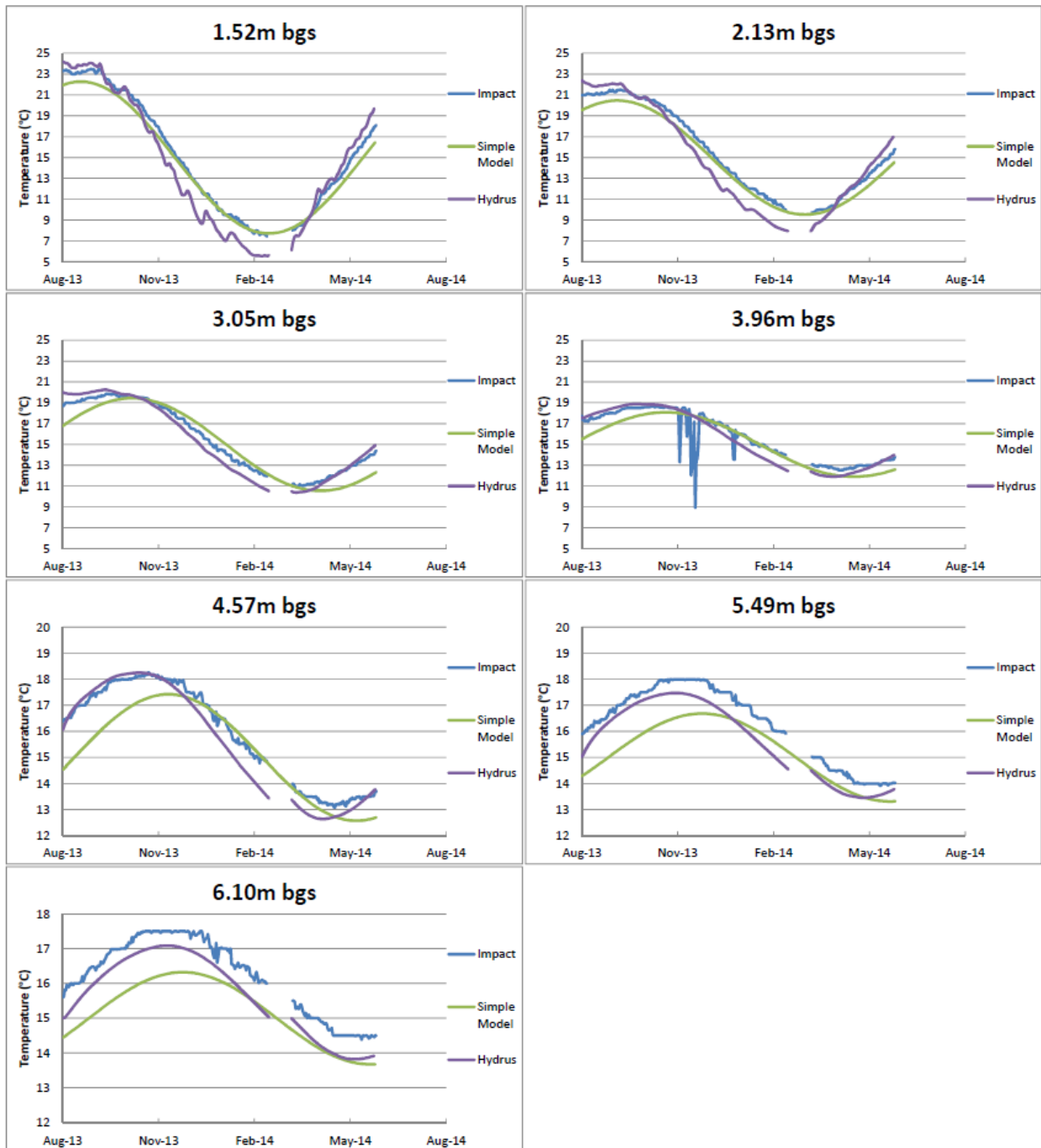


Figure 18. Subsurface temperatures measured at impacted location and calculated as background using the simple analytical model and Hydrus for the field site in Northern New Jersey

Average NSZD rates and cumulative NAPL losses over nine months for the field site in Northern New Jersey using both of the calculated background correction methods are shown in Table 15. These data indicate similar results for the two background correction methods, with average NSZD rates of 633 gal/acre/year using the simple analytical model and 780 gal/acre/year using Hydrus. Cumulative NAPL losses are 481 gal/acre using the simple analytical model and 592 gal/acre using Hydrus. Prior characterization of NSZD rates at this site using CO<sub>2</sub> Traps at the same locations as the temperature monitoring sticks indicate average loss rates of approximately 3,800 gal/acre/year (unreported field data). NSZD rates calculated using the thermal NSZD rate model are considerably less than NSZD rates determined using the CO<sub>2</sub> Trap method. This discrepancy may be due to the incomplete energy balance at this site leading to an underestimation of the energy released due to biodegradation, an overestimation of the true change in enthalpy of the oxidation reactions occurring at the site, and/or underestimation of the energy flow due to convection. Better understanding of these factors could lead to calculations of larger NSZD rates by the thermal NSZD rate model.

Table 15. Average NSZD rate and cumulative NAPL losses for the field site in Northern New Jersey

<b>Background Correction</b>	<b>Average Loss Rate (gal/acre/year)</b>	<b>Cumulative NAPL Losses 9 months (gal/acre)</b>
Hydrus	780	592
Simple Model	633	481

Cumulative NAPL losses calculated using daily NSZD rates are shown in Figure 19. Because daily NSZD rates could not be calculated from late February to late March, the daily NSZD rate is assumed as zero for this time period. Figure 19 indicates that NSZD rates are not constant throughout the year, and NSZD rates calculated using both background correction methods

follow similar trends. NSZD rates calculated using the simple analytical model suggest minimal rates in the fall and spring and positive rates in the winter, while NSZD rates calculated using Hydrus suggest positive rates in the fall and winter and negative rates in the spring. Calculation of negative NSZD rates by the model is likely due to the incomplete energy balance at this site, as well as imperfections of the background correction methods leading to incorrect estimates of background temperatures. In addition, the water table and LNAPL at this site are shallow, and shallow subsurface temperatures are strongly influenced by short-term heating and cooling at the ground surface, making it difficult to isolate the heat released due to NAPL biodegradation for use in the thermal NSZD rate model.

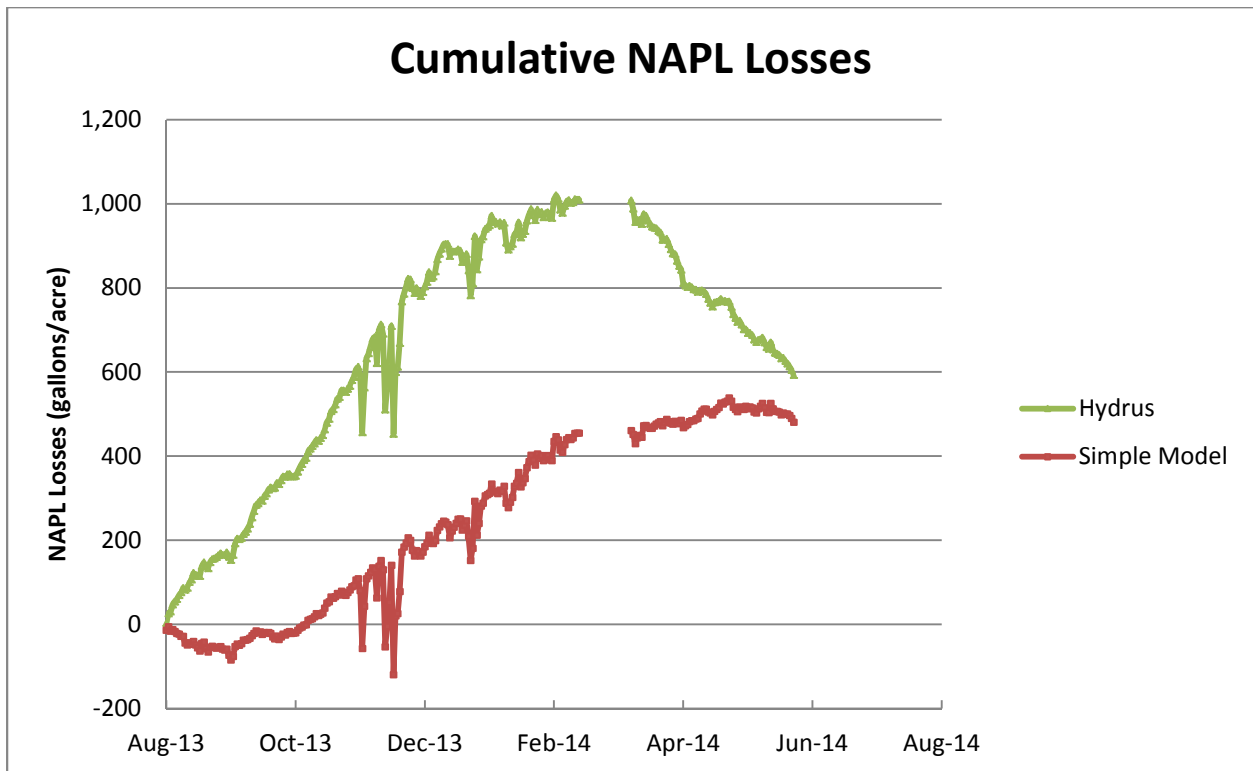


Figure 19. Cumulative NAPL losses at the field site in Northern New Jersey

Figure 20 shows the daily NAPL loss rate in gallons/acre versus the subsurface temperature at 2.13m bgs. This depth represents the approximate center of the vertical extent of the NAPL zone.

Figure 20 indicates no correlation between subsurface temperature and increased NAPL loss rate at this site. This finding is not consistent with Figure 19, which indicates variable NSZD rates throughout the year. It is unclear whether NSZD rates at this site are influenced by seasonal changes in subsurface temperatures.

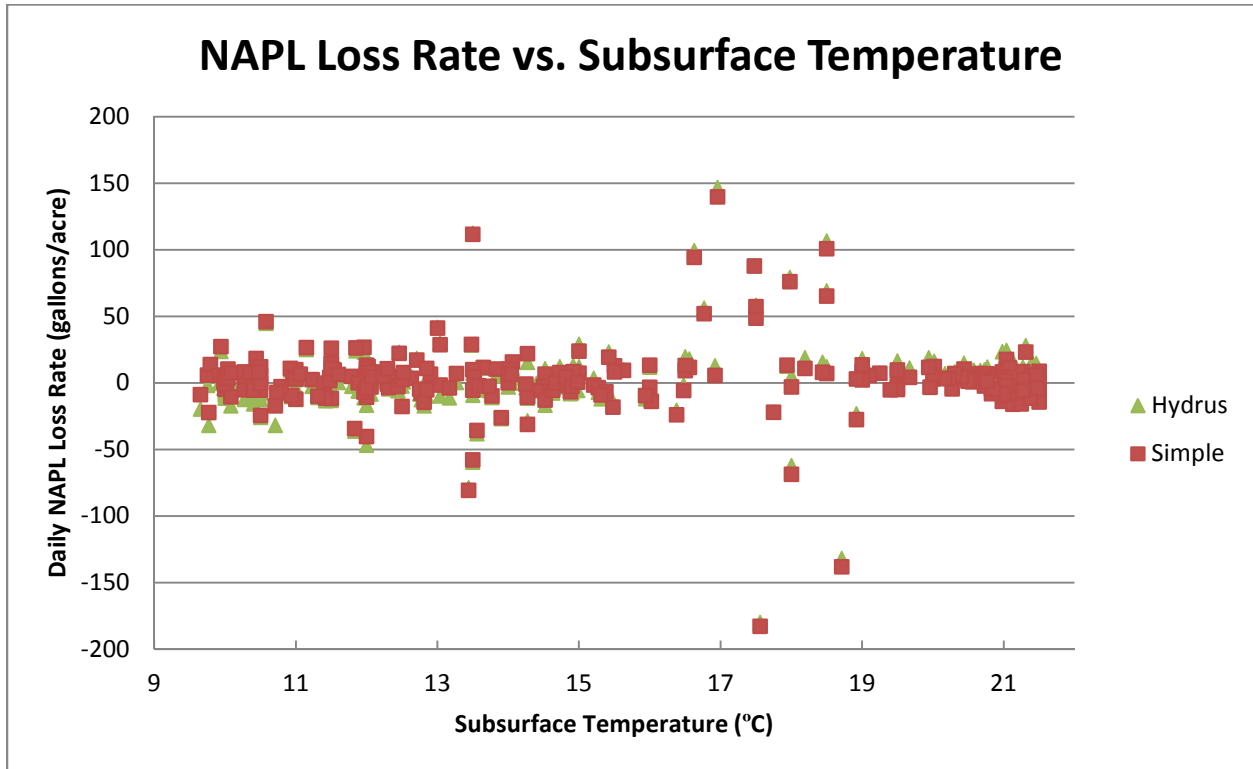


Figure 20. NAPL loss rate versus subsurface temperature at 2.13m bgs at the field site in Northern New Jersey

#### 4.3.5. Southern New Jersey

For the field site in Southern New Jersey, the daily average subsurface temperatures measured at the impacted location as well as the subsurface temperatures calculated as background values using the simple analytical model and Hydrus are plotted in Figure 21. The dataloggers at 2.67m bgs and 6.48m bgs stopped functioning in August 2014, so subsequent data are not available. The datalogger at 1.91m bgs began recording highly variable data beginning in August 2014, and

the subsequent data are not deemed reliable. Subsurface temperatures measured at the impacted location and calculated as background values are very similar at 0.53m bgs, 1.41m bgs, 1.91m bgs, and 2.67m bgs. Temperatures at the impacted location are increasingly warmer than temperatures calculated as background values at greater depths, with temperatures at the impacted location at 7.24m bgs approximately two degrees Celsius warmer than temperatures calculated as background values. At all depths, general agreement exists between the background temperatures calculated using the simple analytical model and Hydrus from approximately February 2013 to September 2014, but disagreement between the two methods occurs prior to February 2013 and after September 2014.

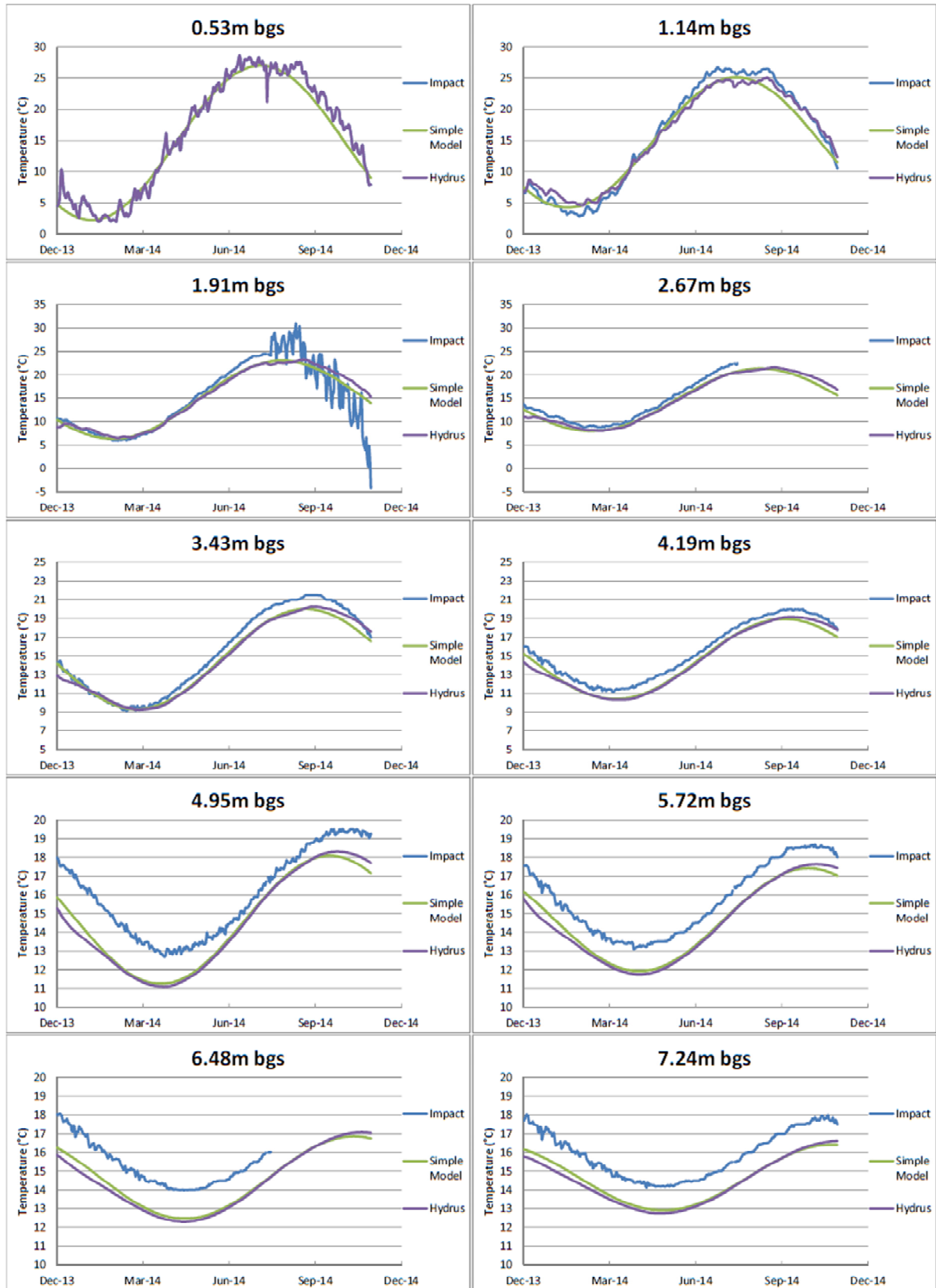


Figure 21. Subsurface temperatures measured at impacted location and calculated as background using the simple analytical model and Hydrus for the field site in Southern New Jersey

Average NSZD rates and cumulative NAPL losses over 11 months for the field site in Southern New Jersey using both of the calculated background correction methods are shown in Table 16. These data indicate similar results for the two background correction methods, with average NSZD rates of 68 gal/acre/year using the simple analytical model and 110 gal/acre/year using Hydrus. Cumulative NAPL losses are 103 gal/acre using the simple analytical model and 76 gal/acre using Hydrus. Prior characterization of NSZD rates at this site using CO<sub>2</sub> Traps at the same locations as the temperature monitoring sticks indicate average loss rates of approximately 4,000 gal/acre/year (Bezold 2015). NSZD rates calculated using the thermal NSZD rate model are more than an order of magnitude less than loss rates determined using the CO<sub>2</sub> Trap method. This discrepancy may be due to the incomplete energy balance at this site leading to an underestimation of the energy released due to biodegradation, an overestimation of the true change in enthalpy of the oxidation reactions occurring at the site, and/or underestimation of the energy flow due to convection. Better understanding of these factors could lead to calculations of larger NSZD rates by the thermal NSZD rate model.

Table 16. Average NSZD rate and cumulative NAPL losses for the field site in Southern New Jersey

<b>Background Correction</b>	<b>Average Loss Rate (gal/acre/year)</b>	<b>Cumulative NAPL Losses 11 months (gal/acre)</b>
Hydrus	110	76
Simple Model	68	103

Cumulative NAPL losses calculated using daily NSZD rates are shown in Figure 22. This figure indicates that NSZD rates calculated using both background correction methods follow similar trends and are variable throughout the year: negative in the winter, positive in the spring, negative in the summer, and positive in the fall. Calculation of negative NSZD rates by the

model is likely due to the incomplete energy balance at this site, as well as imperfections of the background correction methods leading to incorrect estimates of background temperatures. In addition, this site has a shallow water table, and methane oxidation likely occurs at shallow depths by methanotrophic bacteria (Bezold 2015). Because shallow subsurface temperatures are strongly influenced by short-term heating and cooling at the ground surface, it is difficult to isolate the heat released due to NAPL biodegradation for use in the thermal NSZD rate model.

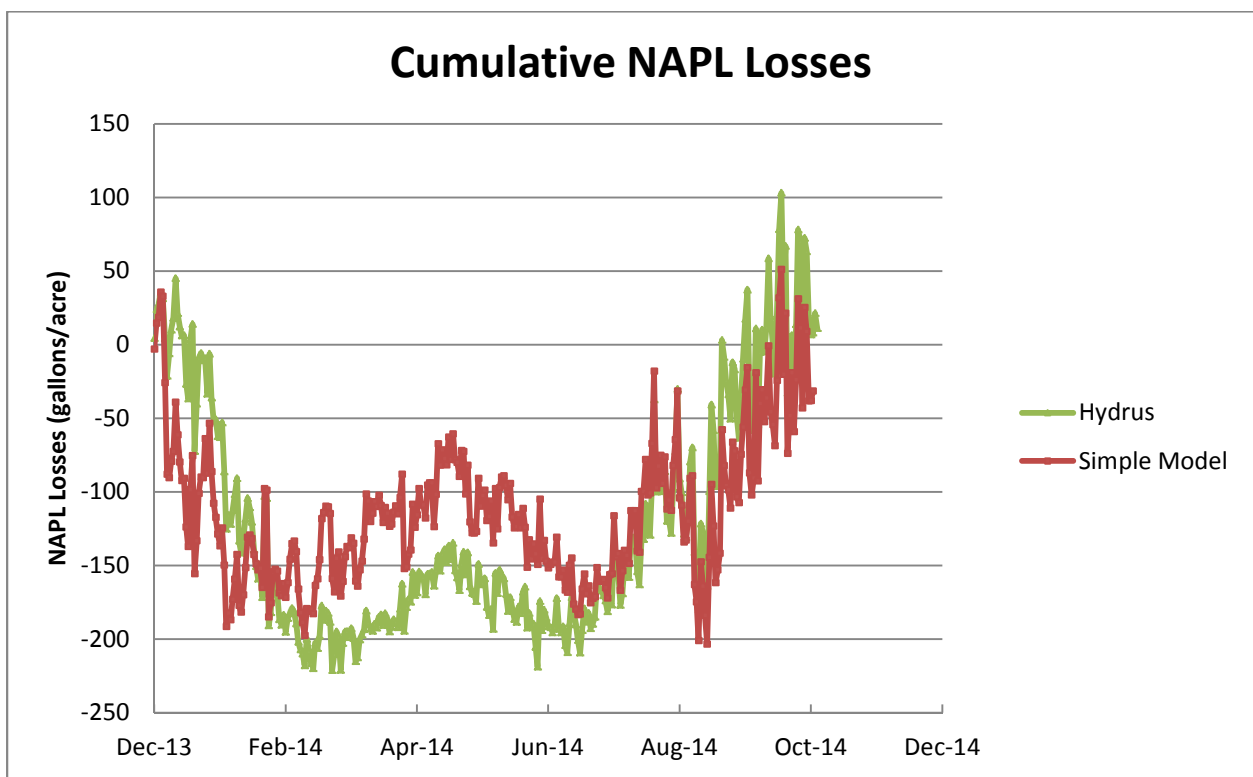


Figure 22. Cumulative NAPL losses at field site in Southern New Jersey

Figure 23 shows the daily NAPL loss rate in gallons/acre versus the subsurface temperature at 3.43m bgs. This depth represents the approximate center of the vertical extent of the NAPL zone. The figure indicates no correlation between subsurface temperature and increased NAPL loss rate at this site. This finding is not consistent with Figure 22, which indicates variable NSZD

rates throughout the year. It is unclear whether NSZD rates at this site are influenced by seasonal changes in subsurface temperatures.

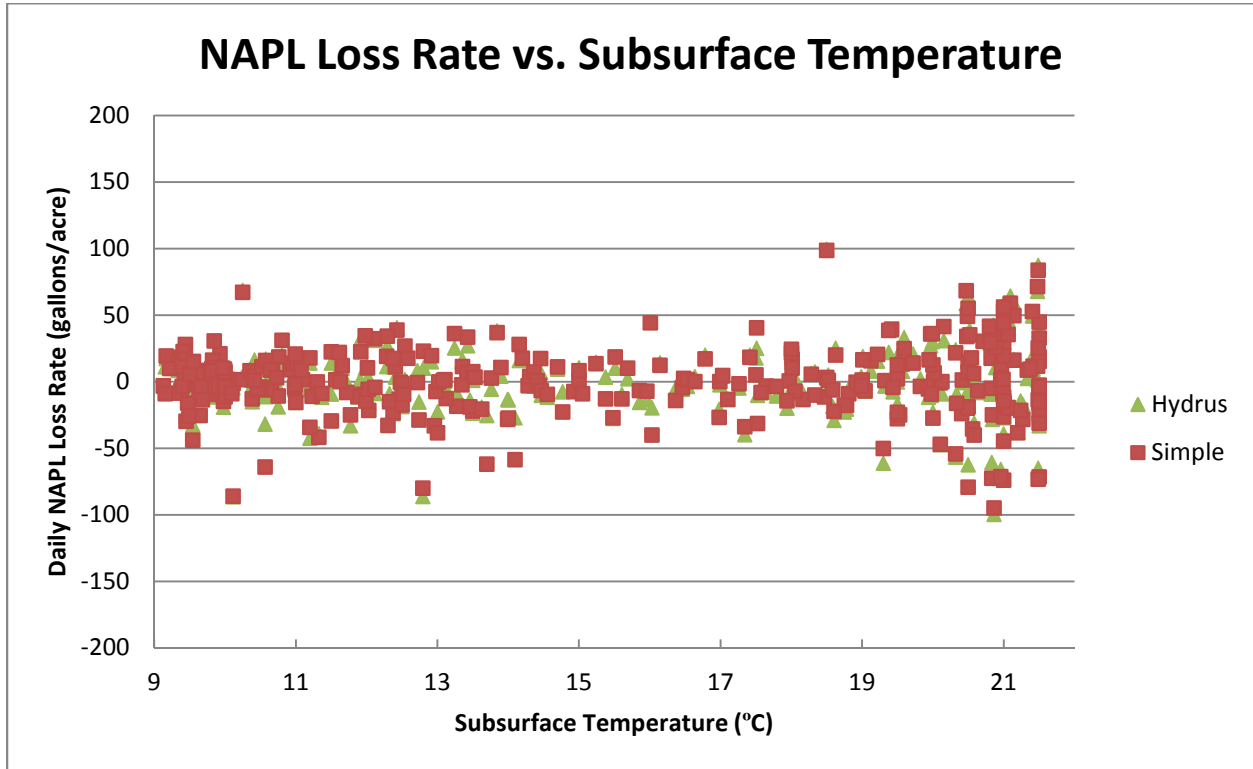


Figure 23. NAPL loss rate versus subsurface temperature at 3.43m bgs at the field site in Southern New Jersey

#### 4.3.6. Parameter Sensitivity Analysis

This section presents the results of the parameter sensitivity analysis. These results indicate which parameters strongly influence the thermal NSZD rate model and require accurate characterization, and which parameters have less influence on the results and can be approximated. The relative effects of each parameter at low and high values are compared to the model output using the base case parameters. The percent difference from the base case scenario for each parameter at low and high values are summarized in Table 17.

Table 17. Results of the parameter sensitivity analysis for the site in Kansas using the background location background correction method

Parameter	Average Loss Rate Percent Difference from Base Case		Cumulative Losses Percent Difference from Base Case	
	Low	High	Low	High
n	-6.5	6.5	-6.5	6.5
K	-0.1	0.1	-0.1	0.1
S <sub>wfc</sub>	0.2	-0.2	0.1	-0.2
κ <sub>unsat</sub>	-19.8	19.8	-19.8	19.8
κ <sub>sat</sub>	0.6	-0.6	0.6	-0.6
C <sub>unsat</sub>	2.4	-2.4	2.4	-2.4
C <sub>sat</sub>	3.7	-3.7	3.7	-3.7
ΔH <sub>r</sub>	25.0	-16.7	25.0	-16.7

The parameter sensitivity analysis indicates that the values of hydraulic conductivity (K), unsaturated zone water saturation (S<sub>wfc</sub>), and saturated zone thermal conductivity (κ<sub>sat</sub>) are relatively inconsequential in the thermal NSZD rate model. Varying these values by 20% produces average loss rates and cumulative NAPL losses that are less than 0.6% different from the base case scenario. Values of unsaturated and saturated zone volumetric heat capacity (C<sub>unsat</sub> and C<sub>sat</sub>, respectively) are somewhat important in the thermal NSZD rate model, as variation of these values produces average loss rates and cumulative NAPL losses within 4% of the base case scenario. Soil porosity (n) is also somewhat important in the thermal NSZD rate model as variation of this value causes average loss rates and cumulative NAPL losses to differ by 6.5% of the base case scenario.

The parameter sensitivity analysis indicates that values of unsaturated zone thermal conductivity (κ<sub>unsat</sub>) and change in enthalpy of the oxidation reaction (ΔH<sub>r</sub>) are significant inputs to the thermal NSZD rate model. Variation of these parameters by 20% led to average loss rates and cumulative NAPL losses approximately 16 to 25% different from the base case scenario.

The unsaturated zone thermal conductivity is used by the thermal NSZD rate model to determine the energy flow out of the top of the NAPL body, and as discussed for the field site in Kansas, this flow accounts for a large proportion of the energy flows in the energy balance. Thus, variation of this value causes significant changes in the average loss rate and cumulative NAPL losses. Estimation of the unsaturated zone thermal conductivity can be improved by direct measurement of the thermal conductivity of field soils. This measurement was taken for soils at the field site in Kansas, as discussed previously, but not for the rest of the field sites as site soils were not available for analysis. In addition, this work assumes that the thermal conductivity of the media is constant, while in reality, it varies as a function of soil moisture. Varying the thermal conductivity as a function of soil moisture in the model would lead to better estimates of the thermal conductivity as it changes spatially and temporally.

The change in enthalpy of the NAPL oxidation reaction is used to calculate the NSZD rate from the energy released during NAPL biodegradation. Thus, variation of this value causes significant changes in the average loss rate and cumulative NAPL losses. The variability in the change in enthalpy of oxidation of aqueous phase decane is large, ranging from -26.58 kJ/mol under methanogenic conditions to -6797.07 kJ/mol under aerobic conditions, as shown previously in Table 8. Estimation of this value could be improved by better knowledge of the reactants and products of biodegradation and the mass flows occurring in the system, which would enable selection of a value appropriate for site conditions.

#### **4.4. Limitations**

The main limitations of the thermal NSZD rate model are that it requires a background correction, it is not accurate for sites with shallow NAPL or methane oxidation fronts, it may

misestimate the timing of NAPL biodegradation, it is sensitive to input parameters that are not well constrained, and it can be influenced by other heat sources in the subsurface. These limitations are discussed in detail in this section.

The thermal NSZD rate model requires temperatures either measured or modeled at a representative background location that is not impacted by NAPL. Differences in ground cover, soil properties, and subsurface heterogeneities can cause heat transfer at modeled and measured background locations to be somewhat different than heat transfer at the impacted location, which can cause large variability in NSZD rates calculated by the model. The quality of the background temperatures determines the accuracy of the thermal NSZD rate model. Results from this thesis suggest that while none of the background correction methods produce exact estimates of background temperatures, temperatures measured at a background stick and modeled using Hydrus provide reasonable estimates of background temperatures, while temperatures modeled using the simple analytical model often provide inaccurate estimates of background temperatures.

The thermal NSZD rate model does not seem to be accurate for sites with NAPL or methane oxidation fronts at shallow depths where subsurface temperatures are highly influenced by the air temperature. At these shallow depths, energy flows near the ground surface are much larger than those due to NAPL biodegradation, making isolation of the heat released due to NAPL biodegradation difficult. NSZD rates calculated using subsurface temperatures are not accurately estimated at sites where the NAPL or methane oxidation front is close to the ground surface, such as the field sites in New Jersey.

The thermal NSZD rate model may represent delayed biodegradation rates due to delayed energy flows. After NAPL is biodegraded to methane, the methane may be stored due to a rising water table or precipitation events. Only when the methane reaches the methane oxidation front is a large energy flow produced that is captured by the thermal NSZD rate model. This delay may cause the thermal NSZD rate model to misestimate the timing of NAPL biodegradation as later in time than it actually occurs.

As discussed in the previous section, the thermal NSZD rate model is sensitive to input values of unsaturated zone thermal conductivity and the change in enthalpy of the oxidation reaction. While the thermal conductivity can be better constrained by direct measurement and the use of spatially and temporally variable values based on soil moisture, better constraint of the change in enthalpy is more difficult as the oxidation reactants and products of biodegradation are unknown, and not all of the enthalpy released during biodegradation may be released as heat to the surrounding environment. This work assumes that the end products of all biodegradation reactions are carbon dioxide and water, and all enthalpy released during oxidation is released as heat to the surrounding environment. However, other oxidation reactions likely occur, some of the NAPL likely degrades to solid phase precipitates or volatile fatty acids, and some of the enthalpy released during oxidation is not released as heat. Consideration of variable electron acceptors, end products, and microbial populations leads to variable values of the change in enthalpy, and variations of this parameter can lead to large variations in the average loss rate and cumulative NAPL losses calculated by the thermal NSZD rate model.

Finally, the thermal NSZD rate model may be influenced by heat sources other than the heat released during NAPL biodegradation. Energy flows caused by other factors, such as heated

water flowing through subsurface pipes, influence the energy balance. NSZD rates calculated using subsurface temperatures are not accurately estimated in locations highly influenced by subsurface heating sources other than the heat released during NAPL biodegradation.

## **5. LABORATORY STUDY OF THERMODYNAMICS OF BIODEGRADATION**

Building on the literature and theory presented in Chapter 2, this chapter describes the laboratory column experiment conducted to evaluate the thermodynamics of biodegradation of a carbon substrate in soil. The following experiment was conducted as a preliminary effort, and some aspects of this work are incomplete. Nevertheless, this material is included as many aspects are intriguing and potentially foundational to future work. First, the objectives of the laboratory experiment are defined. Next, the methods used to carry out the experiment are described. Finally, the results of the laboratory experiment are given.

### **5.1. Objectives**

Three main objectives drove this laboratory experiment. The first objective was to verify whether a measurable increase in temperature, and thus a quantifiable amount of heat, is generated during biodegradation of a carbon substrate in soil. The second objective was to determine whether a subsequent addition of substrate would again produce a measurable increase in temperature. The third objective was to determine whether closing the system to preclude oxygen from entering the soil would change the reaction rate and the amount of heat released.

### **5.2. Methods**

This section details the methods used to carry out the laboratory experiment to study the thermodynamics of biodegradation of a carbon substrate in soil. First, the physical setup of the column in the laboratory is detailed. Second, the addition of the substrate, molasses, is described. Third, the gas sampling procedures and analytical techniques employed are presented. Finally, the methods of molasses loss rate modeling using the thermal NSZD rate model are described.

### 5.2.1. Column Setup

The experiment was conducted in a 14.5 cm ID schedule 80 PVC pipe oriented vertically. A schematic of the column setup is shown in Figure 24. The column was 185 cm high with a wall thickness of 1.2 cm. The column was wrapped with 7.6 cm of R-30 fiberglass insulation (Owens Corning, Toledo, OH) on all sides, which was then covered with plastic wrap to secure the insulation in place. The top of the column was initially open to the atmosphere. The bottom of the column was sealed with a PVC cap secured in place with a hose clamp. A 3.2 mm inner diameter copper pipe was coiled and placed in the bottom of the cap, with an inlet on one side of the cap and an outlet on the other side. A 3.2 mm thick, 14.5 cm diameter copper disc was placed above the copper pipe coil.

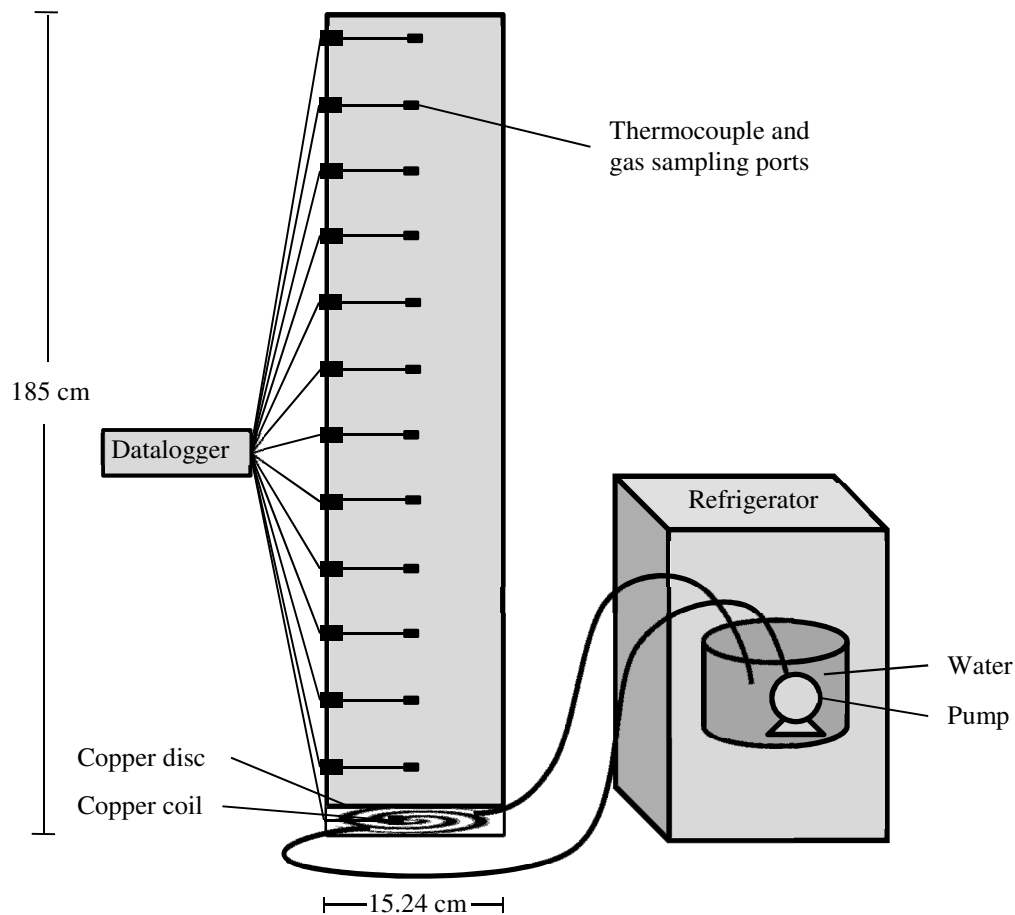


Figure 24. Schematic of experimental column setup

A submersible pump (Mini Submersible/Fountain/Pond Pump, Pacific Hydrostar, Camarillo, CA) was placed in a bucket of water inside of a small refrigerator (Mini Refrigerator/Freezer, Haier, New York City, New York). Cold water (approximately 9°C) was continuously pumped from the bucket, through the copper pipe coil, and back into the bucket to simulate a constant temperature boundary.

Sampling ports were located every 15.2 cm vertically along the column. Sampling ports consisted of 4.8 mm diameter PTFE tubing (Cole-Parmer, Vernon Hills, IL) that extended to the center of the column. A type T (copper-constantan) thermocouple was placed at the center of the column at each sampling port location, with the thermocouple wire extending out of the column through the PTFE tubing. 5 µm Nitex filter fabric (Wildco, Yulee, FL) was wrapped around the end of each PTFE tube and thermocouple to prevent the extraction of sand during sampling. An additional thermocouple was placed at the base of the column below the copper disc to determine the boundary temperature.

Fine sand (20-40 Colorado Silica Sand, Premier Silica) was used as the porous media to fill the column. The sand was poured into the column on top of the copper disc to a height 2.5 cm below the top of the column. Tap water from Fort Collins, CO was then pumped into the column through a port at the base of the column until the sand was fully saturated. Water was pumped at a rate of approximately 20 mL/min, and reached full saturation in approximately 24 hours. The water was then drained via the sampling port located 30.5 cm from the base of the column until the piezometer indicated that the water table was 30.5 cm from the base of the column. 3.85 L of water was drained in approximately 24 days.

### ***5.2.2. Molasses Addition***

For the initial molasses injection, 125 mL of molasses (Unsulphured Blackstrap Molasses, Golden Barrel, Honey Brook, PA) mixed with 375 mL of tap water was added to the column via the injection port located 38.1 cm from the base of the column. To simulate water table fluctuations, 300 mL of water was then drained and re-injected into the column three times via the sampling port located 15.24 cm from the base of the column.

For the second molasses injection, 200 mL of molasses mixed with 200 mL of tap water was added to the column via the injection port located 38.1 cm from the base of the column. 100 mL of water was then drained and re-injected into the column via the sampling port located 15.24 cm from the base of the column.

For the final molasses injection, 200 mL of molasses mixed with 200 mL of tap water was added to the column via the injection port located 38.1 cm from the base of the column. 100 mL of water was then drained and re-injected into the column via the sampling port located 15.24 cm from the base of the column. The top of the column was sealed with a PVC cap secured in place with a hose clamp and fitted with an air lock to preclude oxygen from entering the column but allow gases from the column to escape.

### ***5.2.3. Sampling Procedure and Analytical Technique***

Temperature data were collected at each thermocouple every minute. Temperatures were collected using two Omega thermocouple dataloggers. Average hourly temperatures were calculated and used in the loss rate model.

Gas samples were collected at each sampling port by purging two tubing volumes of gas (3 mL) followed by the collection of a 1 mL sample in a gastight 10 mL syringe (BD, Franklin Lakes, NJ) capped with a stopcock (Cole-Parmer, Vernon Hills, IL). Sample collection started at the bottom of the unsaturated zone in the column and progressed towards the top. Samples were analyzed within one hour of collection using a HP 5890 Series II gas chromatograph equipped with a thermal conductivity detector. 50  $\mu$ L samples were analyzed for percent methane and carbon dioxide using an Alltech Hayesep<sup>®</sup> Q 80/100 column (8'x1/8" x 0.085" SS) with helium as the carrier gas and a constant oven temperature of 40°C. Calibration was performed before the start of the experiment, and calibration curves are included in Appendix B.

#### ***5.2.4. Loss Rate Modeling***

Temperature data collected during the laboratory experiment was used in the thermal NSZD rate model to determine the magnitude and timing of molasses losses. The thermal NSZD rate model was run utilizing the model inputs described in this section. The Mathcad model as applied to the laboratory experiment is included in Appendix A. Because no water was flowing through the system, only the energy flows into and out of the impacted zone via conduction in the vertical direction and the change in storage were considered in the energy balance. The model was run using hourly averages of the temperatures measured in the column.

The background correction was achieved by determining the temperature gradient within the column before molasses was added and then subtracting this background gradient from the measured temperature gradient after molasses was added to the column. This method produced the temperature gradient due to molasses biodegradation.

The values of soil characteristics used in the thermal NSZD rate model are listed in Table 18. The porosity ( $n$ ) was determined to be 0.4 by Tracy (2015). The water saturation in the unsaturated ( $S_{wfc}$ ) and saturated ( $S_w$ ) zones was assumed to be 0.1 and 1, respectively. The area ( $A$ ) inside the column perpendicular to the vertical direction was measured. The thermal conductivity in the unsaturated ( $\kappa_{unsat}$ ) and saturated ( $\kappa_{sat}$ ) zones and the volumetric heat capacity in the unsaturated ( $C_{unsat}$ ) and saturated ( $C_{sat}$ ) zones were measured using a thermal properties analyzer (KD2 Pro, Decagon Devices, Pullman, WA).

Table 18. Soil characteristics used in the thermal NSZD rate model for the laboratory experiment

Parameter (units)	Value
$n$	0.4
$S_{wfc}$	0.1
$S_w$	1
$A$ ( $m^2$ )	0.0186
$\kappa_{unsat}$ (W/mK)	0.41
$\kappa_{sat}$ (W/mK)	1.36
$C_{unsat}$ ( $kJ/m^3K$ )	1252.5
$C_{sat}$ ( $kJ/m^3K$ )	2826.7

The molasses used in this experiment was 45% sugar. Glucose was used to represent the sugar in the molasses for the thermal NSZD rate model (glucose molecular weight = 0.180 kg/mol, density = 1540 kg/m<sup>3</sup>). The standard change in free energy ( $\Delta G_r^o$ ) and enthalpy ( $\Delta H_r^o$ ) of glucose biodegradation via aerobic oxidation and methanogenesis were calculated and used in the thermal NSZD rate model as appropriate based on the results of gas samples taken from the column. These values were calculated as described in Chapter 2, and are listed in Table 19.

Table 19. Standard change in free energy ( $\Delta G_r^o$ ) and enthalpy ( $\Delta H_r^o$ ) for redox reactions of standard phase glucose per mole glucose (calculated using values tabulated in Appendix B)

<b>Standard Phase Glucose Redox Reaction</b>	<b><math>\Delta G_r^o</math> (kJ/mole)</b>	<b><math>\Delta H_r^o</math> (kJ/mole)</b>
$6O_2 + C_6H_{12}O_6 \rightarrow 6CO_2 + 6H_2O$ Aerobic Respiration	-2878.6	-2805.0
$C_6H_{12}O_6 \rightarrow 3CO_2 + 3CH_4$ Methanogenesis	-424.1	-133.3

### 5.3. Results and Discussion

This section contains the results of the laboratory experiment and the application of the thermal NSZD rate model to the laboratory temperature data. First, the results of gas sampling of the column are presented. Then, molasses loss rates and cumulative losses for each molasses injection are presented and discussed.

#### 5.3.1. Gas Sampling

Gas samples taken throughout the laboratory experiment confirmed that biodegradation of the molasses was occurring due to the increase in carbon dioxide concentration following each molasses injection. Gas samples also indicated the timing and relative magnitude of molasses losses within the column. Figure 25 shows the carbon dioxide concentrations at all unsaturated sampling ports throughout the entirety of the laboratory experiment. Figure 25 indicates that carbon dioxide concentrations peaked approximately seven days after the first molasses injection, ten days after the second molasses injection, and twenty days after the third molasses injection. Larger carbon dioxide concentrations were measured at the 76.2cm sampling port following the second molasses injection of 200mL than were measured at the 76.2cm sampling port following the first molasses injection of 125mL; however, smaller carbon dioxide

concentrations were measured at the 91.4cm sampling port and above following the second molasses injection than was measured at each corresponding elevation following the first molasses injection. Slightly lower carbon dioxide concentrations were measured at the 76.2cm sampling port following the third molasses injection of 200mL than was measured at the 76.2cm sampling port following the second molasses injection, but larger carbon dioxide concentrations were measured at the 91.4cm sampling port and above following the third molasses injection than were measured at each corresponding elevation following the first and second molasses injections.

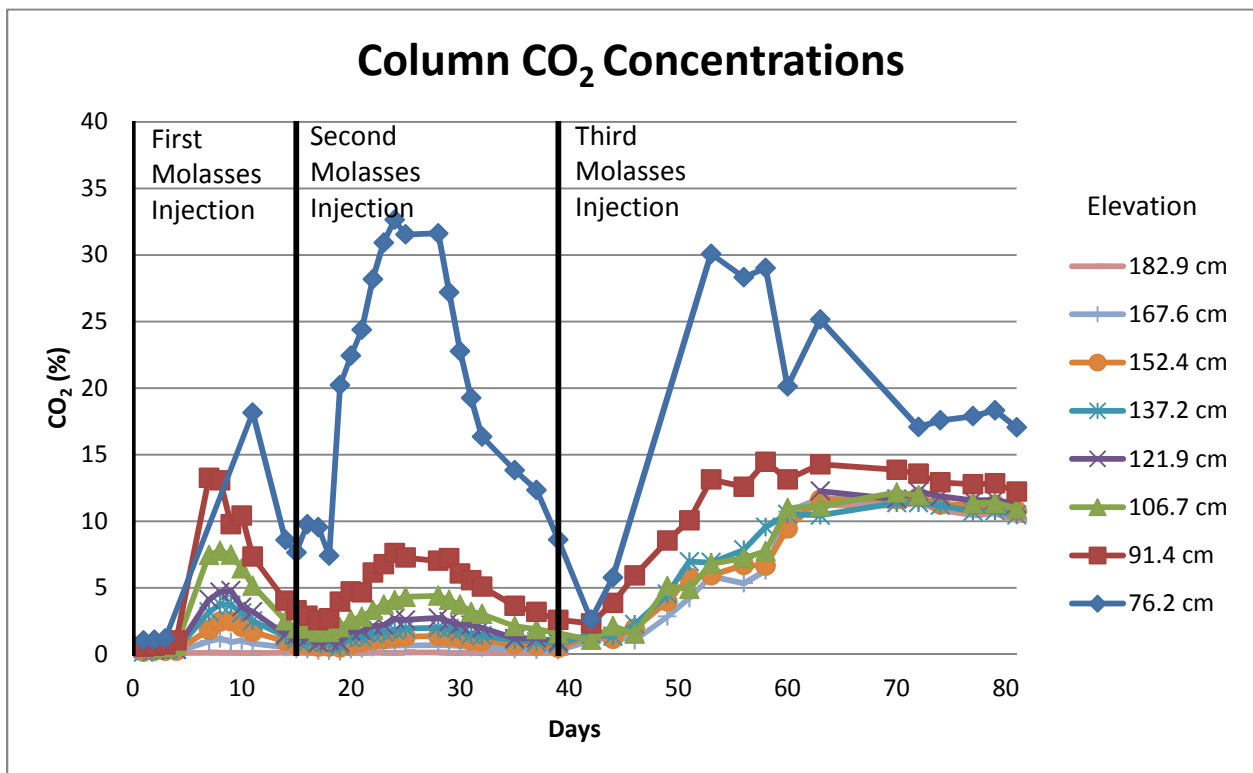


Figure 25. Carbon dioxide concentrations in the column throughout the laboratory experiment

Figure 26 shows the methane concentrations at all unsaturated sampling ports throughout the entirety of the laboratory experiment. Figure 26 indicates that methanogenesis was not observed

following the first molasses injection, but did occur following the second and third molasses injections. Methanogenesis began approximately 21 days following the second molasses injection, likely because all other electron acceptors had been reduced. This finding indicates that a mixture of aerobic and anaerobic oxidation was likely occurring following the second molasses injection. Following the third molasses injection, when the top of the column was sealed to prevent additional oxygen from entering the column, methanogenesis occurred throughout the experimental period. Because methanogenesis was already occurring in the column, the third molasses injection added electron donors for the microbes, leading to increased methanogenesis rates and increased methane production.

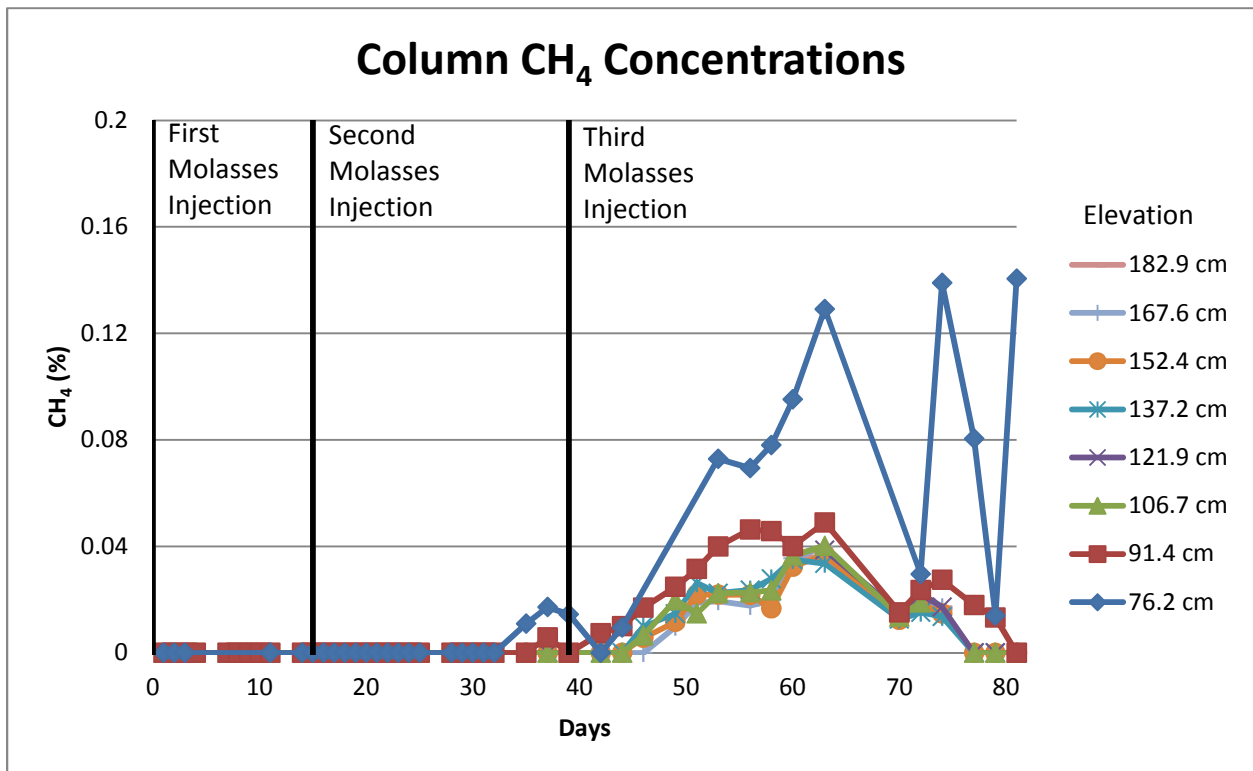


Figure 26. Methane concentrations in the column throughout the laboratory experiment

Figure 27 shows the carbon dioxide profiles in the column after the first, second, and third molasses injections. Three carbon dioxide profiles are shown in each graph: three days after the molasses injection, at the highest carbon dioxide concentrations, and after carbon dioxide concentrations began decreasing. The profiles for the first and second molasses injections show similar trends, with the highest carbon dioxide concentrations at the base of the unsaturated zone and the lowest carbon dioxide concentrations at the top of the column. The carbon dioxide concentration profiles following the third molasses injection exhibit a different trend. The profile three days after the third molasses injection is similar to the profiles three days after the first and second molasses injections. The profile 24 days after the third molasses injection indicates the highest carbon dioxide concentrations at the base of the unsaturated zone and relatively constant carbon dioxide concentrations at higher elevations. The profile 40 days after the molasses injection indicates almost the same carbon dioxide concentrations as 24 days after the molasses injection because the column was sealed and carbon dioxide was not able to diffuse into the atmosphere. The methane profiles following the third molasses injection, which are not plotted, show the same trends.

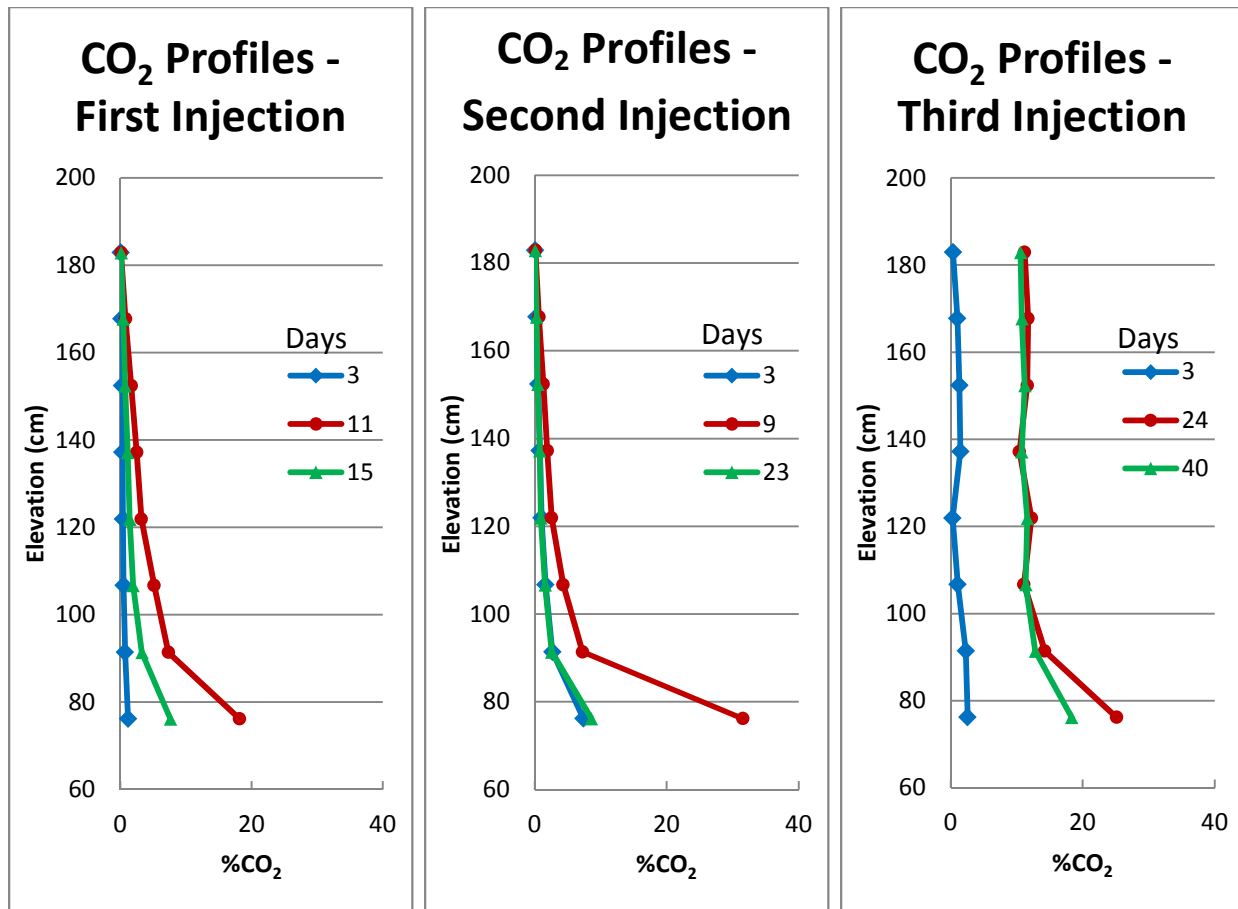


Figure 27. Column carbon dioxide profiles following each molasses injection

### 5.3.2. Loss Rate Modeling

Based on the results of gas sampling during the laboratory experiment, oxidation of the molasses was assumed to be via aerobic oxidation following the first molasses injection, half aerobic oxidation and half methanogenesis following the second molasses injection, and methanogenesis following the third molasses injection. The thermal NSZD rate model utilized the respective change in enthalpy for each of these conditions. The full range of measured temperature data following the first and second molasses injections were used in the thermal NSZD rate model. Temperature data for 30 days following the third molasses injection was used in the thermal NSZD rate model. Based on the soil gas samples, biodegradation was assumed to be negligible

after 30 days. The average glucose loss rate and cumulative glucose losses following each molasses injection are shown in Table 20. The data indicate much smaller losses rates and cumulative losses for the first and second molasses injections than for the third molasses injection because the column was assumed to be entirely methanogenic following the third molasses injection, and the change in enthalpy of methanogenic oxidation of glucose is considerably less than the change in enthalpy of aerobic oxidation of glucose. The thermal NSZD rate model suggests that only 1.6% of the first molasses injection was biodegraded, 4.7% of the second molasses injection was biodegraded, and 125% of the third molasses injection was biodegraded. The thermal NSZD rate model likely underestimated loss rates for the first and second molasses injection and overestimated loss rates for the third molasses injection due to the assumed aerobic and/or anaerobic conditions. In addition, the thermal NSZD rate model likely underestimated loss rates for the first molasses injection due to the assumption that the microbial population was at steady-state. In reality, the microbial population likely grew following the first molasses injection, using some of the energy released during the molasses degradation to grow the population. This energy was not released to the surrounding environment, but was not accounted for by the thermal NSZD rate model. Better characterization of the oxidation reactions that were occurring and the portion of energy used to grow the microbial population would lead to better estimates of loss rates.

Table 20. Average loss rate and cumulative glucose losses for each molasses injection

<b>Molasses Injection</b>	<b>Average Loss Rate (mL/day)</b>	<b>Cumulative Glucose Losses (mL)</b>
First (56.25 mL glucose)	0.06	0.9
Second (90 mL glucose)	0.18	4.2
Third (90 mL glucose)	3.65	112.7

Cumulative molasses losses calculated using hourly molasses loss rates are shown in Figure 28. This figure indicates that molasses loss rates were relatively constant following each molasses injection. This figure also illustrates that molasses loss rates calculated using the thermal NSZD rate model following the third molasses injection are considerably larger than molasses loss rates following the first and second molasses injections. Again, the higher loss rates following the third injection are likely due to the assumption that all glucose was oxidized via methanogenesis to methane and the methane was not oxidized to carbon dioxide.

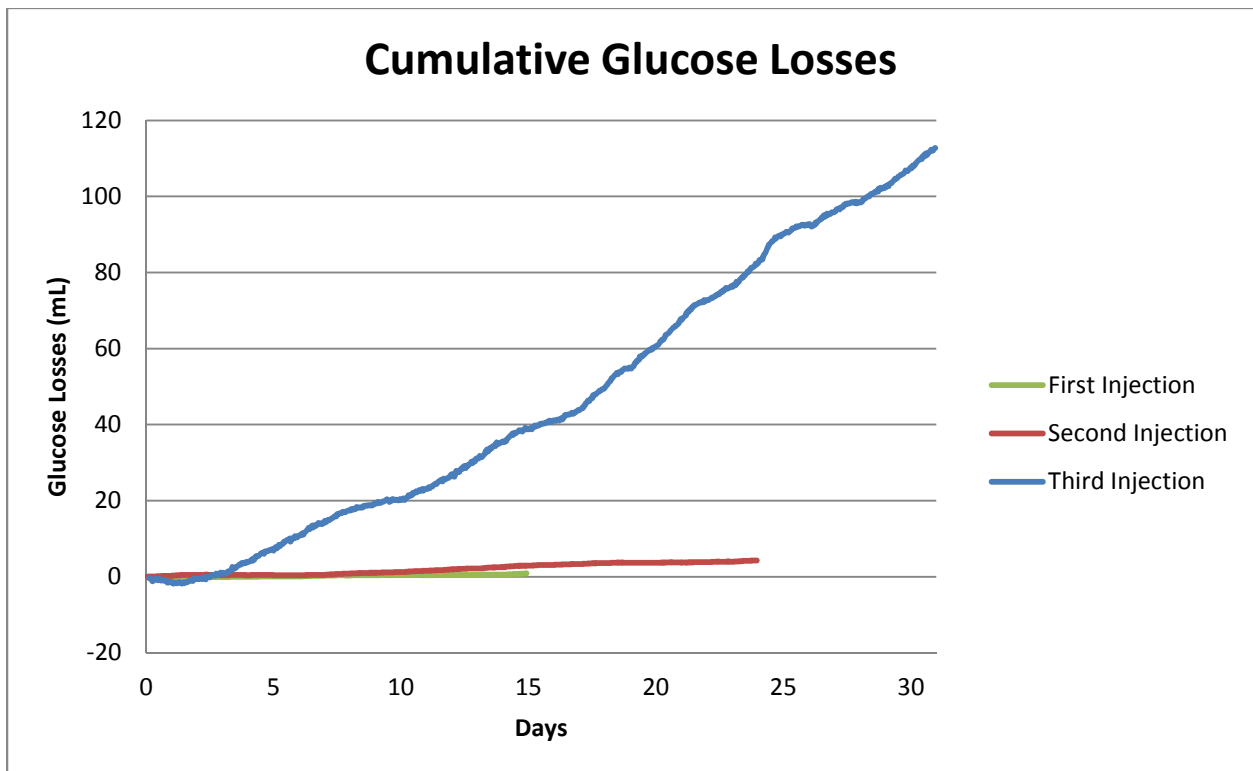


Figure 28. Cumulative glucose losses following each molasses injection

Returning to the premise of the introduction of this chapter, this experiment was conducted as a preliminary effort to understand the thermodynamics of biodegradation of a carbon substrate in soil. Some aspects of this experiment need further refinement and study, as discussed subsequently in Section 6.3 regarding suggestions for future work.

## **6. SUMMARY AND CONCLUSIONS**

This chapter provides a summary of the preceding chapters. First, the main ideas and themes of this thesis are stated. Next, the main results of application of the thermal NSZD rate model to field and laboratory data are summarized. Finally, suggestions for future work to improve the accuracy of the thermal NSZD rate model are presented.

### **6.1. Main Ideas and Themes**

NSZD rates are an important factor to consider when determining remediation strategies for NAPL impacted soil and groundwater. Knowledge of the magnitude and timing of NSZD rates will help site managers advance sustainable remedies for subsurface NAPL. This work was conducted to develop a novel method of providing real-time, continuous estimates of NSZD rates using subsurface temperatures about NAPL bodies.

A thermal NSZD rate model was developed based on subsurface temperatures measured at a NAPL impacted location and measured or modeled temperatures at a representative unimpacted background location. The background temperatures were subtracted from the temperatures measured at the impacted location to determine the temperatures due to NAPL biodegradation. These background corrected temperatures were then used in an energy balance, which considered energy flows due to conduction, convection, and the change in storage of energy within the NAPL impacted area, to determine the rate of energy release during NAPL biodegradation. The rate of energy release was divided by the change in enthalpy of the reaction to determine the NSZD rate.

The results of this work indicate that subsurface temperatures about a NAPL body can be used to resolve NSZD rates. This thermal method has two main advantages over methods utilizing gas fluxes: the thermal method is much less influenced by variable environmental factors, and the thermal method can provide continuous NSZD rates throughout the year. In addition, the thermal method has several qualities that make it a suitable option for monitoring NSZD rates at NAPL or other contaminant impacted sites. The first advantage is that once the temperature monitoring stick(s) are installed, the data can be collected remotely, a considerable convenience for remote sites or sites that are difficult to access. Second, the model used in the thermal method provides real-time data analysis. As soon as subsurface temperature data are available, NSZD rates can be calculated. Finally, the thermal method provides the potential to detect new contaminant releases to the subsurface. Because the model provides real-time data analysis, new releases may cause a jump in NSZD rates calculated by the model, indicating a possible contaminant release.

This work also indicates that the thermal method has limitations. The imperfections of the background corrections, incomplete energy balances, and unknown composition and quantity of reaction products and reactants limit the accuracy of NSZD rates calculated using the thermal NSZD rate model. The thermal NSZD rate model does not seem to be accurate for sites with shallow NAPL or methane oxidation fronts because of difficulties in isolating the heat released due to NAPL biodegradation from short-term heating and cooling at the ground surface. In addition, the thermal NSZD rate model may represent delayed biodegradation rates due to delayed energy flows and may be subject to other heat sources or sinks in the NAPL impacted area. The assumptions of this work likely lead to minimal estimates of true NSZD rates; however, a lack of known NSZD rates to compare the thermal method against makes it difficult to determine the accuracy of the thermal NSZD rate model.

## **6.2. Results of Field and Lab Studies**

The thermal NSZD rate model was applied to data from five field sites to determine continuous NSZD rates. In addition, a laboratory experiment was completed to evaluate the thermodynamics of biodegradation of a carbon substrate in soil. This section summarizes the results of both of these efforts.

### ***6.2.1. Field Scale Application of the Thermal NSZD Rate Model***

At all sites, background temperatures were modeled using a simple analytical model and Hydrus. For the sites in Kansas and Wyoming, background temperatures were also measured at an unimpacted location. Analysis of these background temperatures suggested that measured background temperatures or modeled background temperatures using Hydrus provided reasonable estimates of true background temperatures; however, modeled background temperatures using the simple analytical model often provided poor estimates of true background temperatures.

The field sites in Kansas, Colorado, Wyoming, and Southern New Jersey all had measured subsurface temperatures at the NAPL impacted location that were up to 4°C warmer than temperatures measured or modeled as background values. The field site in Northern New Jersey did not show this trend, likely because the water table and LNAPL at this site are shallow.

Average and cumulative NSZD rates calculated using background temperatures modeled by the simple analytical model often indicated negative loss rates. These negative loss rates further indicate that modeled background temperatures using the simple analytical model provide poor estimates of true background temperatures and inaccurate estimates of NSZD rates. Average

NSZD rates calculated using background temperatures modeled by Hydrus and measured at a background location are consistently lower than average NSZD rates obtained using CO<sub>2</sub> Traps at each field site. The lower NSZD rates are likely due to poor constraint of the value used for the change in enthalpy of NAPL biodegradation. The change in enthalpy is dependent on the oxidation reactants and products as well as the efficiency with which the microbes oxidize the NAPL. For this work, the change in enthalpy term utilized assumes that all NAPL is initially oxidized via methanogenesis and all produced methane is oxidized into carbon dioxide and water, and that all enthalpy released during NAPL biodegradation is released as heat to the surrounding environment. The consistently lower estimates of average NSZD rates by the thermal NSZD rate model as compared to NSZD rates obtained using CO<sub>2</sub> Traps suggests that these assumptions may provide a poor estimate of the true change in enthalpy. It is likely that a portion of the NAPL is degrading to solid phase precipitations or volatile fatty acids, and/or some of the released energy is used by the microbial population and is not released as heat to the surrounding environment during NAPL biodegradation. Consideration of these factors would lead to smaller values of the change in enthalpy and larger NSZD rates more consistent with loss rates determined using CO<sub>2</sub> Traps.

In addition, the apparent low NSZD rate estimates presented in this thesis may be due to underestimation of the temperature gradient due to the placement of thermocouples below the methane oxidation front and/or underestimation of the energy released during biodegradation due to an incomplete energy balance. These factors can be addressed by increasing the number of thermocouples above the NAPL body and by collection of water level data at the site to quantify all energy fluxes in the energy balance.

Comparison of daily NSZD rates to subsurface temperatures at the approximate center of the NAPL zone indicates a possible correlation between these parameters. This correlation was only observed for the field site in Wyoming, where increased subsurface temperatures corresponded to increased NSZD rates. NAPL at this site is somewhat shallow, and subsurface temperatures in the NAPL zone naturally vary over a large range of temperatures.

Data from the field site in Kansas allowed all energy flow terms to be considered in the energy balance. Results from application of the thermal NSZD rate model to this field site suggest that the energy flows due to conduction out of the top of the NAPL body in the z direction, convection of sensible heat by water in the z direction, and the change in energy represent significant proportions of the total rate of energy released. For the remainder of the field sites, the energy flow due to convection of sensible heat by water in the z direction was neglected due to lack of groundwater flow data. This deficiency may cause the thermal NSZD rate model to underestimate the total rate of energy released during NAPL biodegradation and therefore also underestimate NSZD rates.

### ***6.2.2. Laboratory Study of Thermodynamics of Biodegradation***

The results of gas samples taken from the column following each molasses injection provided some insight into the redox reactions occurring in the column. Following each molasses injection, increased carbon dioxide concentrations were observed near the water table that decreased with height in the column. Carbon dioxide concentrations increased with time as biodegradation of the molasses occurred, then decreased as biodegradation rates decreased. Very small concentrations of methane were observed in the column approximately 20 days after the second molasses injection, indicating that methanogenesis was occurring. Increasing

concentrations of methane were observed throughout the column following the third molasses injection.

The laboratory experiment verified that heat was released due to biodegradation following each molasses injection. An increase in the temperature gradient allowed application of the thermal NSZD rate model to the temperature data collected during the laboratory experiment. Average and cumulative molasses loss rates were calculated for each molasses injection event. Assumptions of molasses biodegradation via aerobic respiration following the first molasses injection and half aerobic respiration and half methanogenesis following the second molasses injection led to cumulative molasses losses of less than 5% of molasses injected. The assumption of molasses biodegradation via methanogenesis following the third molasses injection led to a cumulative molasses loss of more than 100% of the molasses injected. These results suggest a poor estimate of the true change in enthalpy occurring during the experiment. Processes lower on the redox ladder are likely dominating, but oxidation is not occurring solely via methanogenesis.

### **6.3. Future Work**

The energy balance and thermal NSZD rate model described in this thesis represent a preliminary attempt at quantifying the heat released during NAPL biodegradation and converting it to a NAPL loss rate. Continued work on this novel effort will result in more accurate estimates of NSZD rates. Suggestions for future work are made herein. These suggestions include characterization of all biodegradation reactants and products, studies to better understand how much energy is used by microorganisms during biodegradation, and the creation of a numerical model of energy fluxes in the subsurface.

### ***6.3.1. Characterization of Biodegradation Reactants and Products***

As discussed previously, the thermal NSZD rate model is sensitive to the value input for the change in enthalpy of the NAPL biodegradation. This value depends on the reactants and products of the biodegradation reactions, and knowledge of these variables would allow better estimation of the change in enthalpy value used in the thermal NSZD rate model. Initially, a thorough literature search of soil and water quality parameters at NAPL impacted sites may help determine the oxidation reactions occurring at these sites. Further, this knowledge could be acquired through characterization of the mass fluxes occurring in the subsurface at NAPL impacted sites. Analysis of inflowing and outflowing water in the NAPL impacted zone would indicate which electron acceptors are present and which reaction end products are formed and leave the system. Analysis of soils would indicate which reaction end products are formed and stay in the system. Analysis of soil gases would indicate whether a portion of the NAPL is only degraded to methane and not fully degraded to carbon dioxide. Characterization of NAPL biodegradation reactants and end products would indicate which oxidation reactions are occurring, leading to better estimates of the change in enthalpy value used in the thermal NSZD rate model and better estimates of NSZD rates.

### ***6.3.2. Characterization of Microbial Use of Energy***

As discussed previously, the value input for the change in enthalpy of the NAPL oxidation reaction depends on the proportion of energy that is released as heat to the surrounding environment during NAPL biodegradation. Even when the microbial population is at steady-state, some of the energy is likely taken out of the system when microbes move out of the system, and some energy is used to generate biomass material that cannot be degraded,

indicating that not all of the enthalpy released during NAPL biodegradation is released as heat to the surrounding environment. A thorough review of the literature on this topic may lead to better understanding of the proportion of energy used by the microbes that is not released as heat, which will lead to better estimates of NSZD rates.

### ***6.3.3. Numerical Modeling***

Numerical modeling in one, two, and three dimensions may lead to better understanding of thermal fluxes about subsurface NAPL bodies. One of the limitations of the thermal NSZD rate model described in this thesis is its requirement of subsurface temperatures at a representative background location. However, use of a detailed numerical model may eliminate the necessity for the background correction. Numerical modeling will also provide validation of the energy released during NAPL biodegradation.

## 7. REFERENCES

- Amos, R. T., K. U. Mayer, B. A. Bekins, G. N. Delin, and R. L. Williams (2005), Use of dissolved and vapor-phase gases to investigate methanogenic degradation of petroleum hydrocarbon contamination in the subsurface, *Water Resources Research*, 41(2).
- Bezold, Z. (2015), Investigation of Temperature Effects on Subsurface Attenuation of Nitroaromatic Compounds, CSU Thesis, Colorado State University Libraries.
- Carslaw, H. S., and J. C. Jaeger (1959), *Conduction of Heat in Solids*, 2nd ed., 510 pp., Clarendon Press, Oxford.
- Christensen, T. H., P. L. Bjerg, S. A. Banwart, R. Jakobsen, G. Heron, and H. J. Albrechtsen (2000), Characterization of redox conditions in groundwater contaminant plumes, *Journal of Contaminant Hydrology*, 45(3-4), 165-241.
- CRC Handbook of Chemistry and Physics*, (2014), CRC Press, West Palm Beach, FL.
- ITRC, (2009), Evaluating Natural Source Zone Depletion at Sites with LNAPL, Interstate Technology & Regulatory Council, LNAPLs Team, Washington, D.C.
- Dean, J. A., and N. A. Lange (1999), *Lange's Handbook of Chemistry*, McGraw-Hill, New York.
- DeVries, D. A. (1958), Simultaneous transfer of heat and moisture in porous media, pp. 909-916, Transactions, American Geophysical Union.
- DeVries, D. A., and N. Afgan (1975), *Heat and Mass Transfer in the Biosphere*, Scripta Book Co. [distributed by] Wiley, Washington.
- Dewalle, F. B., E. S. K. Chian, and E. Hammerberg (1978), Gas-production from solid-waste in landfills, *Journal of the Environmental Engineering Division-Asce*, 104(3), 415-432.
- Hanson, J. L., N. Yesiller, and N. K. Oettle (2010), Spatial and temporal temperature distributions in municipal solid waste landfills, *Journal of Environmental Engineering-Asce*, 136(8), 804-814.
- Hartz, K. E., R. E. Klink, and R. K. Ham (1982), Temperature effects – methane generation from landfill samples, *Journal of the Environmental Engineering Division-Asce*, 108(4), 629-638.
- Heijnen, J. J., and J. P. Vandijken (1992), In search of a thermodynamic description of biomass yields for the chemotrophic growth of microorganisms, *Biotechnology and Bioengineering*, 39(8), 833-858.
- Hillel, D. (1980), *Fundamentals of Soil Physics*, 413 pp., Academic Press, New York.

- Hollesen, J., B. Elberling, and P. E. Jansson (2011), Modelling temperature-dependent heat production over decades in High Arctic coal waste rock piles, *Cold Regions Science and Technology*, 65(2), 258-268.
- Huang, G. F., Q. T. Wu, J. W. C. Wong, and B. B. Nagar (2006), Transformation of organic matter during co-composting of pig manure with sawdust, *Bioresource Technology*, 97(15), 1834-1842.
- Johnson, P., P. Lundegard, and Z. Liu (2006), Source zone natural attenuation at petroleum hydrocarbon spill sites - I: Site-specific assessment approach, *Groundwater Monitoring and Remediation*, 26(4), 82-92.
- Kiaalhosseini, S. (2014), Novel Methods for Characterization of Contaminated Sites – Electrical Resistivity Method, Magnetic Resonance Imaging, and Cryogenic Coring, CSU Dissertation Proposal, Colorado State University.
- Kumar, S. (2011), Composting of municipal solid waste, *Critical Reviews in Biotechnology*, 31(2), 112-136.
- Liu, J. S., V. Vojinovic, R. Patino, and U. von Stockar (2007), A comparison of various Gibbs energy dissipation correlations for predicting microbial growth yields, *Thermochimica Acta*, 458(1-2), 38-46.
- Lundegard, P. D., and P. C. Johnson (2006), Source zone natural attenuation at petroleum hydrocarbon spill sites - II: Application to a former oil field, *Groundwater Monitoring and Remediation*, 26(4), 93-106.
- Mahler, N., T. Sale, and M. Lyverse (2012), A mass balance approach to resolving LNAPL stability, *Groundwater*, 50(6), 861-871.
- Mataalvarez, J., and A. Martinezviturtia (1986), Laboratory simulation of municipal solid-waste fermentation with leachate recycle, *Journal of Chemical Technology and Biotechnology*, 36(12), 547-556.
- McCoy, K., J. Zimbron, T. Sale, and M. Lyverse (2014), Measurement of natural losses of LNAPL using CO<sub>2</sub> Traps, *Groundwater*.
- McCoy, K. M. (2012), Resolving natural losses of LNAPL using CO<sub>2</sub> Traps, CSU Thesis, Colorado State University Libraries.
- Molins, S., U. K. Mayer, R. T. Amos, and B.A. Bekins (2010), Vadose zone attenuation of organic compounds at a crude oil spill site - Interactions between biogeochemical reactions and multicomponent gas transport, *Journal of Contaminant Hydrology*, 112(1-4), 15-29.

- Plyasunov, A. V., and E. L. Shock (2000), Thermodynamic functions of hydration of hydrocarbons at 298.15 K and 0.1 MPa, *Geochimica Et Cosmochimica Acta*, 64(3), 439-468.
- Rees, J. F. (1980a), Optimization of methane production and refuse decomposition in landfills by temperature control, *Journal of Chemical Technology and Biotechnology*, 30(8), 458-465
- Rees, J. F. (1980b), The fate of carbon-compounds in the landfill disposal of organic-matter, *Journal of Chemical Technology and Biotechnology*, 30(4), 161-175.
- Rittmann, B. E., and P. L. McCarty (2001), *Environmental Biotechnology Principles and Applications*, 754 pp., McGraw-Hill, Boston.
- Saito, H., J. Simunek, and B. P. Mohanty (2006), Numerical analysis of coupled water, vapor, and heat transport in the vadose zone, *Vadose Zone Journal*, 5(2), 784-800.
- Sale, T. (2003), Answers to frequently asked questions about managing risk at LNAPL sites. *API Soil and Water Research Bulletin* 18:1-20.
- Shock, E. L., H. C. Helgeson, and D. A. Sverjensky (1989), Calculation of the thermodynamic and transport properties of aqueous species at high pressures and temperatures – standard partial molal properties of inorganic neutral species, *Geochimica Et Cosmochimica Acta*, 53(9), 2157-2183.
- Sihota, N. I., O. Singurindy, and K. U. Mayer (2011), CO<sub>2</sub>-efflux measurements for evaluating source zone natural attenuation rates in a petroleum hydrocarbon contaminated aquifer, *Environmental Science & Technology*, 45(2), 482-488.
- Sweeney, R. E., and G. T. Ririe (2014), Temperature as a tool to evaluate aerobic biodegradation in hydrocarbon contaminated soil, *Groundwater Monitoring and Remediation*, 34(3), 41-50.
- Tchobanoglous, G. (1993), *Integrated Solid Waste Management Engineering Principles and Management Issues*, 978 pp., McGraw-Hill, New York.
- Tracy, M. (2015), Method Comparison for Analysis of LNAPL Natural Source Zone Depletion Using CO<sub>2</sub> Fluxes, CSU Thesis, Colorado State University Libraries.
- TRC (2012), LNAPL Distribution and Recoverability Assessment.
- VanBriesen, J. M. (2001), Thermodynamic yield predictions for biodegradation through oxygenase activation reactions, *Biodegradation*, 12(4), 265-281.
- VanBriesen, J. M. (2002), Evaluation of methods to predict bacterial yield using thermodynamics, *Biodegradation*, 13(3), 171-190.

Wiedemeier, T. H., H. S. Rifai, C. J. Newell, and J. T. Wilson (1999), *Natural Attenuation of Fuels and Chlorinated Solvents in the Subsurface*, John Wiley & Sons, New York.

Wiedemeier, T. H., J. T. Wilson, J. E. Hansen, F. H. Chapelle, and M. A. Swanson (1996), Technical Protocol for Evaluating Natural Attenuation of Chlorinated Solvents in Groundwater. Revision 1, DTIC Document.

Wu, J. Q., and D. L. Nofziger (1999), Incorporating temperature effects on pesticide degradation into a management model, *Journal of Environmental Quality*, 28(1), 92-100.

Xiao, J. H., and J. M. VanBriesen (2006), Expanded thermodynamic model for microbial true yield prediction, *Biotechnology and Bioengineering*, 93(1), 110-121

## 8. APPENDIX A

### 8.1. Thermal NSZD Rate Model Using Background Location Correction

#### Data Input Files:

##### Temperature Probes:

N1 :=  ...\N1Daily.dat

N2 :=  C:\Ca...W2Daily\_corrected.txt

N3 :=  C:\Ca...W3Daily\_corrected.txt

N4 :=  ...\N4Daily.dat

B1 :=  ...\B1Daily.dat

##### Water Levels at Temperature Probes:

N1DTW :=  ...\N1DTW.csv

N2DTW :=  ...\N2DTW.csv

N3DTW :=  ...\N3DTW.csv

#### Parameter Inputs:

Number of days:  $N := N_{\text{data}} = 373$   
 $i := 1..N - 2$   
 $\Delta t := 1\text{day}$

##### Depths:

$z_1 := 0.5\text{ft}$   
 $z_2 := 1\text{ft}$   
 $z_3 := 10\text{ft}$   
 $z_4 := 12\text{ft}$   
 $z_5 := 19\text{ft}$   
 $z_6 := 27\text{ft}$   
 $z_7 := 35\text{ft}$   
 $z_8 := 37\text{ft}$   
 $b := z_7 - z_3$

##### Other:

$n := 0.25$   
 $S_{\text{wfc}} := 0.1$   
 $S_{\text{w}} := 1$   
 $L_{\text{w}} := 2257000 \frac{\text{J}}{\text{kg}}$   
 $\rho_{\text{wv}} := 23 \frac{\text{gm}}{\text{m}^3}$   
 $L_{\text{o}} := L_{\text{w}} \cdot \rho_{\text{wv}} = 51911 \text{ Pa}$

##### Reference Volume Characteristics:

$w := 1\text{ft}$   
 $L := 1000\text{-ft}$   
 $K_{\text{sat}} := 0.005 \frac{\text{cm}}{\text{s}}$   
 $L_{\text{o}} = 51911 \cdot \frac{\text{J}}{\text{m}^3}$

### Average Saturated Thickness:

$$B_{\text{sat}} := \begin{cases} \text{for } i \in 1..N \\ B_{\text{sat}_i} \leftarrow z_7 - \frac{N1DTW_i + N2DTW_i + N3DTW_i}{3} \cdot \text{ft} \\ B_{\text{sat}} \end{cases}$$

### Thermal Conductivities:

#### Unsaturated Zone:

$$\kappa_{\text{unsat}} := 0.0023 \cdot \frac{\text{cal}}{\text{cm} \cdot \text{sec}}$$

$$\kappa_{\text{unsat}} = 0.963 \cdot \frac{\text{W}}{\text{m}}$$

#### Saturated Zone:

$$\kappa_{\text{sat}} := 0.0035 \cdot \frac{\text{cal}}{\text{cm} \cdot \text{sec}}$$

$$\kappa_{\text{sat}} = 1.465 \cdot \frac{\text{W}}{\text{m}}$$

### Heat Capacities:

$$\rho_s := 2.65 \cdot \frac{\text{gm}}{\text{cm}^3} \quad c_s := 44.4 \cdot \frac{\text{J}}{\text{mol}} \cdot \frac{\text{mol}}{60.08 \cdot \text{gm}} \quad C_s := c_s \cdot \rho_s$$

$$\rho_w := 1 \cdot \frac{\text{gm}}{\text{cm}^3} \quad c_w := 4.1855 \cdot \frac{1000\text{J}}{\text{kg}} \quad C_w := c_w \cdot \rho_w$$

$$\rho_a := 1.205 \cdot \frac{\text{kg}}{\text{m}^3} \quad c_a := 1.005 \cdot \frac{1000\text{J}}{\text{kg}} \quad C_a := c_a \cdot \rho_a$$

#### Unsaturated Zone:

$$C_{\text{unsat}} := [(1 - n) \cdot c_s \cdot \rho_s + n \cdot S_{\text{wfc}} \cdot c_w \cdot \rho_w + (n - S_{\text{wfc}}) \cdot c_a \cdot \rho_a]$$

$$C_{\text{unsat}} = 1573610.765 \cdot \frac{\text{J}}{\text{m}^3}$$

#### Saturated Zone:

$$C_{\text{sat}} := [(1 - n) \cdot c_s \cdot \rho_s + n \cdot S_w \cdot c_w \cdot \rho_w + (n - S_w) \cdot c_a \cdot \rho_a]$$

$$C_{\text{sat}} = 2514258.342 \cdot \frac{\text{J}}{\text{m}^3}$$

## Groundwater Gradient and Direction

Well Coordinates

Water levels in four wells

$$M_{xy} := \begin{pmatrix} 2275519.91 & 312281.22 \\ 2276249.95 & 310350.91 \\ 2276366.24 & 312003.41 \\ 2275123.03 & 310382.84 \end{pmatrix}$$

wl :=



.. \D... \WLdata.csv

$N_{data} := \text{cols}(wl) = 373$      $j := 1..N_{data}$

XX := for j ∈ 1..N<sub>data</sub>

$$zz \leftarrow \begin{pmatrix} wl_{1,j} \\ wl_{2,j} \\ wl_{3,j} \\ wl_{4,j} \end{pmatrix}$$

$R \leftarrow \text{regress}(M_{xy}, zz, 1)$

$\text{Slope}_x \leftarrow R_4$

$\text{Slope}_y \leftarrow R_5$

$ZZ_{j,1} \leftarrow \text{Slope}_x$

$ZZ_{j,2} \leftarrow \text{Slope}_y$

$ZZ_{j,3} \leftarrow \sqrt{\text{Slope}_x^2 + \text{Slope}_y^2}$

$ZZ_{j,4} \leftarrow \text{atan}\left(\frac{-\text{Slope}_y}{-\text{Slope}_x}\right)$  if  $\text{Slope}_x \leq 0 \wedge \text{Slope}_y \leq 0$

$ZZ_{j,4} \leftarrow \text{atan}\left(\frac{\text{Slope}_x}{-\text{Slope}_y}\right) + \frac{\pi}{2}$  if  $\text{Slope}_x > 0 \wedge \text{Slope}_y \leq 0$

$ZZ_{j,4} \leftarrow \text{atan}\left(\frac{\text{Slope}_y}{\text{Slope}_x}\right) + \pi$  if  $\text{Slope}_x \geq 0 \wedge \text{Slope}_y \geq 0$

$ZZ_{j,4} \leftarrow \text{atan}\left(\frac{-\text{Slope}_x}{\text{Slope}_y}\right) + \frac{3 \cdot \pi}{2}$  if  $\text{Slope}_x \leq 0 \wedge \text{Slope}_y \geq 0$

ZZ

$\theta_j := XX_{j,4}$

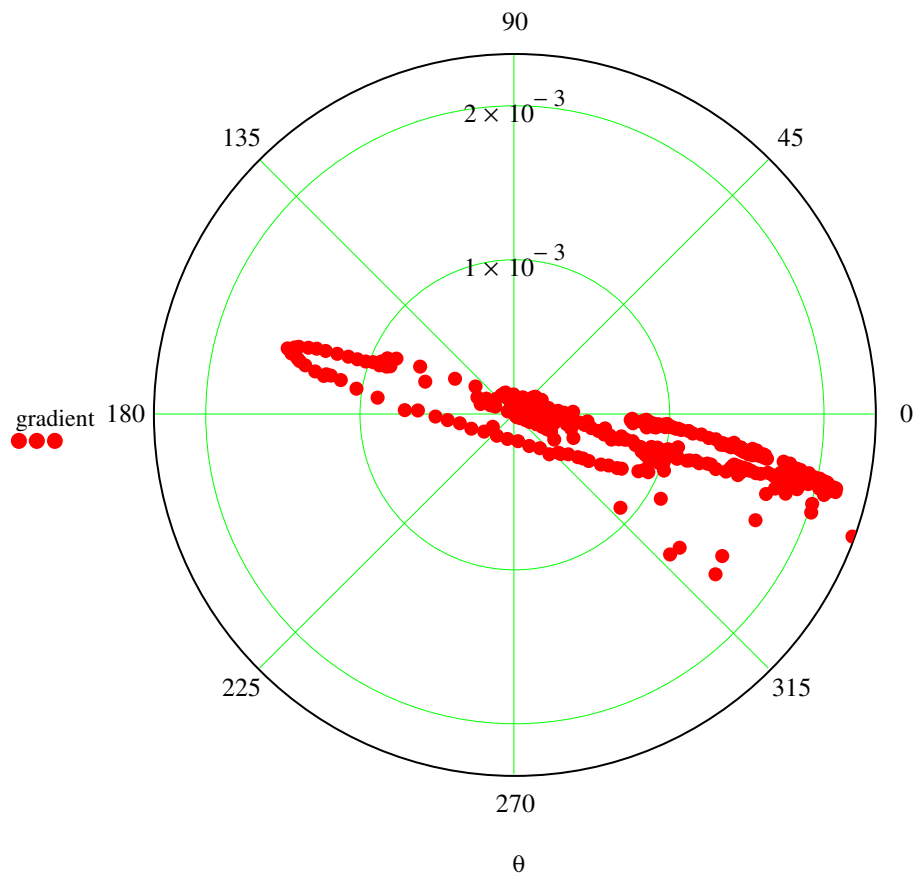
$\text{gradient}_j := XX_{j,3}$

	1
1	5.898
2	0.456
3	0.427
4	6.091
5	0.498
6	6.032
7	0.466
8	0.557
9	0.674
10	0.698
11	0.717
12	0.717
13	0.641
14	0.534
15	0.492
16	...

$\theta =$

	1
1	$4.1581 \cdot 10^{-4}$
2	$1.7425 \cdot 10^{-4}$
3	$1.8121 \cdot 10^{-4}$
4	$3.4782 \cdot 10^{-4}$
5	$1.8932 \cdot 10^{-4}$
6	$3.8325 \cdot 10^{-4}$
7	$2.0227 \cdot 10^{-4}$
8	$1.8383 \cdot 10^{-4}$
9	$1.7832 \cdot 10^{-4}$
10	$1.665 \cdot 10^{-4}$
11	$1.5701 \cdot 10^{-4}$
12	$1.4476 \cdot 10^{-4}$
13	$1.474 \cdot 10^{-4}$
14	$1.4972 \cdot 10^{-4}$
15	$1.5872 \cdot 10^{-4}$
16	...

gradient =



## Storage Calculations:

$$d := \begin{pmatrix} -0.5 \\ -1 \\ -10 \\ -12 \\ -19 \\ -27 \\ -35 \\ -37 \end{pmatrix}$$

M := augment(d)

p := 4

$$\text{AN1} := \left| \begin{array}{l} \text{for } i \in 1..N \\ \quad \text{T11} \leftarrow \left| \begin{array}{l} \text{for } p \in 1..8 \\ \quad \text{XX}_{p,i} \leftarrow N1_{i,p+1} \\ \quad \text{XX} \end{array} \right. \\ \text{T11} \end{array} \right.$$

$$\text{AN2} := \left| \begin{array}{l} \text{for } i \in 1..N \\ \quad \text{T11} \leftarrow \left| \begin{array}{l} \text{for } p \in 1..8 \\ \quad \text{XX}_{p,i} \leftarrow N2_{i,p+1} \\ \quad \text{XX} \end{array} \right. \\ \text{T11} \end{array} \right.$$

$$\text{AN5} := \left| \begin{array}{l} \text{for } i \in 1..N \\ \quad \text{T55} \leftarrow \left| \begin{array}{l} \text{for } p \in 1..8 \\ \quad \text{XX}_{p,i} \leftarrow B1_{i,p+1} \\ \quad \text{XX} \end{array} \right. \\ \text{T55} \end{array} \right.$$

$$\text{AN5} := \left| \begin{array}{l} \text{for } i \in 1..N \\ \quad \text{T55} \leftarrow \left| \begin{array}{l} \text{for } p \in 1..8 \\ \quad \text{XX}_{p,i} \leftarrow B1_{i,p+1} \\ \quad \text{XX} \end{array} \right. \\ \text{T55} \end{array} \right.$$

$$\text{N1S} := \left| \begin{array}{l} \text{for } j \in 1..N \\ \quad \text{C} \leftarrow \text{AN1}^{\langle j \rangle} \\ \quad \text{D} \leftarrow \text{AN5}^{\langle j \rangle} \\ \quad \text{E} \leftarrow \text{regress}(M, C, p) \\ \quad \text{F} \leftarrow \text{regress}(M, D, p) \\ \quad \text{G}(x) \leftarrow \text{interp}[E, M, C, (x)] \\ \quad \text{H}(x) \leftarrow \text{interp}[F, M, D, (x)] \\ \quad \text{I} \leftarrow \left| \begin{array}{l} \text{for } i \in -0.5, -0.6.. -37 \\ \quad \text{XX} \leftarrow \int_{-10}^{-35} G(i) \, di \\ \quad \text{XX} \end{array} \right. \\ \quad \text{J} \leftarrow \left| \begin{array}{l} \text{for } i \in -0.5, -0.6.. -37 \\ \quad \text{XX} \leftarrow \int_{-10}^{-35} H(i) \, di \\ \quad \text{XX} \end{array} \right. \\ \quad \text{K}_j \leftarrow -(I - J)ft \\ \text{K} \end{array} \right.$$

$$\text{N2S} := \left| \begin{array}{l} \text{for } j \in 1..N \\ \quad \text{C} \leftarrow \text{AN2}^{\langle j \rangle} \\ \quad \text{D} \leftarrow \text{AN5}^{\langle j \rangle} \\ \quad \text{E} \leftarrow \text{regress}(M, C, p) \\ \quad \text{F} \leftarrow \text{regress}(M, D, p) \\ \quad \text{G}(x) \leftarrow \text{interp}[E, M, C, (x)] \\ \quad \text{H}(x) \leftarrow \text{interp}[F, M, D, (x)] \\ \quad \text{I} \leftarrow \left| \begin{array}{l} \text{for } i \in -0.5, -0.6.. -37 \\ \quad \text{XX} \leftarrow \int_{-10}^{-35} G(i) \, di \\ \quad \text{XX} \end{array} \right. \\ \quad \text{J} \leftarrow \left| \begin{array}{l} \text{for } i \in -0.5, -0.6.. -37 \\ \quad \text{XX} \leftarrow \int_{-10}^{-35} H(i) \, di \\ \quad \text{XX} \end{array} \right. \\ \quad \text{K}_j \leftarrow -(I - J)ft \\ \text{K} \end{array} \right.$$

```

AN3 := | for i ∈ 1..N
      | T11 ← | for p ∈ 1..8
      |       | XXp,i ← N3i,p+1
      |       | XX
      | T11

```

```

AN4 := | for i ∈ 1..N
      | T11 ← | for p ∈ 1..8
      |       | XXp,i ← N4i,p+1
      |       | XX
      | T11

```

```

AN5 := | for i ∈ 1..N
      | T55 ← | for p ∈ 1..8
      |       | XXp,i ← B1i,p+1
      |       | XX
      | T55

```

```

AN5 := | for i ∈ 1..N
      | T55 ← | for p ∈ 1..8
      |       | XXp,i ← B1i,p+1
      |       | XX
      | T55

```

```

N3S := | for j ∈ 1..N
      | C ← AN3<j>
      | D ← AN5<j>
      | E ← regress(M, C, p)
      | F ← regress(M, D, p)
      | G(x) ← interp[E, M, C, (x)]
      | H(x) ← interp[F, M, D, (x)]
      | I ← | for i ∈ -0.5, -0.6.. -37
      |     | XX ← ∫-10-35 G(i) di
      |     | XX
      | J ← | for i ∈ -0.5, -0.6.. -37
      |     | XX ← ∫-10-35 H(i) di
      |     | XX
      | Kj ← -(I - J) ft
      | K

```

```

N4S := | for j ∈ 1..N
      | C ← AN4<j>
      | D ← AN5<j>
      | E ← regress(M, C, p)
      | F ← regress(M, D, p)
      | G(x) ← interp[E, M, C, (x)]
      | H(x) ← interp[F, M, D, (x)]
      | I ← | for i ∈ -0.5, -0.6.. -37
      |     | XX ← ∫-10-35 G(i) di
      |     | XX
      | J ← | for i ∈ -0.5, -0.6.. -37
      |     | XX ← ∫-10-35 H(i) di
      |     | XX
      | Kj ← -(I - J) ft
      | K

```

### Background Corrected Temperatures:

$$T_{c05ft} := \left| \begin{array}{l} \text{for } i \in 1..N-2 \\ \left| \begin{array}{l} N_{avg05_i} \leftarrow \frac{N1_{i,2} + N2_{i,2} + N3_{i,2}}{3} \\ N_{avg05ft_i} \leftarrow N_{avg05_i} - B1_{i,2} \end{array} \right. \\ N_{avg05ft} \end{array} \right.$$

$$T_{c19ft} := \left| \begin{array}{l} \text{for } i \in 1..N-2 \\ \left| \begin{array}{l} N_{avg19_i} \leftarrow \frac{N1_{i,6} + N2_{i,6} + N3_{i,6}}{3} \\ N_{avg19ft_i} \leftarrow N_{avg19_i} - B1_{i,6} \end{array} \right. \\ N_{avg19ft} \end{array} \right.$$

$$T_{c1ft} := \left| \begin{array}{l} \text{for } i \in 1..N-2 \\ \left| \begin{array}{l} N_{avg1_i} \leftarrow \frac{N1_{i,3} + N2_{i,3} + N3_{i,3}}{3} \\ N_{avg1ft_i} \leftarrow N_{avg1_i} - B1_{i,3} \end{array} \right. \\ N_{avg1ft} \end{array} \right.$$

$$T_{c27ft} := \left| \begin{array}{l} \text{for } i \in 1..N-2 \\ \left| \begin{array}{l} N_{avg27_i} \leftarrow \frac{N1_{i,7} + N2_{i,7} + N3_{i,7}}{3} \\ N_{avg27ft_i} \leftarrow N_{avg27_i} - B1_{i,7} \end{array} \right. \\ N_{avg27ft} \end{array} \right.$$

$$T_{c10ft} := \left| \begin{array}{l} \text{for } i \in 1..N-2 \\ \left| \begin{array}{l} N_{avg10_i} \leftarrow \frac{N1_{i,4} + N2_{i,4} + N3_{i,4}}{3} \\ N_{avg10ft_i} \leftarrow N_{avg10_i} - B1_{i,4} \end{array} \right. \\ N_{avg10ft} \end{array} \right.$$

$$T_{c35ft} := \left| \begin{array}{l} \text{for } i \in 1..N-2 \\ \left| \begin{array}{l} N_{avg35_i} \leftarrow \frac{N1_{i,8} + N2_{i,8} + N3_{i,8}}{3} \\ N_{avg35ft_i} \leftarrow N_{avg35_i} - B1_{i,8} \end{array} \right. \\ N_{avg35ft} \end{array} \right.$$

$$T_{c12ft} := \left| \begin{array}{l} \text{for } i \in 1..N-2 \\ \left| \begin{array}{l} N_{avg12_i} \leftarrow \frac{N1_{i,5} + N2_{i,5} + N3_{i,5}}{3} \\ N_{avg12ft_i} \leftarrow N_{avg12_i} - B1_{i,5} \end{array} \right. \\ N_{avg12ft} \end{array} \right.$$

$$T_{c37ft} := \left| \begin{array}{l} \text{for } i \in 1..N-2 \\ \left| \begin{array}{l} N_{avg37_i} \leftarrow \frac{N1_{i,9} + N2_{i,9} + N3_{i,9}}{3} \\ N_{avg37ft_i} \leftarrow N_{avg37_i} - B1_{i,9} \end{array} \right. \\ N_{avg37ft} \end{array} \right.$$

### Average Temperature Difference Between Background and Reference Volume:

$$T_c := \left| \begin{array}{l} \text{for } i \in 1..N-2 \\ \left| \begin{array}{l} N_{avg_i} \leftarrow \frac{N1_{i,9} + N2_{i,9} + N3_{i,9}}{3} \\ N_{avgsource_i} \leftarrow N_{avg_i} - B1_{i,9} \end{array} \right. \\ N_{avgsource} \end{array} \right.$$

### Fluxes due to Conduction:

$$E_{inzcond_i} := -\kappa_{unsat} \cdot \left( \frac{T_{c1ft_i} - T_{c10ft_i}}{z_3 - z_2} \right) \cdot L \cdot w \quad E_{outzcond_i} := \kappa_{sat} \cdot \left( \frac{T_{c35ft_i} - T_{c37ft_i}}{z_8 - z_7} \right) \cdot L \cdot w$$

### Flux due to Convection of Sensible Heat by Water (z):

$$E_{zconvw} := \left| \begin{array}{l} \text{for } i \in 1..N-2 \\ \left| \begin{array}{l} \text{Conv}w_{z_i} \leftarrow \left( \frac{B_{sat_i} - B_{sat_{i+1}}}{\Delta t} \right) \cdot n \cdot L \cdot w \cdot C_w \cdot T_{c_i} \text{ if } B_{sat_{i+1}} < B_{sat_i} \\ \text{Conv}w_{z_i} \leftarrow 0 \text{ otherwise} \end{array} \right. \\ \text{Conv}w_z \end{array} \right.$$

### Flux due to Convection of Sensible Heat by Vapor (z):

$$E_{zconvv} := \left| \begin{array}{l} \text{for } i \in 1..N-2 \\ \left| \begin{array}{l} \text{Conv}v_{z_i} \leftarrow \left( \frac{B_{sat_i} - B_{sat_{i+1}}}{\Delta t} \right) \cdot n \cdot L \cdot w \cdot C_a \cdot T_{c_i} \text{ if } B_{sat_i} < B_{sat_{i+1}} \\ \text{Conv}v_{z_i} \leftarrow 0 \text{ otherwise} \end{array} \right. \\ \text{Conv}v_z \end{array} \right.$$

### Flux due to Convection of Latent Heat by Vapor (z):

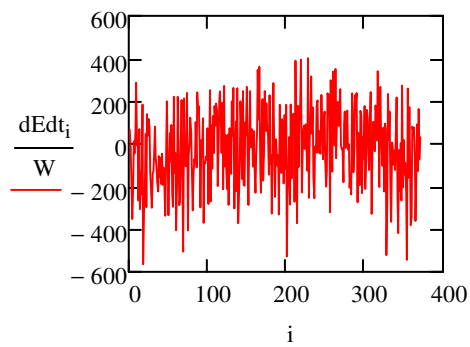
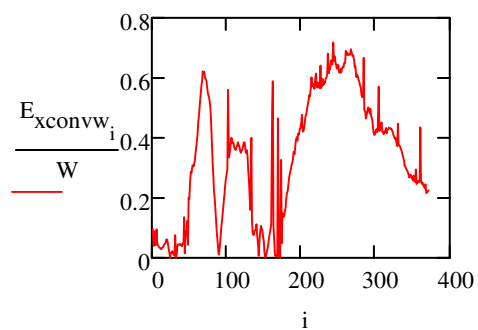
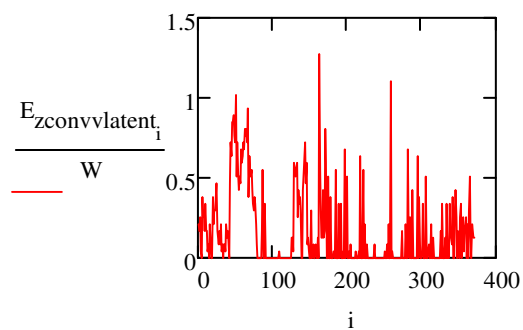
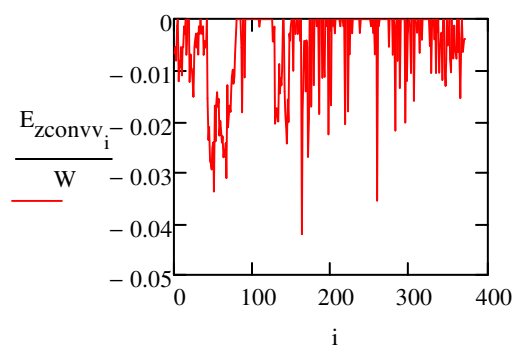
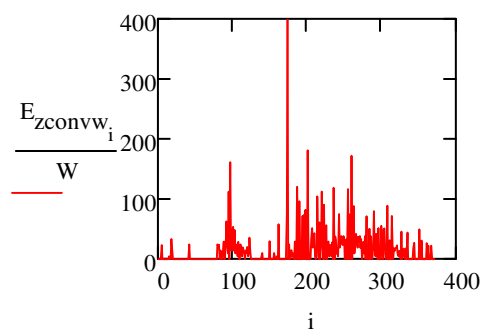
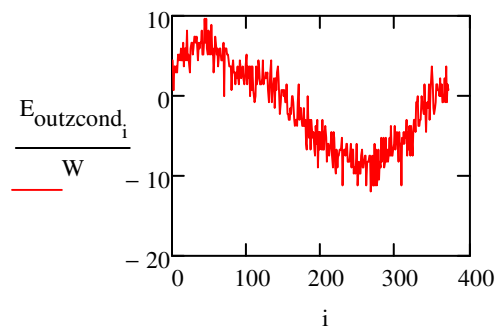
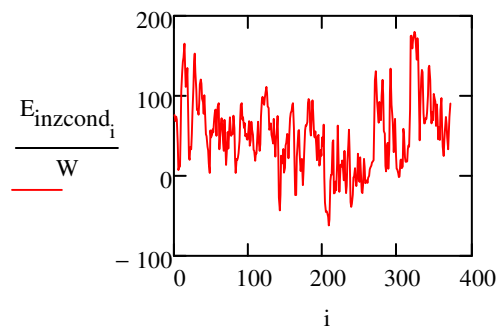
$$E_{zconvvlatent} := \left| \begin{array}{l} \text{for } i \in 1..N-2 \\ \left| \begin{array}{l} \text{Latent}vapor_i \leftarrow - \left( \frac{B_{sat_i} - B_{sat_{i+1}}}{\Delta t} \right) \cdot n \cdot L \cdot w \cdot L_w \cdot \rho_{wv} \text{ if } B_{sat_i} < B_{sat_{i+1}} \\ \text{Latent}vapor_i \leftarrow 0 \text{ otherwise} \end{array} \right. \\ \text{Latent}vapor \end{array} \right.$$

### Flux due to Convection of Sensible Heat by Water (x):

$$E_{xconvw_i} := \left| \cos(\theta)_i \right| \cdot \text{gradient}_i \cdot K_{sat} \cdot B_{sat_i} \cdot w \cdot C_w \cdot T_{c_i}$$

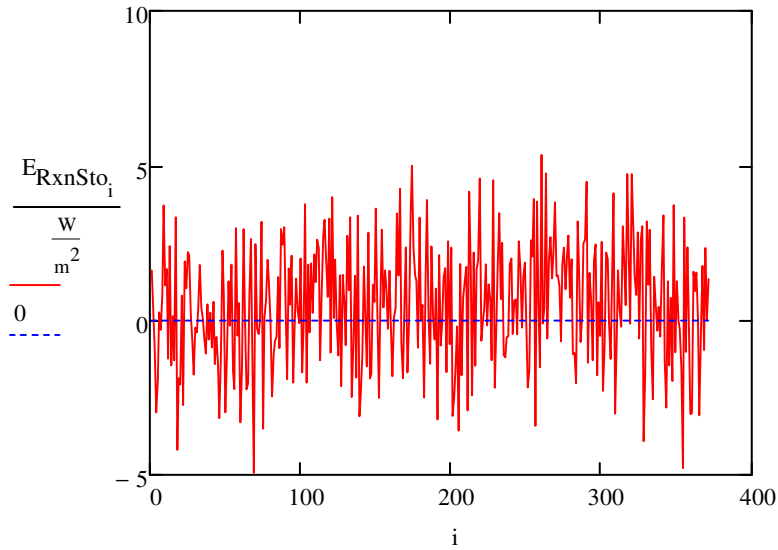
### Change in Energy:

$$dEdt_i := \left[ \left( \frac{B_{sat_i}}{b} \right) \cdot C_{sat} + \left( \frac{b - B_{sat_i}}{b} \right) \cdot C_{unsat} \right] \cdot \left[ \frac{\left( \frac{N1S_{i+1} + N2S_{i+1} + N3S_{i+1}}{3} \right) - \left( \frac{N1S_i + N2S_i + N3S_i}{3} \right)}{\Delta t} \right] \cdot L \cdot w$$



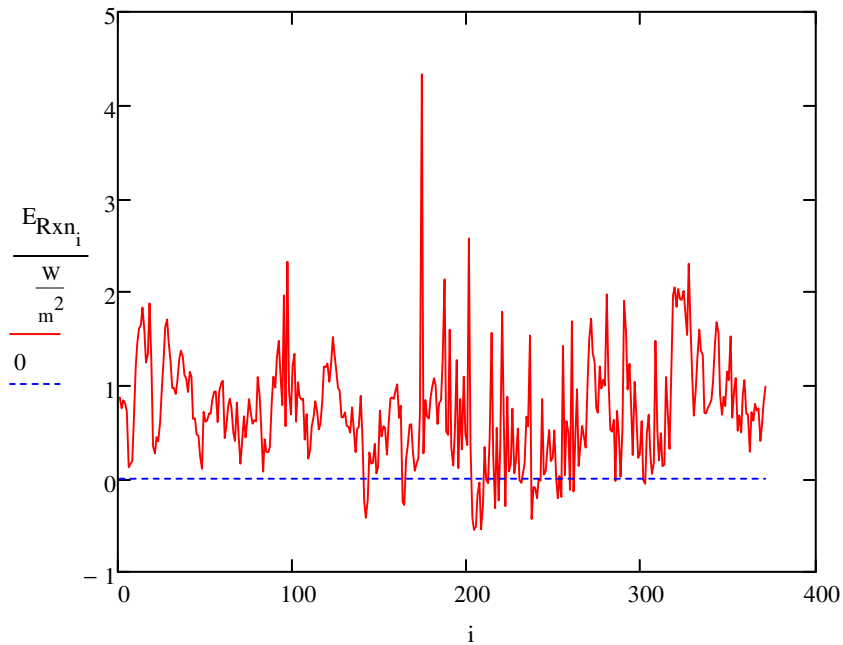
**Flux Due to Reactions**  
**Background Flux Method with Storage:**

$$E_{RxnSto} := \frac{E_{xconvw} + E_{inzcond} + E_{zconvw} + E_{outzcond} + E_{zconvv} + E_{zconvvlatent} + dEdt}{L \cdot w}$$



**Flux Due to Reactions**  
**Background Flux Method without Storage:**

$$E_{Rxn} := \frac{E_{xconvw} + E_{inzcond} + E_{zconvw} + E_{outzcond} + E_{zconvv} + E_{zconvvlatent}}{L \cdot w}$$



## Loss Rate:

### Decane Properties:

$$\Delta G_{\text{rdecane}} := -4206550 \frac{\text{J}}{\text{mol}} \quad \Delta H_{\text{rdecane}} := -6791690 \frac{\text{J}}{\text{mol}}$$

$$\text{MW}_{\text{decane}} := 142.29 \frac{\text{gm}}{\text{mol}}$$

$$\Delta H_{\text{rdecane}\%} := \frac{\Delta H_{\text{rdecane}}}{\Delta G_{\text{rdecane}}} = 1.615$$

$$\rho_{\text{decane}} := 0.730 \frac{\text{gm}}{\text{cm}^3}$$

### Heat Due to Reactions:

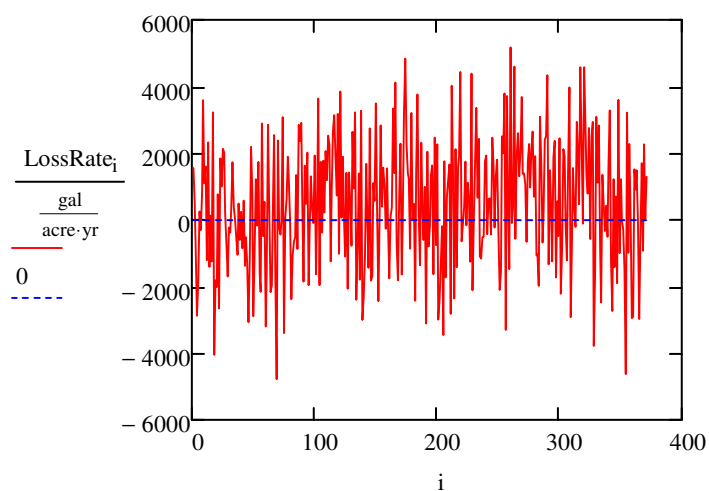
$$\Delta G_{\text{rXdecane}} := -662000 \frac{\text{J}}{\text{mol}} \quad Y_{\text{XD}} := 0.268$$

$$\text{Adjusted}\Delta G_{\text{rdecane}} := \Delta G_{\text{rXdecane}} \cdot Y_{\text{XD}} \cdot 10 = -1774160 \frac{\text{J}}{\text{mol}}$$

$$\Delta H_{\text{T}} := \text{Adjusted}\Delta G_{\text{rdecane}} \cdot \Delta H_{\text{rdecane}\%} = -2864472.009 \frac{\text{J}}{\text{mol}}$$

### Decane Loss Rate without Storage:

$$\text{LossRate} := \frac{-E_{\text{RxnSto}} \cdot \text{MW}_{\text{decane}}}{\Delta H_{\text{rdecane}} \cdot \rho_{\text{decane}}}$$



	1	
1	1567.735	
2	490.274	
3	-831.893	
4	-2874.802	
5	-1856.641	
6	256.675	
7	-295.92	
8	805.173	· $\frac{\text{gal}}{\text{acre}\cdot\text{yr}}$
9	3600.853	
10	1101.267	
11	1609.004	
12	-1195.969	
13	2332.647	
14	-1401.84	
15	132.206	
16	...	

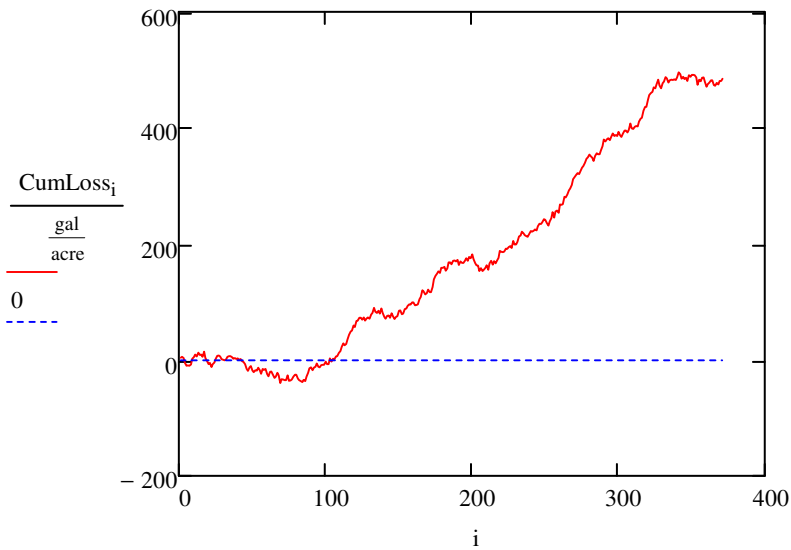
$$\text{AvgLossRate} := \frac{\sum_i \text{LossRate}_i}{N}$$

$$\text{AvgLossRate} = 475.119 \frac{\text{gal}}{\text{acre}\cdot\text{yr}}$$

## Cumulative Losses:

$$\text{cumsum}(v) := \begin{cases} w_{\text{ORIGIN}} \leftarrow v_{\text{ORIGIN}} \\ \text{for } k \in \text{ORIGIN} + 1 \dots \text{last}(v) \\ w_k \leftarrow w_{k-1} + v_k \\ w \end{cases}$$

CumLoss := cumsum(LossRate) · 1·day



	1
1	4.292
2	5.635
3	3.357
4	-4.514
5	-9.597
6	-8.895
7	-9.705
8	-7.5
9	2.359
10	5.374
11	9.779
12	6.505
13	12.891
14	9.053
15	9.415
16	...

CumLoss =  $\frac{\text{gal}}{\text{acre}}$

.....\bkgdailylossrates.csv

LossRate  
 $\frac{\text{gal}}{\text{acre} \cdot \text{yr}}$

....\bkgcumloss.csv

CumLoss  
 $\frac{\text{gal}}{\text{acre}}$

## 8.2. Thermal NSZD Rate Model Using Simple Analytical Model

### Data Input Files:

#### Temperature Probes:

N1 :=  ...\
 N2 :=  C:\Cs...\N2Daily\_corrected.txt  
 N3 :=  C:\Cs...\N3Daily\_corrected.txt  
 N4 :=  ...\

#### Water Levels at Temperature Probes:

N1DTW :=  ...\
 N2DTW :=  ...\
 N3DTW :=  ...\

### Parameter Inputs:

Number of days:  $N := N_{\text{data}} = 373$   
 $i := 1..N - 2$   
 $\Delta t := 1\text{day}$

#### Depths:

$z_1 := 0.5\text{ft}$   
 $z_2 := 1\text{ft}$   
 $z_3 := 10\text{ft}$   
 $z_4 := 12\text{ft}$   
 $z_5 := 19\text{ft}$   
 $z_6 := 27\text{ft}$   
 $z_7 := 35\text{ft}$   
 $z_8 := 37\text{ft}$   
 $b := z_7 - z_3$

#### Other:

$n := 0.25$   
 $S_{\text{wfc}} := 0.1$   
 $S_{\text{w}} := 1$   
 $L_{\text{w}} := 2257000 \frac{\text{J}}{\text{kg}}$   
 $\rho_{\text{wv}} := 23 \frac{\text{gm}}{\text{m}^3}$   
 $L_{\text{o}} := L_{\text{w}} - \rho_{\text{wv}} = 51911 \text{Pa}$

#### Reference Volume Characteristics:

$w := 1\text{ft}$   
 $L := 1000\text{-ft}$   
 $K_{\text{sat}} := 0.005 \frac{\text{cm}}{\text{s}}$

**Average Saturated Thickness:**

$$B_{\text{sat}} := \begin{cases} \text{for } i \in 1..N \\ B_{\text{sat}_i} \leftarrow z_7 - \frac{N1DTW_i + N2DTW_i + N3DTW_i}{3} \cdot \text{ft} \\ B_{\text{sat}} \end{cases}$$

**Thermal Conductivities:**

**Unsaturated Zone:**

$$\kappa_{\text{unsat}} := 0.0023 \cdot \frac{\text{cal}}{\text{cm} \cdot \text{sec}}$$

$$\kappa_{\text{unsat}} = 0.963 \cdot \frac{\text{W}}{\text{m}}$$

**Saturated Zone:**

$$\kappa_{\text{sat}} := 0.0035 \cdot \frac{\text{cal}}{\text{cm} \cdot \text{sec}}$$

$$\kappa_{\text{sat}} = 1.465 \cdot \frac{\text{W}}{\text{m}}$$

**Heat Capacities:**

$$\rho_s := 2.65 \cdot \frac{\text{gm}}{\text{cm}^3} \quad c_s := 44.4 \cdot \frac{\text{J}}{\text{mol}} \cdot \frac{\text{mol}}{60.08 \cdot \text{gm}} \quad C_s := c_s \cdot \rho_s$$

$$\rho_w := 1 \cdot \frac{\text{gm}}{\text{cm}^3} \quad c_w := 4.1855 \cdot \frac{1000\text{J}}{\text{kg}} \quad C_w := c_w \cdot \rho_w$$

$$\rho_a := 1.205 \cdot \frac{\text{kg}}{\text{m}^3} \quad c_a := 1.005 \cdot \frac{1000\text{J}}{\text{kg}} \quad C_a := c_a \cdot \rho_a$$

**Unsaturated Zone:**

$$C_{\text{unsat}} := [(1 - n) \cdot c_s \cdot \rho_s + n \cdot S_{\text{wfc}} \cdot c_w \cdot \rho_w + (n - S_{\text{wfc}}) \cdot c_a \cdot \rho_a]$$

$$C_{\text{unsat}} = 1573610.765 \cdot \frac{\text{J}}{\text{m}^3}$$

**Saturated Zone:**

$$C_{\text{sat}} := [(1 - n) \cdot c_s \cdot \rho_s + n \cdot S_w \cdot c_w \cdot \rho_w + (n - S_w) \cdot c_a \cdot \rho_a]$$

$$C_{\text{sat}} = 2514258.342 \cdot \frac{\text{J}}{\text{m}^3}$$

## Groundwater Gradient and Direction

Well Coordinates

Water levels in four wells

$$M_{xy} := \begin{pmatrix} 2275519.91 & 312281.22 \\ 2276249.95 & 310350.91 \\ 2276366.24 & 312003.41 \\ 2275123.03 & 310382.84 \end{pmatrix}$$

wl :=



..\D...\WLdata.csv

$N_{data} := \text{cols}(wl) = 373 \quad j := 1..N_{data}$

XX := for j ∈ 1..N<sub>data</sub>

$$zz \leftarrow \begin{pmatrix} wl_{1,j} \\ wl_{2,j} \\ wl_{3,j} \\ wl_{4,j} \end{pmatrix}$$

R ← regress( $M_{xy}$ , zz, 1)

Slope<sub>x</sub> ← R<sub>4</sub>

Slope<sub>y</sub> ← R<sub>5</sub>

ZZ<sub>j,1</sub> ← Slope<sub>x</sub>

ZZ<sub>j,2</sub> ← Slope<sub>y</sub>

ZZ<sub>j,3</sub> ←  $\sqrt{\text{Slope}_x^2 + \text{Slope}_y^2}$

ZZ<sub>j,4</sub> ←  $\text{atan}\left(\frac{-\text{Slope}_y}{-\text{Slope}_x}\right)$  if Slope<sub>x</sub> ≤ 0 ∧ Slope<sub>y</sub> ≤ 0

ZZ<sub>j,4</sub> ←  $\text{atan}\left(\frac{\text{Slope}_x}{-\text{Slope}_y}\right) + \frac{\pi}{2}$  if Slope<sub>x</sub> > 0 ∧ Slope<sub>y</sub> ≤ 0

ZZ<sub>j,4</sub> ←  $\text{atan}\left(\frac{\text{Slope}_y}{\text{Slope}_x}\right) + \pi$  if Slope<sub>x</sub> ≥ 0 ∧ Slope<sub>y</sub> ≥ 0

ZZ<sub>j,4</sub> ←  $\text{atan}\left(\frac{-\text{Slope}_x}{\text{Slope}_y}\right) + \frac{3 \cdot \pi}{2}$  if Slope<sub>x</sub> ≤ 0 ∧ Slope<sub>y</sub> > 0

ZZ

$\theta_j := XX_{j,4}$

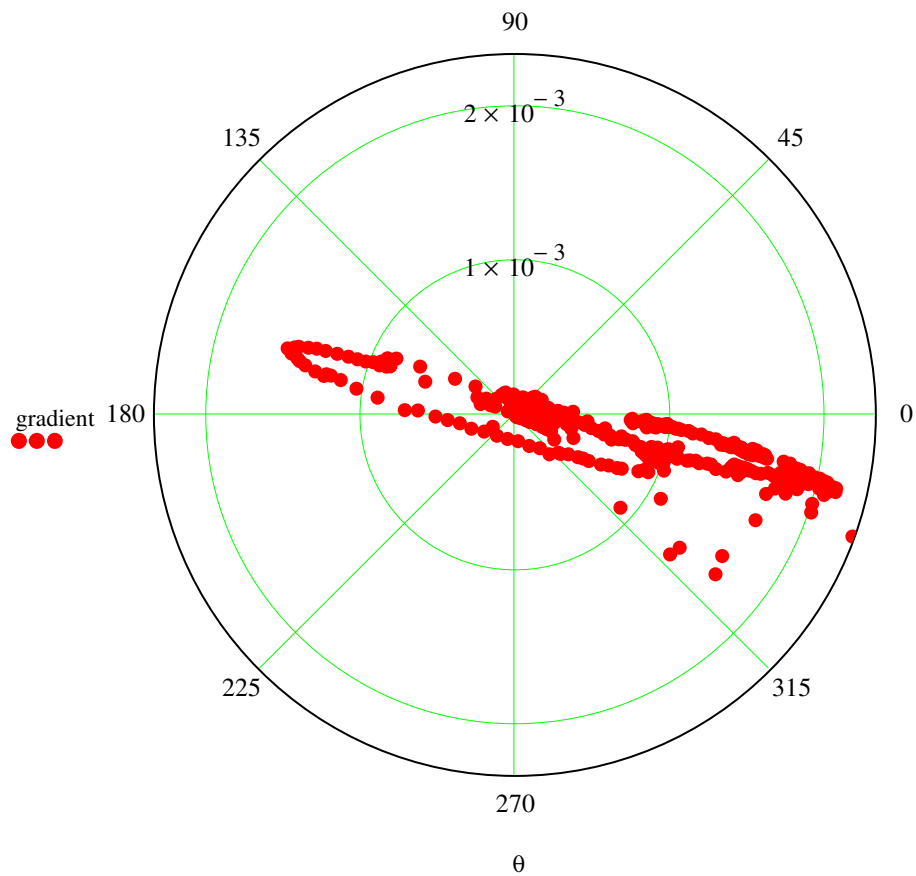
gradient<sub>j</sub> := XX<sub>j,3</sub>

	1
1	5.898
2	0.456
3	0.427
4	6.091
5	0.498
6	6.032
7	0.466
8	0.557
9	0.674
10	0.698
11	0.717
12	0.717
13	0.641
14	0.534
15	0.492
16	...

$\theta =$

	1
1	$4.1581 \cdot 10^{-4}$
2	$1.7425 \cdot 10^{-4}$
3	$1.8121 \cdot 10^{-4}$
4	$3.4782 \cdot 10^{-4}$
5	$1.8932 \cdot 10^{-4}$
6	$3.8325 \cdot 10^{-4}$
7	$2.0227 \cdot 10^{-4}$
8	$1.8383 \cdot 10^{-4}$
9	$1.7832 \cdot 10^{-4}$
10	$1.665 \cdot 10^{-4}$
11	$1.5701 \cdot 10^{-4}$
12	$1.4476 \cdot 10^{-4}$
13	$1.474 \cdot 10^{-4}$
14	$1.4972 \cdot 10^{-4}$
15	$1.5872 \cdot 10^{-4}$
16	...

gradient =



**Carslaw Jaeger Model:**

$$T_a := 14.5 \quad A_o := 15.94 \quad t_0 := 263.5 \cdot \text{day} \quad \omega := \frac{2 \cdot \pi}{365 \cdot \text{day}}$$

$$D_{\text{Hunsat}} := \frac{\kappa_{\text{unsat}}}{C_{\text{unsat}}} = 6.1195 \times 10^{-7} \cdot \frac{\text{m}^2}{\text{s}} \quad D_{\text{Hsat}} := \frac{\kappa_{\text{sat}}}{C_{\text{sat}}} = 5.8283 \times 10^{-7} \cdot \frac{\text{m}^2}{\text{s}}$$

$$d_{\text{unsat}} := \sqrt{\frac{2 \cdot D_{\text{Hunsat}}}{\omega}} = 2.478 \text{ m} \quad d_{\text{sat}} := \sqrt{\frac{2 \cdot D_{\text{Hsat}}}{\omega}} = 2.419 \text{ m}$$

NN := for i ∈ 1..N

XX<sub>i,1</sub> ← i

$$\text{XX}_{i,2} \leftarrow T_a + A_o \cdot e^{\frac{-z_1}{d_{\text{unsat}}}} \cdot \sin \left[ \frac{2 \cdot \pi \cdot (i \cdot \text{day} - t_0)}{365 \cdot \text{day}} - \frac{z_1}{d_{\text{unsat}}} - \frac{\pi}{2} \right]$$

$$\text{XX}_{i,3} \leftarrow T_a + A_o \cdot e^{\frac{-z_2}{d_{\text{unsat}}}} \cdot \sin \left[ \frac{2 \cdot \pi \cdot (i \cdot \text{day} - t_0)}{365 \cdot \text{day}} - \frac{z_2}{d_{\text{unsat}}} - \frac{\pi}{2} \right]$$

$$\text{XX}_{i,4} \leftarrow T_a + A_o \cdot e^{\frac{-z_3}{d_{\text{unsat}}}} \cdot \sin \left[ \frac{2 \cdot \pi \cdot (i \cdot \text{day} - t_0)}{365 \cdot \text{day}} - \frac{z_3}{d_{\text{unsat}}} - \frac{\pi}{2} \right]$$

$$\text{XX}_{i,5} \leftarrow T_a + A_o \cdot e^{\frac{-z_4}{d_{\text{unsat}}}} \cdot \sin \left[ \frac{2 \cdot \pi \cdot (i \cdot \text{day} - t_0)}{365 \cdot \text{day}} - \frac{z_4}{d_{\text{unsat}}} - \frac{\pi}{2} \right]$$

$$\text{XX}_{i,6} \leftarrow T_a + A_o \cdot e^{\frac{-z_5}{d_{\text{sat}}}} \cdot \sin \left[ \frac{2 \cdot \pi \cdot (i \cdot \text{day} - t_0)}{365 \cdot \text{day}} - \frac{z_5}{d_{\text{sat}}} - \frac{\pi}{2} \right]$$

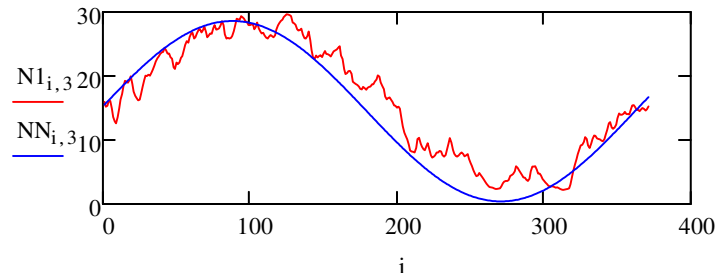
$$\text{XX}_{i,7} \leftarrow T_a + A_o \cdot e^{\frac{-z_6}{d_{\text{sat}}}} \cdot \sin \left[ \frac{2 \cdot \pi \cdot (i \cdot \text{day} - t_0)}{365 \cdot \text{day}} - \frac{z_6}{d_{\text{sat}}} - \frac{\pi}{2} \right]$$

$$\text{XX}_{i,8} \leftarrow T_a + A_o \cdot e^{\frac{-z_7}{d_{\text{sat}}}} \cdot \sin \left[ \frac{2 \cdot \pi \cdot (i \cdot \text{day} - t_0)}{365 \cdot \text{day}} - \frac{z_7}{d_{\text{sat}}} - \frac{\pi}{2} \right]$$

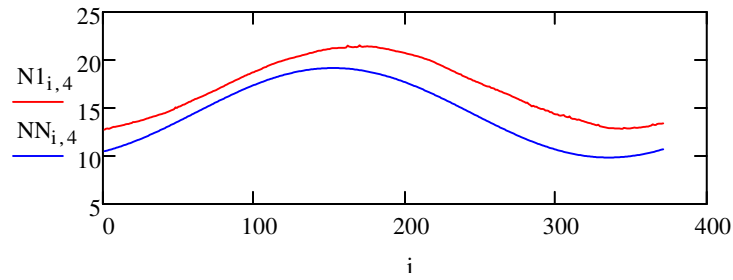
$$\text{XX}_{i,9} \leftarrow T_a + A_o \cdot e^{\frac{-z_8}{d_{\text{sat}}}} \cdot \sin \left[ \frac{2 \cdot \pi \cdot (i \cdot \text{day} - t_0)}{365 \cdot \text{day}} - \frac{z_8}{d_{\text{sat}}} - \frac{\pi}{2} \right]$$

XX

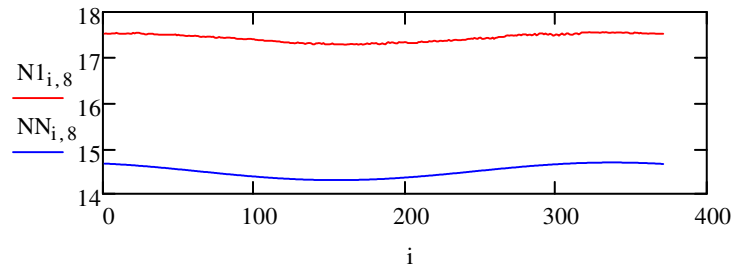
N1 vs. Model Temperatures at 1ft bgs



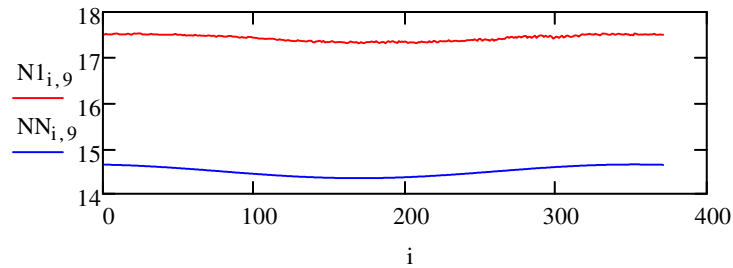
N1 vs. Model Temperatures at 10ft bgs



N1 vs. Model Temperatures at 35ft bgs



N1 vs. Model Temperatures at 37ft bgs



**Storage Calculations:**

$$d := \begin{pmatrix} -0.5 \\ -1 \\ -10 \\ -12 \\ -19 \\ -27 \\ -35 \\ -37 \end{pmatrix} \quad \begin{array}{l} M := \text{augment}(d) \\ p := 4 \end{array}$$

$$\text{AN1} := \left| \begin{array}{l} \text{for } i \in 1..N \\ \quad \text{T11} \leftarrow \left| \begin{array}{l} \text{for } p \in 1..8 \\ \quad \text{XX}_{p,i} \leftarrow N1_{i,p+1} \\ \quad \text{XX} \end{array} \right. \\ \text{T11} \end{array} \right.$$

$$\text{AN2} := \left| \begin{array}{l} \text{for } i \in 1..N \\ \quad \text{T11} \leftarrow \left| \begin{array}{l} \text{for } p \in 1..8 \\ \quad \text{XX}_{p,i} \leftarrow N2_{i,p+1} \\ \quad \text{XX} \end{array} \right. \\ \text{T11} \end{array} \right.$$

$$\text{AN5} := \left| \begin{array}{l} \text{for } i \in 1..N \\ \quad \text{T55} \leftarrow \left| \begin{array}{l} \text{for } p \in 1..8 \\ \quad \text{XX}_{p,i} \leftarrow NN_{i,p+1} \\ \quad \text{XX} \end{array} \right. \\ \text{T55} \end{array} \right.$$

$$\text{AN5} := \left| \begin{array}{l} \text{for } i \in 1..N \\ \quad \text{T55} \leftarrow \left| \begin{array}{l} \text{for } p \in 1..8 \\ \quad \text{XX}_{p,i} \leftarrow NN_{i,p+1} \\ \quad \text{XX} \end{array} \right. \\ \text{T55} \end{array} \right.$$

$$\text{N1S} := \left| \begin{array}{l} \text{for } j \in 1..N \\ \quad \text{C} \leftarrow \text{AN1}^{\langle j \rangle} \\ \quad \text{D} \leftarrow \text{AN5}^{\langle j \rangle} \\ \quad \text{E} \leftarrow \text{regress}(M, C, p) \\ \quad \text{F} \leftarrow \text{regress}(M, D, p) \\ \quad \text{G}(x) \leftarrow \text{interp}[E, M, C, (x)] \\ \quad \text{H}(x) \leftarrow \text{interp}[F, M, D, (x)] \\ \quad \text{I} \leftarrow \left| \begin{array}{l} \text{for } i \in -0.5, -0.6.. -37 \\ \quad \text{XX} \leftarrow \int_{-10}^{-35} G(i) \, di \\ \quad \text{XX} \end{array} \right. \\ \quad \text{J} \leftarrow \left| \begin{array}{l} \text{for } i \in -0.5, -0.6.. -37 \\ \quad \text{XX} \leftarrow \int_{-10}^{-35} H(i) \, di \\ \quad \text{XX} \end{array} \right. \\ \quad \text{K}_j \leftarrow -(I - J)ft \\ \text{K} \end{array} \right.$$

$$\text{N2S} := \left| \begin{array}{l} \text{for } j \in 1..N \\ \quad \text{C} \leftarrow \text{AN2}^{\langle j \rangle} \\ \quad \text{D} \leftarrow \text{AN5}^{\langle j \rangle} \\ \quad \text{E} \leftarrow \text{regress}(M, C, p) \\ \quad \text{F} \leftarrow \text{regress}(M, D, p) \\ \quad \text{G}(x) \leftarrow \text{interp}[E, M, C, (x)] \\ \quad \text{H}(x) \leftarrow \text{interp}[F, M, D, (x)] \\ \quad \text{I} \leftarrow \left| \begin{array}{l} \text{for } i \in -0.5, -0.6.. -37 \\ \quad \text{XX} \leftarrow \int_{-10}^{-35} G(i) \, di \\ \quad \text{XX} \end{array} \right. \\ \quad \text{J} \leftarrow \left| \begin{array}{l} \text{for } i \in -0.5, -0.6.. -37 \\ \quad \text{XX} \leftarrow \int_{-10}^{-35} H(i) \, di \\ \quad \text{XX} \end{array} \right. \\ \quad \text{K}_j \leftarrow -(I - J)ft \\ \text{K} \end{array} \right.$$

```

AN3 := | for i ∈ 1..N
      | T11 ← | for p ∈ 1..8
      |       | XXp,i ← N3i,p+1
      |       | XX
      | T11

```

```

AN4 := | for i ∈ 1..N
      | T11 ← | for p ∈ 1..8
      |       | XXp,i ← N4i,p+1
      |       | XX
      | T11

```

```

AN5 := | for i ∈ 1..N
      | T55 ← | for p ∈ 1..8
      |       | XXp,i ← NNi,p+1
      |       | XX
      | T55

```

```

AN5 := | for i ∈ 1..N
      | T55 ← | for p ∈ 1..8
      |       | XXp,i ← NNi,p+1
      |       | XX
      | T55

```

```

N3S := | for j ∈ 1..N
      | C ← AN3<j>
      | D ← AN5<j>
      | E ← regress(M, C, p)
      | F ← regress(M, D, p)
      | G(x) ← interp[E, M, C, (x)]
      | H(x) ← interp[F, M, D, (x)]
      | I ← | for i ∈ -0.5, -0.6.. -37
      |     | XX ← ∫-10-35 G(i) di
      |     | XX
      | J ← | for i ∈ -0.5, -0.6.. -37
      |     | XX ← ∫-10-35 H(i) di
      |     | XX
      | Kj ← -(I - J) ft
      | K

```

```

N4S := | for j ∈ 1..N
      | C ← AN4<j>
      | D ← AN5<j>
      | E ← regress(M, C, p)
      | F ← regress(M, D, p)
      | G(x) ← interp[E, M, C, (x)]
      | H(x) ← interp[F, M, D, (x)]
      | I ← | for i ∈ -0.5, -0.6.. -37
      |     | XX ← ∫-10-35 G(i) di
      |     | XX
      | J ← | for i ∈ -0.5, -0.6.. -37
      |     | XX ← ∫-10-35 H(i) di
      |     | XX
      | Kj ← -(I - J) ft
      | K

```

### Background Corrected Temperatures:

$$T_{c05ft} := \left| \begin{array}{l} \text{for } i \in 1..N-2 \\ \left| \begin{array}{l} N_{avg05_i} \leftarrow \frac{N1_{i,2} + N2_{i,2} + N3_{i,2}}{3} \\ N_{avg05ft_i} \leftarrow N_{avg05_i} - NN_{i,2} \end{array} \right. \\ N_{avg05ft} \end{array} \right.$$

$$T_{c19ft} := \left| \begin{array}{l} \text{for } i \in 1..N-2 \\ \left| \begin{array}{l} N_{avg19_i} \leftarrow \frac{N1_{i,6} + N2_{i,6} + N3_{i,6}}{3} \\ N_{avg19ft_i} \leftarrow N_{avg19_i} - NN_{i,6} \end{array} \right. \\ N_{avg19ft} \end{array} \right.$$

$$T_{c1ft} := \left| \begin{array}{l} \text{for } i \in 1..N-2 \\ \left| \begin{array}{l} N_{avg1_i} \leftarrow \frac{N1_{i,3} + N2_{i,3} + N3_{i,3}}{3} \\ N_{avg1ft_i} \leftarrow N_{avg1_i} - NN_{i,3} \end{array} \right. \\ N_{avg1ft} \end{array} \right.$$

$$T_{c27ft} := \left| \begin{array}{l} \text{for } i \in 1..N-2 \\ \left| \begin{array}{l} N_{avg27_i} \leftarrow \frac{N1_{i,7} + N2_{i,7} + N3_{i,7}}{3} \\ N_{avg27ft_i} \leftarrow N_{avg27_i} - NN_{i,7} \end{array} \right. \\ N_{avg27ft} \end{array} \right.$$

$$T_{c10ft} := \left| \begin{array}{l} \text{for } i \in 1..N-2 \\ \left| \begin{array}{l} N_{avg10_i} \leftarrow \frac{N1_{i,4} + N2_{i,4} + N3_{i,4}}{3} \\ N_{avg10ft_i} \leftarrow N_{avg10_i} - NN_{i,4} \end{array} \right. \\ N_{avg10ft} \end{array} \right.$$

$$T_{c35ft} := \left| \begin{array}{l} \text{for } i \in 1..N-2 \\ \left| \begin{array}{l} N_{avg35_i} \leftarrow \frac{N1_{i,8} + N2_{i,8} + N3_{i,8}}{3} \\ N_{avg35ft_i} \leftarrow N_{avg35_i} - NN_{i,8} \end{array} \right. \\ N_{avg35ft} \end{array} \right.$$

$$T_{c12ft} := \left| \begin{array}{l} \text{for } i \in 1..N-2 \\ \left| \begin{array}{l} N_{avg12_i} \leftarrow \frac{N1_{i,5} + N2_{i,5} + N3_{i,5}}{3} \\ N_{avg12ft_i} \leftarrow N_{avg12_i} - NN_{i,5} \end{array} \right. \\ N_{avg12ft} \end{array} \right.$$

$$T_{c37ft} := \left| \begin{array}{l} \text{for } i \in 1..N-2 \\ \left| \begin{array}{l} N_{avg37_i} \leftarrow \frac{N1_{i,9} + N2_{i,9} + N3_{i,9}}{3} \\ N_{avg37ft_i} \leftarrow N_{avg37_i} - NN_{i,9} \end{array} \right. \\ N_{avg37ft} \end{array} \right.$$

### Average Temperature Difference Between Background and Reference Volume:

$$T_c := \left| \begin{array}{l} \text{for } i \in 1..N-2 \\ \left| \begin{array}{l} N_{avg_i} \leftarrow \frac{N1_{i,9} + N2_{i,9} + N3_{i,9}}{3} \\ N_{avgsource_i} \leftarrow N_{avg_i} - NN_{i,9} \end{array} \right. \\ N_{avgsource} \end{array} \right.$$

### Fluxes due to Conduction:

$$E_{inzcond_i} := -\kappa_{unsat} \cdot \left( \frac{T_{c1ft_i} - T_{c10ft_i}}{z_3 - z_2} \right) \cdot L \cdot w \quad E_{outzcond_i} := \kappa_{sat} \cdot \left( \frac{T_{c35ft_i} - T_{c37ft_i}}{z_8 - z_7} \right) \cdot L \cdot w$$

### Flux due to Convection of Sensible Heat by Water (z):

$$E_{zconvw} := \left| \begin{array}{l} \text{for } i \in 1..N-2 \\ \left| \begin{array}{l} Ad_{bottom_i} \leftarrow \left( \frac{B_{sat_i} - B_{sat_{i+1}}}{\Delta t} \right) \cdot n \cdot L \cdot w \cdot C_w \cdot T_{c_i} \text{ if } B_{sat_{i+1}} < B_{sat_i} \\ Ad_{bottom_i} \leftarrow 0 \text{ otherwise} \end{array} \right. \\ Ad_{bottom} \end{array} \right.$$

### Flux due to Convection of Sensible Heat by Vapor (z):

$$E_{zconvv} := \left| \begin{array}{l} \text{for } i \in 1..N-2 \\ \left| \begin{array}{l} Ad_{gas_i} \leftarrow - \left( \frac{B_{sat_i} - B_{sat_{i+1}}}{\Delta t} \right) \cdot n \cdot L \cdot w \cdot C_a \cdot T_{c_i} \text{ if } B_{sat_i} < B_{sat_{i+1}} \\ Ad_{gas_i} \leftarrow 0 \text{ otherwise} \end{array} \right. \\ Ad_{gas} \end{array} \right.$$

### Flux due to Convection of Latent Heat by Vapor (z):

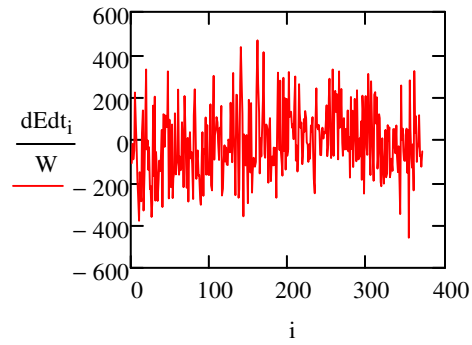
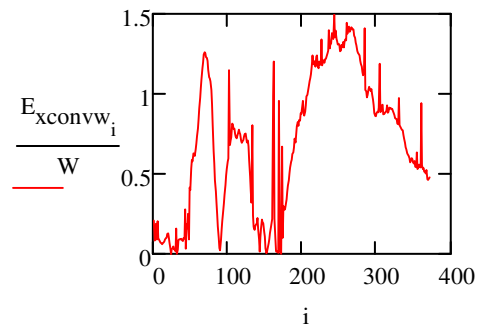
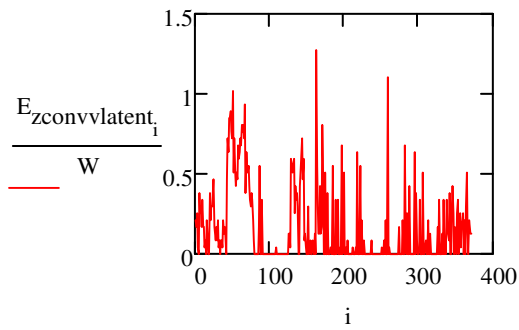
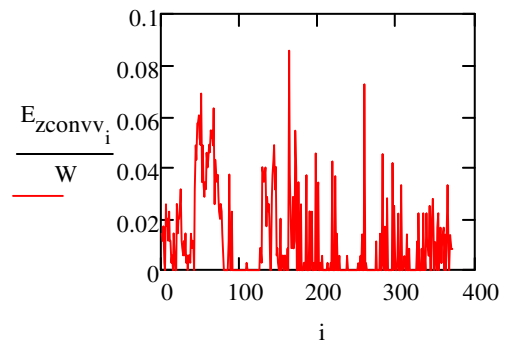
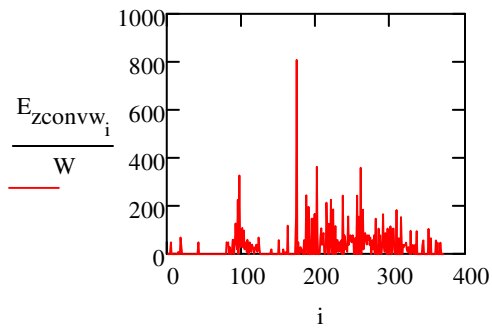
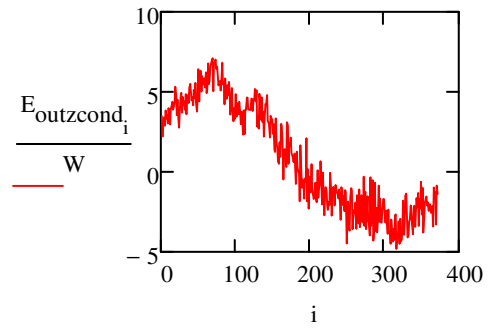
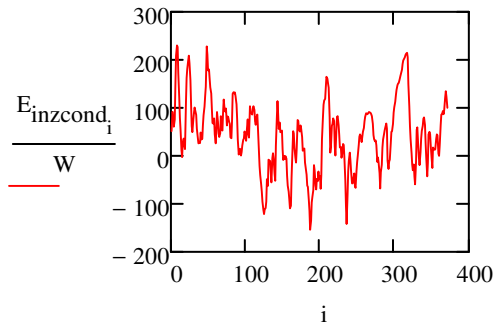
$$E_{zconvlatent} := \left| \begin{array}{l} \text{for } i \in 1..N-2 \\ \left| \begin{array}{l} Latent_{vapor_i} \leftarrow - \left( \frac{B_{sat_i} - B_{sat_{i+1}}}{\Delta t} \right) \cdot n \cdot L \cdot w \cdot L_o \text{ if } B_{sat_i} < B_{sat_{i+1}} \\ Latent_{vapor_i} \leftarrow 0 \text{ otherwise} \end{array} \right. \\ Latent_{vapor} \end{array} \right.$$

### Flux due to Convection of Sensible Heat by Water (x):

$$E_{xconvw_i} := \left| \cos(\theta)_i \right| \cdot gradient_i \cdot K_{sat} \cdot B_{sat_i} \cdot w \cdot C_w \cdot T_{c_i}$$

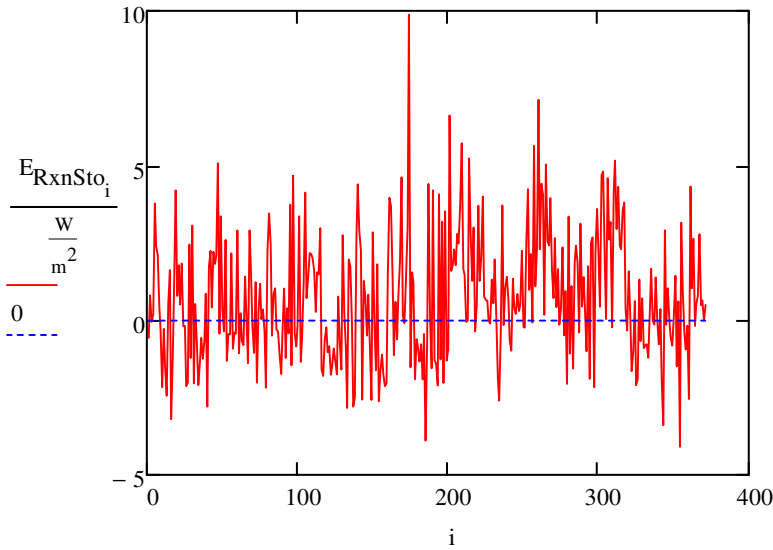
### Change in Energy:

$$dEdt_i := \left[ \left( \frac{B_{sat_i}}{b} \right) \cdot C_{sat} + \left( \frac{b - B_{sat_i}}{b} \right) \cdot C_{unsat} \right] \cdot \left[ \frac{\left( \frac{N1S_{i+1} + N2S_{i+1} + N3S_{i+1}}{3} \right) - \left( \frac{N1S_i + N2S_i + N3S_i}{3} \right)}{\Delta t} \right] \cdot L \cdot w$$



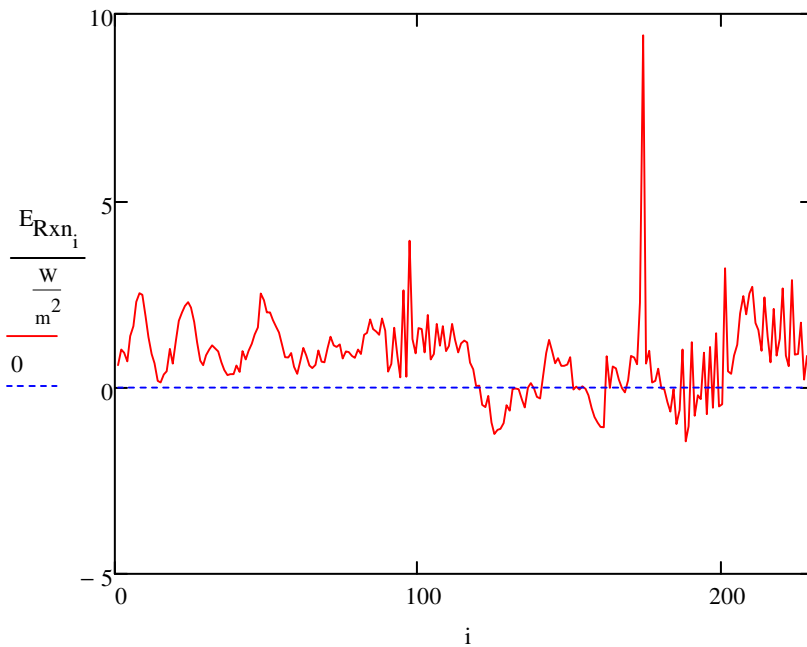
**Flux Due to Reactions**  
**Background Flux Method with Storage:**

$$E_{RxnSto_i} := \frac{E_{xconvw} + E_{inzcond} + E_{zconvw} + E_{outzcond} + E_{zconvv} + E_{zconvvlatent} + dEdt}{L \cdot w}$$



**Flux Due to Reactions**  
**Background Flux Method without Storage:**

$$E_{Rxn_i} := \frac{E_{xconvw} + E_{inzcond} + E_{zconvw} + E_{outzcond} + E_{zconvv} + E_{zconvvlatent}}{L \cdot w}$$



## Loss Rate:

### Decane Properties:

$$\Delta G_{\text{rdecane}} := -4206550 \frac{\text{J}}{\text{mol}} \quad \Delta H_{\text{rdecane}} := -6791690 \frac{\text{J}}{\text{mol}}$$

$$\Delta H_{\text{rdecane}\%} := \frac{\Delta H_{\text{rdecane}}}{\Delta G_{\text{rdecane}}} = 1.615$$

$$\text{MW}_{\text{decane}} := 142.29 \frac{\text{gm}}{\text{mol}}$$

$$\rho_{\text{decane}} := 0.730 \frac{\text{gm}}{\text{cm}^3}$$

### Heat Due to Reactions:

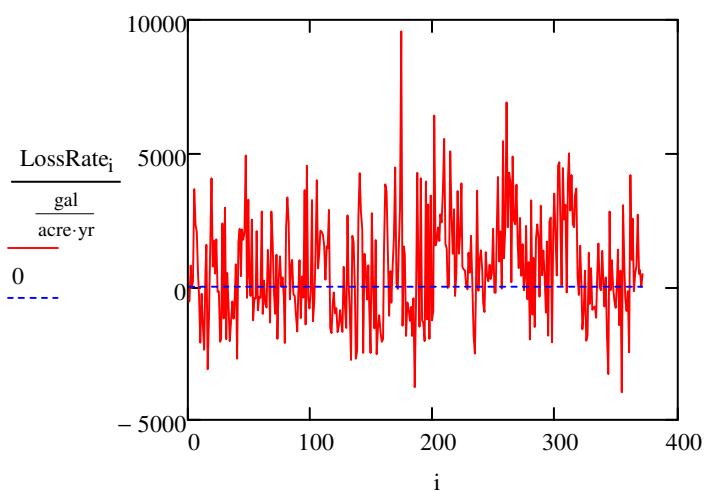
$$\Delta G_{\text{rXdecane}} := -662000 \frac{\text{J}}{\text{mol}} \quad Y_{\text{XD}} := 0.268$$

$$\text{Adjusted}\Delta G_{\text{rdecane}} := \Delta G_{\text{rXdecane}} \cdot Y_{\text{XD}} \cdot 10 = -1774160 \frac{\text{J}}{\text{mol}}$$

$$\Delta H_{\text{T}} := \text{Adjusted}\Delta G_{\text{rdecane}} \cdot \Delta H_{\text{rdecane}\%} = -2864472.009 \frac{\text{J}}{\text{mol}}$$

### Decane Loss Rate without Storage:

$$\text{LossRate} := \frac{-E_{\text{RxnSto}} \cdot \text{MW}_{\text{decane}}}{\Delta H_{\text{rdecane}} \cdot \rho_{\text{decane}}}$$



	1
1	-542.529
2	790.241
3	-39.424
4	180.809
5	3666.997
6	2335.173
7	2050.262
8	440.855
9	-334.052
10	-2091.055
11	-261.076
12	-1420.987
13	-2359.194
14	506.72
15	1579.907
16	...

LossRate =  $\frac{\text{gal}}{\text{acre}\cdot\text{yr}}$

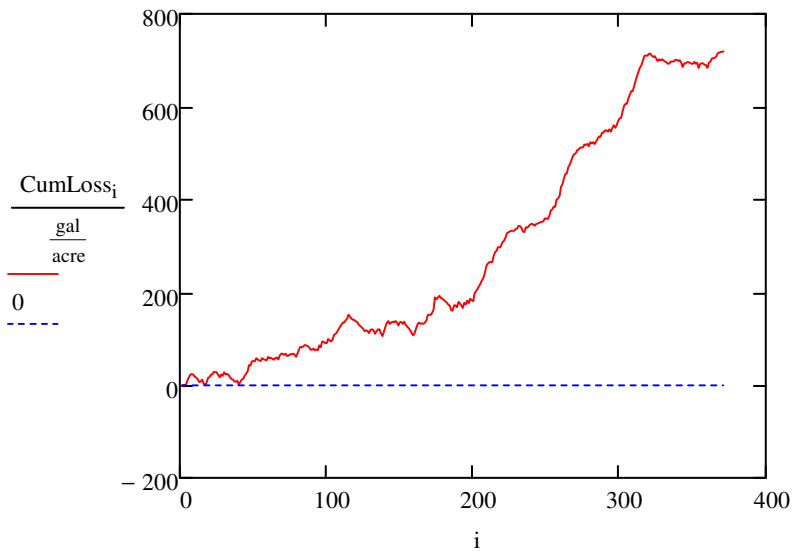
$$\text{AvgLossRate} := \frac{\sum_i \text{LossRate}_i}{N}$$

$$\text{AvgLossRate} = 705.035 \frac{\text{gal}}{\text{acre}\cdot\text{yr}}$$

## Cumulative Losses:

$$\text{cumsum}(v) := \begin{cases} w_{\text{ORIGIN}} \leftarrow v_{\text{ORIGIN}} \\ \text{for } k \in \text{ORIGIN} + 1 \dots \text{last}(v) \\ w_k \leftarrow w_{k-1} + v_k \\ w \end{cases}$$

$$\text{CumLoss} := \text{cumsum}(\text{LossRate}) \cdot 1 \cdot \text{day}$$



	1	
	-1.485	
	0.678	
	0.57	
	1.065	
	11.105	
	17.499	
	23.112	
CumLoss =	24.319	· $\frac{\text{gal}}{\text{acre}}$
	23.405	
	17.679	
	16.965	
	13.074	
	6.615	
	8.002	
	12.328	
	...	

... \CJdailylosses.csv

LossRate  
 $\frac{\text{gal}}{\text{acre} \cdot \text{yr}}$

... \CJcumloss.csv

CumLoss  
 $\frac{\text{gal}}{\text{acre}}$

### 8.3. Thermal NSZD Rate Model Using Hydrus

#### Data Input Files:

##### Temperature Probes:

N1 :=  ...\

N2 :=  C:\Ca...\

N3 :=  C:\Ca...\

N4 :=  ...\

H1 :=  ..\

##### Water Levels at Temperature Probes:

N1DTW :=  ...\

N2DTW :=  ...\

N3DTW :=  ...\

#### Parameter Inputs:

Number of days:  $N := N_{\text{data}} = 373$   
 $i := 9..N - 2$   
 $\Delta t := 1\text{day}$

##### Depths:

$z_1 := 0.5\text{ft}$   
 $z_2 := 1\text{ft}$   
 $z_3 := 10\text{ft}$   
 $z_4 := 12\text{ft}$   
 $z_5 := 19\text{ft}$   
 $z_6 := 27\text{ft}$   
 $z_7 := 35\text{ft}$   
 $z_8 := 37\text{ft}$   
 $b := z_7 - z_3$

##### Other:

$n := 0.25$   
 $S_{\text{wfc}} := 0.1$   
 $S_{\text{w}} := 1$   
 $L_{\text{w}} := 2257000 \frac{\text{J}}{\text{kg}}$   
 $\rho_{\text{wv}} := 23 \frac{\text{gm}}{\text{m}^3}$   
 $L_{\text{o}} := L_{\text{w}} \cdot \rho_{\text{wv}} = 51911 \text{Pa}$

##### Reference Volume Characteristics:

$w := 1\text{ft}$   
 $L := 1000\text{-ft}$   
 $K_{\text{sat}} := 0.005 \frac{\text{cm}}{\text{s}}$

### Average Saturated Thickness:

$$B_{\text{sat}} := \begin{cases} \text{for } i \in 1..N \\ B_{\text{sat}_i} \leftarrow z_7 - \frac{N1DTW_i + N2DTW_i + N3DTW_i}{3} \cdot \text{ft} \\ B_{\text{sat}} \end{cases}$$

### Thermal Conductivities:

#### Unsaturated Zone:

$$\kappa_{\text{unsat}} := 0.0023 \cdot \frac{\text{cal}}{\text{cm} \cdot \text{sec}}$$

$$\kappa_{\text{unsat}} = 0.963 \cdot \frac{\text{W}}{\text{m}}$$

#### Saturated Zone:

$$\kappa_{\text{sat}} := 0.0035 \cdot \frac{\text{cal}}{\text{cm} \cdot \text{sec}}$$

$$\kappa_{\text{sat}} = 1.465 \cdot \frac{\text{W}}{\text{m}}$$

### Heat Capacities:

$$\rho_s := 2.65 \cdot \frac{\text{gm}}{\text{cm}^3} \quad c_s := 44.4 \cdot \frac{\text{J}}{\text{mol}} \cdot \frac{\text{mol}}{60.08 \cdot \text{gm}} \quad C_s := c_s \cdot \rho_s$$

$$\rho_w := 1 \cdot \frac{\text{gm}}{\text{cm}^3} \quad c_w := 4.1855 \cdot \frac{1000\text{J}}{\text{kg}} \quad C_w := c_w \cdot \rho_w$$

$$\rho_a := 1.205 \cdot \frac{\text{kg}}{\text{m}^3} \quad c_a := 1.005 \cdot \frac{1000\text{J}}{\text{kg}} \quad C_a := c_a \cdot \rho_a$$

#### Unsaturated Zone:

$$C_{\text{unsat}} := [(1 - n) \cdot c_s \cdot \rho_s + n \cdot S_{\text{wfc}} \cdot c_w \cdot \rho_w + (n - S_{\text{wfc}}) \cdot c_a \cdot \rho_a]$$

$$C_{\text{unsat}} = 1573610.765 \cdot \frac{\text{J}}{\text{m}^3}$$

#### Saturated Zone:

$$C_{\text{sat}} := [(1 - n) \cdot c_s \cdot \rho_s + n \cdot S_w \cdot c_w \cdot \rho_w + (n - S_w) \cdot c_a \cdot \rho_a]$$

$$C_{\text{sat}} = 2514258.342 \cdot \frac{\text{J}}{\text{m}^3}$$

## Groundwater Gradient and Direction

Well Coordinates

Water levels in four wells

$$M_{xy} := \begin{pmatrix} 2275519.91 & 312281.22 \\ 2276249.95 & 310350.91 \\ 2276366.24 & 312003.41 \\ 2275123.03 & 310382.84 \end{pmatrix}$$

wl :=



.. \D... \WLdata.csv

$N_{data} := \text{cols}(wl) = 373$      $j := 1..N_{data}$

XX := for j ∈ 1..N<sub>data</sub>

$$zz \leftarrow \begin{pmatrix} wl_{1,j} \\ wl_{2,j} \\ wl_{3,j} \\ wl_{4,j} \end{pmatrix}$$

$R \leftarrow \text{regress}(M_{xy}, zz, 1)$

$\text{Slope}_x \leftarrow R_4$

$\text{Slope}_y \leftarrow R_5$

$ZZ_{j,1} \leftarrow \text{Slope}_x$

$ZZ_{j,2} \leftarrow \text{Slope}_y$

$ZZ_{j,3} \leftarrow \sqrt{\text{Slope}_x^2 + \text{Slope}_y^2}$

$ZZ_{j,4} \leftarrow \text{atan}\left(\frac{-\text{Slope}_y}{-\text{Slope}_x}\right)$  if  $\text{Slope}_x \leq 0 \wedge \text{Slope}_y \leq 0$

$ZZ_{j,4} \leftarrow \text{atan}\left(\frac{\text{Slope}_x}{-\text{Slope}_y}\right) + \frac{\pi}{2}$  if  $\text{Slope}_x > 0 \wedge \text{Slope}_y \leq 0$

$ZZ_{j,4} \leftarrow \text{atan}\left(\frac{\text{Slope}_y}{\text{Slope}_x}\right) + \pi$  if  $\text{Slope}_x \geq 0 \wedge \text{Slope}_y \geq 0$

$ZZ_{j,4} \leftarrow \text{atan}\left(\frac{-\text{Slope}_x}{\text{Slope}_y}\right) + \frac{3 \cdot \pi}{2}$  if  $\text{Slope}_x \leq 0 \wedge \text{Slope}_y > 0$

ZZ

$\theta_j := XX_{j,4}$

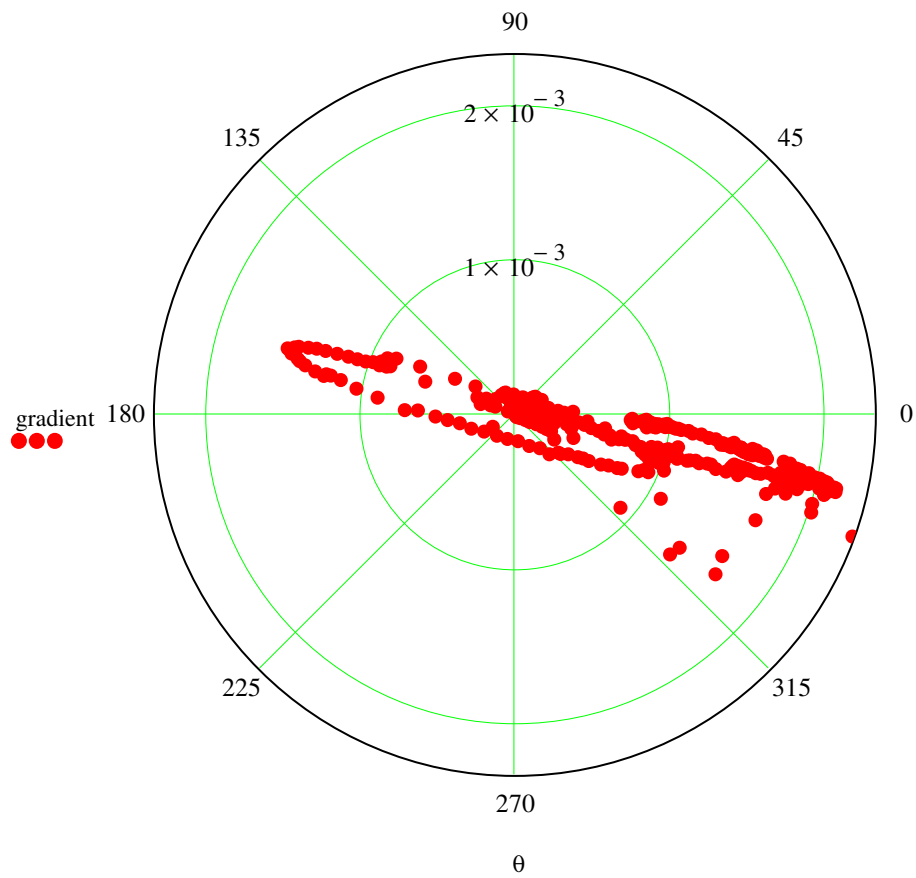
$\text{gradient}_j := XX_{j,3}$

	1
1	5.898
2	0.456
3	0.427
4	6.091
5	0.498
6	6.032
7	0.466
8	0.557
9	0.674
10	0.698
11	0.717
12	0.717
13	0.641
14	0.534
15	0.492
16	...

$\theta =$

	1
1	$4.1581 \cdot 10^{-4}$
2	$1.7425 \cdot 10^{-4}$
3	$1.8121 \cdot 10^{-4}$
4	$3.4782 \cdot 10^{-4}$
5	$1.8932 \cdot 10^{-4}$
6	$3.8325 \cdot 10^{-4}$
7	$2.0227 \cdot 10^{-4}$
8	$1.8383 \cdot 10^{-4}$
9	$1.7832 \cdot 10^{-4}$
10	$1.665 \cdot 10^{-4}$
11	$1.5701 \cdot 10^{-4}$
12	$1.4476 \cdot 10^{-4}$
13	$1.474 \cdot 10^{-4}$
14	$1.4972 \cdot 10^{-4}$
15	$1.5872 \cdot 10^{-4}$
16	...

gradient =



**Storage Calculations:**

$$d := \begin{pmatrix} -0.5 \\ -1 \\ -10 \\ -12 \\ -19 \\ -27 \\ -35 \\ -37 \end{pmatrix} \quad \begin{array}{l} M := \text{augment}(d) \\ p := 4 \end{array}$$

$$\text{AN1} := \left| \begin{array}{l} \text{for } i \in 1..N \\ \quad \text{T11} \leftarrow \left| \begin{array}{l} \text{for } p \in 1..8 \\ \quad \text{XX}_{p,i} \leftarrow N1_{i,p+1} \\ \quad \text{XX} \end{array} \right. \\ \text{T11} \end{array} \right.$$

$$\text{AN2} := \left| \begin{array}{l} \text{for } i \in 1..N \\ \quad \text{T11} \leftarrow \left| \begin{array}{l} \text{for } p \in 1..8 \\ \quad \text{XX}_{p,i} \leftarrow N2_{i,p+1} \\ \quad \text{XX} \end{array} \right. \\ \text{T11} \end{array} \right.$$

$$\text{AN5} := \left| \begin{array}{l} \text{for } i \in 1..N \\ \quad \text{T55} \leftarrow \left| \begin{array}{l} \text{for } p \in 1..8 \\ \quad \text{XX}_{p,i} \leftarrow H1_{i,p+1} \\ \quad \text{XX} \end{array} \right. \\ \text{T55} \end{array} \right.$$

$$\text{AN5} := \left| \begin{array}{l} \text{for } i \in 1..N \\ \quad \text{T55} \leftarrow \left| \begin{array}{l} \text{for } p \in 1..8 \\ \quad \text{XX}_{p,i} \leftarrow H1_{i,p+1} \\ \quad \text{XX} \end{array} \right. \\ \text{T55} \end{array} \right.$$

$$\text{N1S} := \left| \begin{array}{l} \text{for } j \in 1..N \\ \quad \text{C} \leftarrow \text{AN1}^{\langle j \rangle} \\ \quad \text{D} \leftarrow \text{AN5}^{\langle j \rangle} \\ \quad \text{E} \leftarrow \text{regress}(M, C, p) \\ \quad \text{F} \leftarrow \text{regress}(M, D, p) \\ \quad \text{G}(x) \leftarrow \text{interp}[E, M, C, (x)] \\ \quad \text{H}(x) \leftarrow \text{interp}[F, M, D, (x)] \\ \quad \text{I} \leftarrow \left| \begin{array}{l} \text{for } i \in -0.5, -0.6.. -37 \\ \quad \text{XX} \leftarrow \int_{-10}^{-35} G(i) \, di \\ \quad \text{XX} \end{array} \right. \\ \quad \text{J} \leftarrow \left| \begin{array}{l} \text{for } i \in -0.5, -0.6.. -37 \\ \quad \text{XX} \leftarrow \int_{-10}^{-35} H(i) \, di \\ \quad \text{XX} \end{array} \right. \\ \quad \text{K}_j \leftarrow -(I - J)ft \\ \text{K} \end{array} \right.$$

$$\text{N2S} := \left| \begin{array}{l} \text{for } j \in 1..N \\ \quad \text{C} \leftarrow \text{AN2}^{\langle j \rangle} \\ \quad \text{D} \leftarrow \text{AN5}^{\langle j \rangle} \\ \quad \text{E} \leftarrow \text{regress}(M, C, p) \\ \quad \text{F} \leftarrow \text{regress}(M, D, p) \\ \quad \text{G}(x) \leftarrow \text{interp}[E, M, C, (x)] \\ \quad \text{H}(x) \leftarrow \text{interp}[F, M, D, (x)] \\ \quad \text{I} \leftarrow \left| \begin{array}{l} \text{for } i \in -0.5, -0.6.. -37 \\ \quad \text{XX} \leftarrow \int_{-10}^{-35} G(i) \, di \\ \quad \text{XX} \end{array} \right. \\ \quad \text{J} \leftarrow \left| \begin{array}{l} \text{for } i \in -0.5, -0.6.. -37 \\ \quad \text{XX} \leftarrow \int_{-10}^{-35} H(i) \, di \\ \quad \text{XX} \end{array} \right. \\ \quad \text{K}_j \leftarrow -(I - J)ft \\ \text{K} \end{array} \right.$$

$$\text{AN3} := \left| \begin{array}{l} \text{for } i \in 1..N \\ \quad \text{T11} \leftarrow \left| \begin{array}{l} \text{for } p \in 1..8 \\ \quad \text{XX}_{p,i} \leftarrow N3_{i,p+1} \\ \quad \text{XX} \end{array} \right. \\ \text{T11} \end{array} \right|$$

$$\text{AN4} := \left| \begin{array}{l} \text{for } i \in 1..N \\ \quad \text{T11} \leftarrow \left| \begin{array}{l} \text{for } p \in 1..8 \\ \quad \text{XX}_{p,i} \leftarrow N4_{i,p+1} \\ \quad \text{XX} \end{array} \right. \\ \text{T11} \end{array} \right|$$

$$\text{AN5} := \left| \begin{array}{l} \text{for } i \in 1..N \\ \quad \text{T55} \leftarrow \left| \begin{array}{l} \text{for } p \in 1..8 \\ \quad \text{XX}_{p,i} \leftarrow H1_{i,p+1} \\ \quad \text{XX} \end{array} \right. \\ \text{T55} \end{array} \right|$$

$$\text{AN5} := \left| \begin{array}{l} \text{for } i \in 1..N \\ \quad \text{T55} \leftarrow \left| \begin{array}{l} \text{for } p \in 1..8 \\ \quad \text{XX}_{p,i} \leftarrow H1_{i,p+1} \\ \quad \text{XX} \end{array} \right. \\ \text{T55} \end{array} \right|$$

$$\text{N3S} := \left| \begin{array}{l} \text{for } j \in 1..N \\ \quad \text{C} \leftarrow \text{AN3}^{\langle j \rangle} \\ \quad \text{D} \leftarrow \text{AN5}^{\langle j \rangle} \\ \quad \text{E} \leftarrow \text{regress}(M, C, p) \\ \quad \text{F} \leftarrow \text{regress}(M, D, p) \\ \quad \text{G}(x) \leftarrow \text{interp}[E, M, C, (x)] \\ \quad \text{H}(x) \leftarrow \text{interp}[F, M, D, (x)] \\ \quad \text{I} \leftarrow \left| \begin{array}{l} \text{for } i \in -0.5, -0.6.. -37 \\ \quad \text{XX} \leftarrow \int_{-10}^{-35} G(i) \, di \\ \quad \text{XX} \end{array} \right. \\ \quad \text{J} \leftarrow \left| \begin{array}{l} \text{for } i \in -0.5, -0.6.. -37 \\ \quad \text{XX} \leftarrow \int_{-10}^{-35} H(i) \, di \\ \quad \text{XX} \end{array} \right. \\ \quad \text{K}_j \leftarrow -(I - J) \, ft \\ \text{K} \end{array} \right|$$

$$\text{N4S} := \left| \begin{array}{l} \text{for } j \in 1..N \\ \quad \text{C} \leftarrow \text{AN4}^{\langle j \rangle} \\ \quad \text{D} \leftarrow \text{AN5}^{\langle j \rangle} \\ \quad \text{E} \leftarrow \text{regress}(M, C, p) \\ \quad \text{F} \leftarrow \text{regress}(M, D, p) \\ \quad \text{G}(x) \leftarrow \text{interp}[E, M, C, (x)] \\ \quad \text{H}(x) \leftarrow \text{interp}[F, M, D, (x)] \\ \quad \text{I} \leftarrow \left| \begin{array}{l} \text{for } i \in -0.5, -0.6.. -37 \\ \quad \text{XX} \leftarrow \int_{-10}^{-35} G(i) \, di \\ \quad \text{XX} \end{array} \right. \\ \quad \text{J} \leftarrow \left| \begin{array}{l} \text{for } i \in -0.5, -0.6.. -37 \\ \quad \text{XX} \leftarrow \int_{-10}^{-35} H(i) \, di \\ \quad \text{XX} \end{array} \right. \\ \quad \text{K}_j \leftarrow -(I - J) \, ft \\ \text{K} \end{array} \right|$$

### Background Corrected Temperatures:

$$T_{c05ft} := \left| \begin{array}{l} \text{for } i \in 1..N-2 \\ \left| \begin{array}{l} N_{avg05_i} \leftarrow \frac{N1_{i,2} + N2_{i,2} + N3_{i,2}}{3} \\ N_{avg05ft_i} \leftarrow N_{avg05_i} - H1_{i,2} \end{array} \right. \\ N_{avg05ft} \end{array} \right.$$

$$T_{c19ft} := \left| \begin{array}{l} \text{for } i \in 1..N-2 \\ \left| \begin{array}{l} N_{avg19_i} \leftarrow \frac{N1_{i,6} + N2_{i,6} + N3_{i,6}}{3} \\ N_{avg19ft_i} \leftarrow N_{avg19_i} - H1_{i,6} \end{array} \right. \\ N_{avg19ft} \end{array} \right.$$

$$T_{c1ft} := \left| \begin{array}{l} \text{for } i \in 1..N-2 \\ \left| \begin{array}{l} N_{avg1_i} \leftarrow \frac{N1_{i,3} + N2_{i,3} + N3_{i,3}}{3} \\ N_{avg1ft_i} \leftarrow N_{avg1_i} - H1_{i,3} \end{array} \right. \\ N_{avg1ft} \end{array} \right.$$

$$T_{c27ft} := \left| \begin{array}{l} \text{for } i \in 1..N-2 \\ \left| \begin{array}{l} N_{avg27_i} \leftarrow \frac{N1_{i,7} + N2_{i,7} + N3_{i,7}}{3} \\ N_{avg27ft_i} \leftarrow N_{avg27_i} - H1_{i,7} \end{array} \right. \\ N_{avg27ft} \end{array} \right.$$

$$T_{c10ft} := \left| \begin{array}{l} \text{for } i \in 1..N-2 \\ \left| \begin{array}{l} N_{avg10_i} \leftarrow \frac{N1_{i,4} + N2_{i,4} + N3_{i,4}}{3} \\ N_{avg10ft_i} \leftarrow N_{avg10_i} - H1_{i,4} \end{array} \right. \\ N_{avg10ft} \end{array} \right.$$

$$T_{c35ft} := \left| \begin{array}{l} \text{for } i \in 1..N-2 \\ \left| \begin{array}{l} N_{avg35_i} \leftarrow \frac{N1_{i,8} + N2_{i,8} + N3_{i,8}}{3} \\ N_{avg35ft_i} \leftarrow N_{avg35_i} - H1_{i,8} \end{array} \right. \\ N_{avg35ft} \end{array} \right.$$

$$T_{c12ft} := \left| \begin{array}{l} \text{for } i \in 1..N-2 \\ \left| \begin{array}{l} N_{avg12_i} \leftarrow \frac{N1_{i,5} + N2_{i,5} + N3_{i,5}}{3} \\ N_{avg12ft_i} \leftarrow N_{avg12_i} - H1_{i,5} \end{array} \right. \\ N_{avg12ft} \end{array} \right.$$

$$T_{c37ft} := \left| \begin{array}{l} \text{for } i \in 1..N-2 \\ \left| \begin{array}{l} N_{avg37_i} \leftarrow \frac{N1_{i,9} + N2_{i,9} + N3_{i,9}}{3} \\ N_{avg37ft_i} \leftarrow N_{avg37_i} - H1_{i,9} \end{array} \right. \\ N_{avg37ft} \end{array} \right.$$

### Average Temperature Difference Between Background and Reference Volume:

$$T_c := \left| \begin{array}{l} \text{for } i \in 1..N-2 \\ \left| \begin{array}{l} N_{avg_i} \leftarrow \frac{N1_{i,9} + N2_{i,9} + N3_{i,9}}{3} \\ N_{avgsource_i} \leftarrow N_{avg_i} - H1_{i,9} \end{array} \right. \\ N_{avgsource} \end{array} \right.$$

### Fluxes due to Conduction:

$$E_{inzcond_i} := -\kappa_{unsat} \cdot \left( \frac{T_{c1ft_i} - T_{c10ft_i}}{z_3 - z_2} \right) \cdot L \cdot w \quad E_{outzcond_i} := \kappa_{sat} \cdot \left( \frac{T_{c35ft_i} - T_{c37ft_i}}{z_8 - z_7} \right) \cdot L \cdot w$$

### Flux due to Convection of Sensible Heat by Water (z):

$$E_{zconvw} := \left| \begin{array}{l} \text{for } i \in 9..N-2 \\ \left| \begin{array}{l} Ad_{bottom_i} \leftarrow \left( \frac{B_{sat_i} - B_{sat_{i+1}}}{\Delta t} \right) \cdot n \cdot L \cdot w \cdot C_w \cdot T_{c_i} \text{ if } B_{sat_{i+1}} < B_{sat_i} \\ Ad_{bottom_i} \leftarrow 0 \text{ otherwise} \end{array} \right. \\ Ad_{bottom} \end{array} \right.$$

### Flux due to Convection of Sensible Heat by Vapor (z):

$$E_{zconvv} := \left| \begin{array}{l} \text{for } i \in 9..N-2 \\ \left| \begin{array}{l} Ad_{gas_i} \leftarrow - \left( \frac{B_{sat_i} - B_{sat_{i+1}}}{\Delta t} \right) \cdot n \cdot L \cdot w \cdot C_a \cdot T_{c_i} \text{ if } B_{sat_i} < B_{sat_{i+1}} \\ Ad_{gas_i} \leftarrow 0 \text{ otherwise} \end{array} \right. \\ Ad_{gas} \end{array} \right.$$

### Flux due to Convection of Latent Heat by Vapor (z):

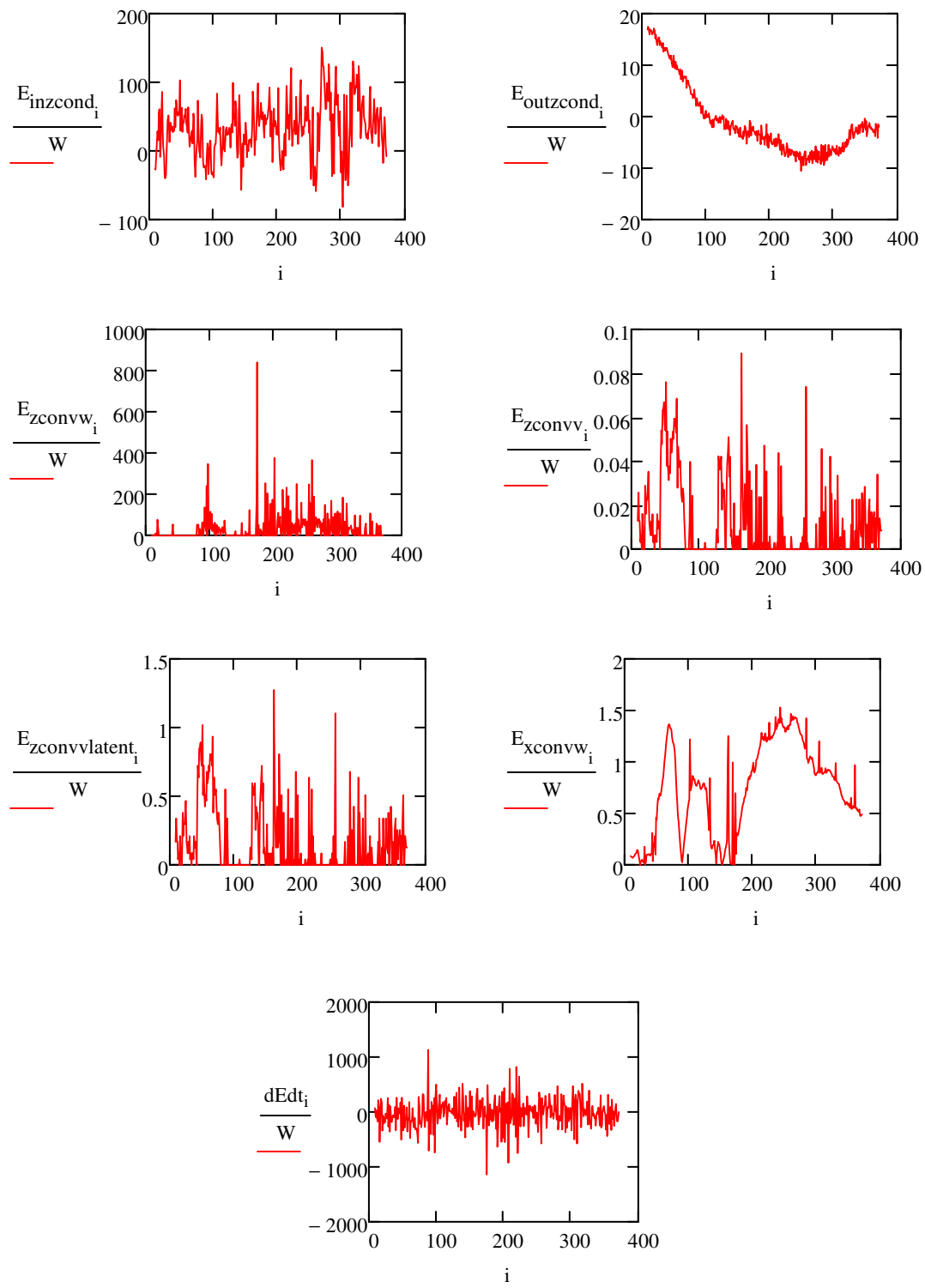
$$E_{zconvlatent} := \left| \begin{array}{l} \text{for } i \in 9..N-2 \\ \left| \begin{array}{l} Latent_{vapor_i} \leftarrow - \left( \frac{B_{sat_i} - B_{sat_{i+1}}}{\Delta t} \right) \cdot n \cdot L \cdot w \cdot L_o \text{ if } B_{sat_i} < B_{sat_{i+1}} \\ Latent_{vapor_i} \leftarrow 0 \text{ otherwise} \end{array} \right. \\ Latent_{vapor} \end{array} \right.$$

### Flux due to Convection of Sensible Heat by Water (x):

$$E_{xconvw_i} := |\cos(\theta)_i| \cdot gradient_i \cdot K_{sat} \cdot B_{sat_i} \cdot w \cdot C_w \cdot T_{c_i}$$

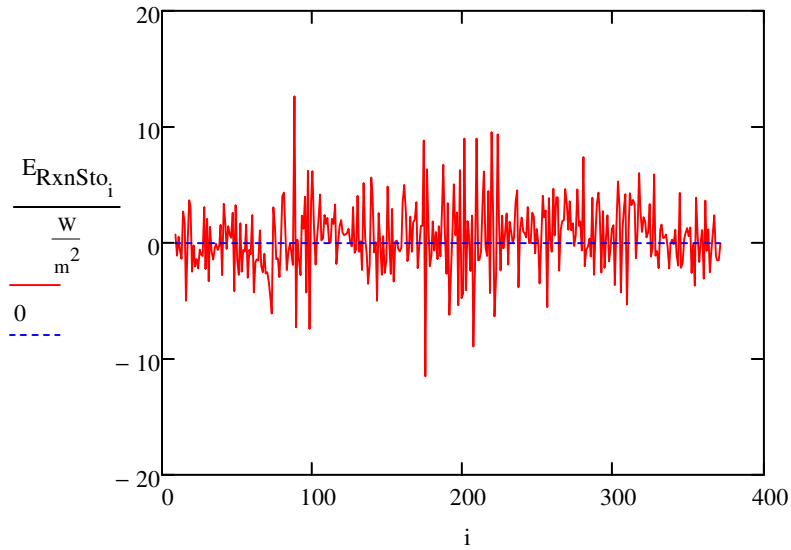
### Change in Energy:

$$dEdt_i := \left[ \left( \frac{B_{sat_i}}{b} \right) \cdot C_{sat} + \left( \frac{b - B_{sat_i}}{b} \right) \cdot C_{unsat} \right] \cdot \left[ \frac{\left( \frac{N1S_{i+1} + N2S_{i+1} + N3S_{i+1}}{3} \right) - \left( \frac{N1S_i + N2S_i + N3S_i}{3} \right)}{\Delta t} \right] \cdot L \cdot w$$



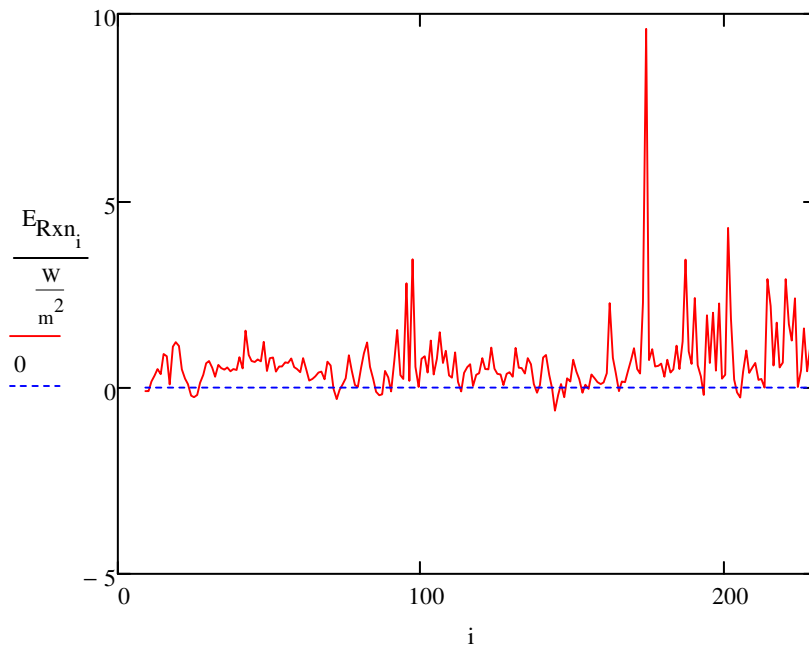
**Flux Due to Reactions**  
**Background Flux Method with Storage:**

$$E_{RxnSto} := \frac{E_{xconvw} + E_{inzcond} + E_{zconvw} + E_{outzcond} + E_{zconvv} + E_{zconvvlatent} + dEdt}{L \cdot w}$$



**Flux Due to Reactions**  
**Background Flux Method without Storage:**

$$E_{Rxn} := \frac{E_{xconvw} + E_{inzcond} + E_{zconvw} + E_{outzcond} + E_{zconvv} + E_{zconvvlatent}}{L \cdot w}$$



## Loss Rate:

### Decane Properties:

$$\Delta G_{\text{rdecane}} := -4206550 \frac{\text{J}}{\text{mol}} \quad \Delta H_{\text{rdecane}} := -6791690 \frac{\text{J}}{\text{mol}}$$

$$\text{MW}_{\text{decane}} := 142.29 \frac{\text{gm}}{\text{mol}}$$

$$\Delta H_{\text{rdecane}\%} := \frac{\Delta H_{\text{rdecane}}}{\Delta G_{\text{rdecane}}} = 1.615$$

$$\rho_{\text{decane}} := 0.730 \frac{\text{gm}}{\text{cm}^3}$$

### Heat Due to Reactions:

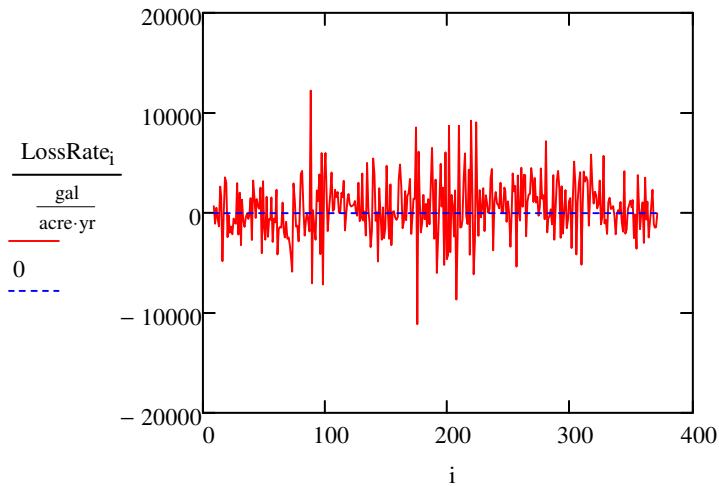
$$\Delta G_{\text{rXdecane}} := -662000 \frac{\text{J}}{\text{mol}} \quad Y_{\text{XD}} := 0.268$$

$$\text{Adjusted}\Delta G_{\text{rdecane}} := \Delta G_{\text{rXdecane}} \cdot Y_{\text{XD}} \cdot 10 = -1774160 \frac{\text{J}}{\text{mol}}$$

$$\Delta H_{\text{T}} := \text{Adjusted}\Delta G_{\text{rdecane}} \cdot \Delta H_{\text{rdecane}\%} = -2864472.009 \frac{\text{J}}{\text{mol}}$$

### Decane Loss Rate without Storage:

$$\text{LossRate} := \frac{-E_{\text{RxnSto}} \cdot \text{MW}_{\text{decane}}}{\Delta H_{\text{rdecane}} \cdot \rho_{\text{decane}}}$$



	1	
1		0
2		0
3		0
4		0
5		0
6		0
7		0
8		0
9		709.205
10		-1042.881
11		534.13
12		-564.766
13		-1308.428
14		2657.292
15		1693.619
16		...

LossRate =  $\frac{\text{gal}}{\text{acre}\cdot\text{yr}}$

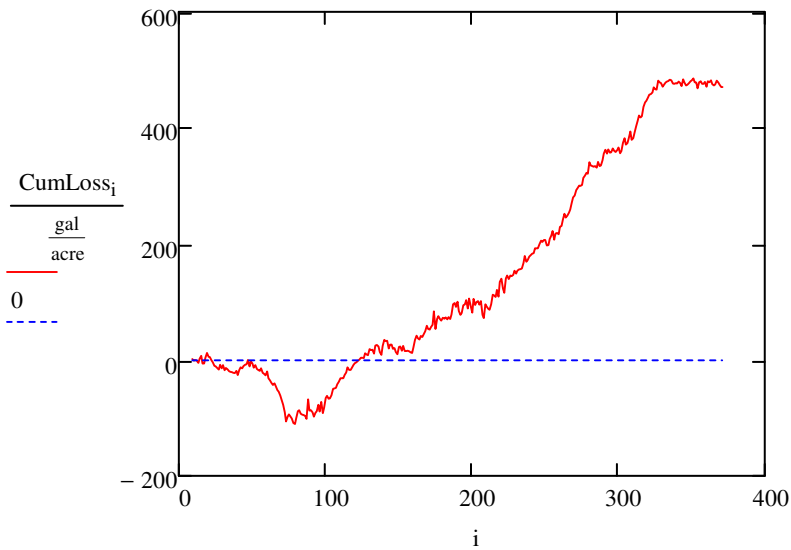
$$\text{AvgLossRate} := \frac{\sum_i \text{LossRate}_i}{N}$$

$$\text{AvgLossRate} = 461.18 \frac{\text{gal}}{\text{acre}\cdot\text{yr}}$$

## Cumulative Losses:

$$\text{cumsum}(v) := \begin{cases} w_{\text{ORIGIN}} \leftarrow v_{\text{ORIGIN}} \\ \text{for } k \in \text{ORIGIN} + 1 \dots \text{last}(v) \\ w_k \leftarrow w_{k-1} + v_k \\ w \end{cases}$$

$$\text{CumLoss} := \text{cumsum}(\text{LossRate}) \cdot 1 \cdot \text{day}$$



	1	
1	0	
2	0	
3	0	
4	0	
5	0	
6	0	
7	0	
8	0	
9	1.942	. gal acre
10	-0.914	
11	0.549	
12	-0.997	
13	-4.58	
14	2.696	
15	7.333	
16	...	

CumLoss =

  
 ..\..\Hydruslossrates.csv  
LossRate  
 gal  
 acre·yr

  
 ....\Hydruscumloss.csv  
CumLoss  
 gal  
 acre

## 8.4. Thermal NSZD Rate Model As Applied to the Laboratory Experiment

### Data Input Files:

#### Temperature Probes:

N1 :=



...\LabData1.csv

### Parameter Inputs:

Number of days:  $N := \text{rows}(N1) = 359$

$i := 1..N - 1$

$\Delta t := 1\text{hr}$

#### Depths:

$z_1 := 0.5\text{ft}$

$z_2 := 1\text{ft}$

$z_3 := 1.5\text{ft}$

$z_4 := 2\text{ft}$

$z_5 := 2.5\text{ft}$

$z_6 := 3\text{ft}$

$z_7 := 3.5\text{ft}$

$z_8 := 4\text{ft}$

$z_9 := 4.5\text{ft}$

$z_{10} := 5\text{ft}$

$z_{11} := 5.5\text{ft}$

$b := z_5 - z_2$

#### Other:

$n := 0.4$

$S_{wfc} := 0.1$

$S_w := 1$

$L_w := 2257000 \frac{\text{J}}{\text{kg}}$

$\rho_{wv} := 23 \frac{\text{gm}}{\text{m}^3}$

$L_o := L_w \cdot \rho_{wv} = 51911 \text{ Pa}$

#### Reference Volume Characteristics:

$w := 1\text{in}$

$L := 28.89\text{-in}$

### Average Saturated Thickness:

$B_{\text{sat}} := 10\text{-in}$

**Thermal Conductivities:**

**Unsaturated Zone:**

$$\kappa_{\text{unsat}} := 0.41 \frac{\text{W}}{\text{m}}$$

$$\kappa_{\text{unsat}} = 0.41 \cdot \frac{\text{W}}{\text{m}}$$

**Saturated Zone:**

$$\kappa_{\text{sat}} := 1.36 \frac{\text{W}}{\text{m}}$$

$$\kappa_{\text{sat}} = 1.36 \cdot \frac{\text{W}}{\text{m}}$$

**Heat Capacities:**

**Unsaturated Zone:**

$$C_{\text{unsat}} := 1252500 \frac{\text{J}}{\text{m}^3}$$

$$C_{\text{unsat}} = 1252500 \cdot \frac{\text{J}}{\text{m}^3}$$

**Saturated Zone:**

$$C_{\text{sat}} := 2826666 \frac{\text{J}}{\text{m}^3}$$

$$C_{\text{sat}} = 2826666 \cdot \frac{\text{J}}{\text{m}^3}$$

**Background Fluxes:**

$$BF_{\text{sat}} := \frac{2.6}{\text{ft}} \quad BF_{\text{unsat}} := \frac{0.8}{\text{ft}}$$

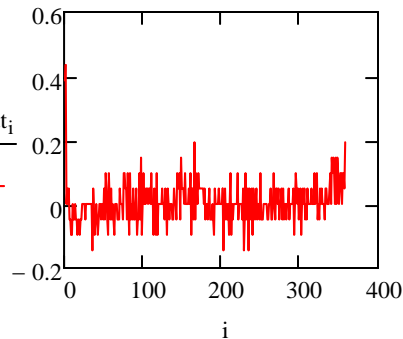
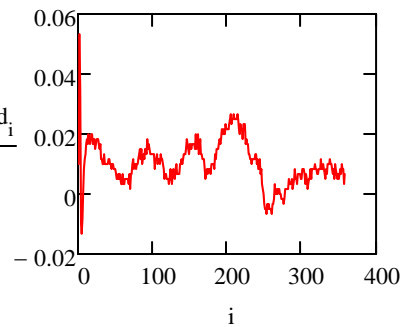
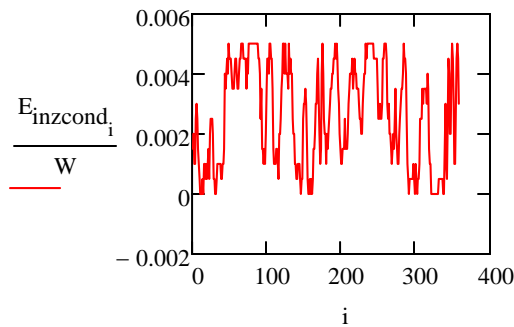
**Fluxes due to Conduction:**

$$E_{\text{inzcond}_i} := \kappa_{\text{unsat}} \cdot \left( \frac{N1_{i,8} - N1_{i,7}}{0.5\text{ft}} - BF_{\text{unsat}} \right) \cdot L \cdot w$$

$$E_{\text{outzcond}_i} := \kappa_{\text{sat}} \cdot \left( \frac{N1_{i,4} - N1_{i,3}}{0.5\text{ft}} - BF_{\text{sat}} \right) \cdot L \cdot w$$

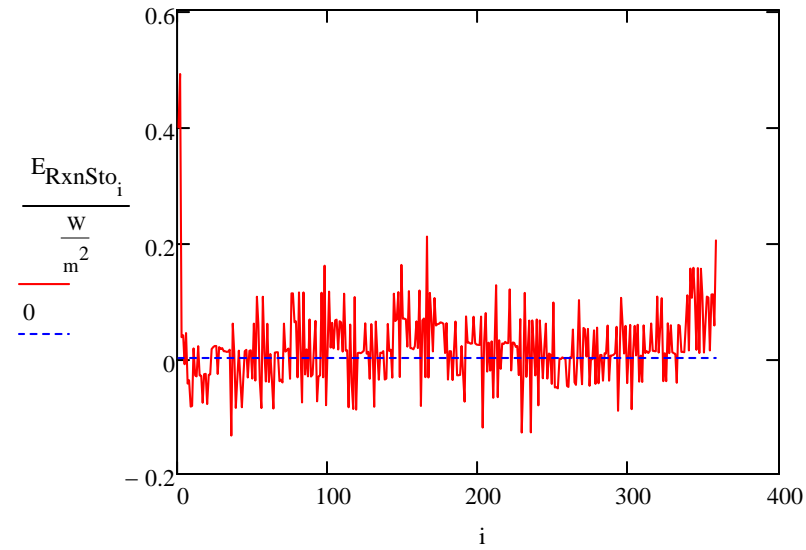
**Change in Energy:**

$$dEdt_i := \left( (0.5C_{\text{sat}} + 0.5C_{\text{unsat}}) \right) \cdot \left( \frac{N1_{i+1,5} - N1_{i,5}}{1\Delta t} \right) \cdot b \cdot L \cdot w$$



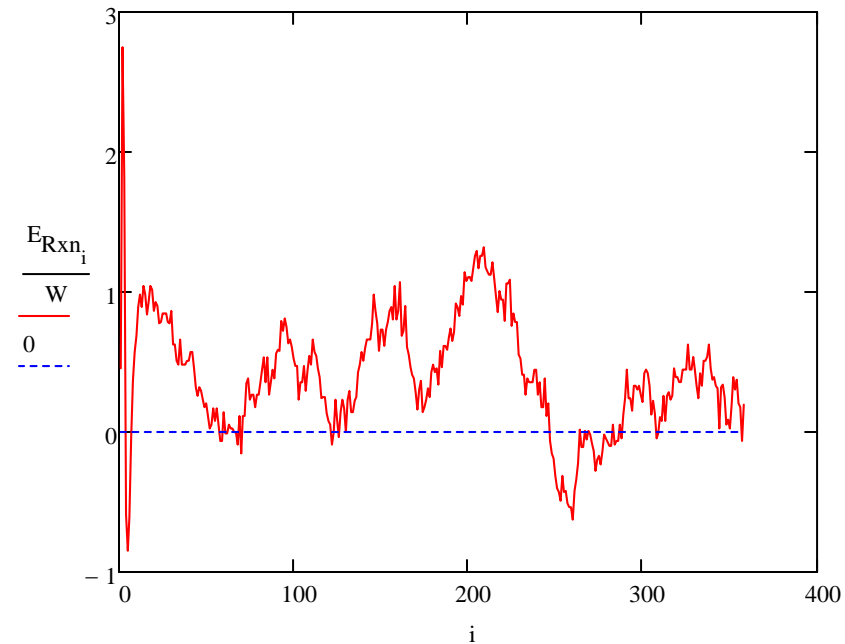
**Flux Due to Reactions  
Background Flux Method with Storage:**

$$E_{\text{RxnSto}} := E_{\text{inzcond}} + E_{\text{outzcond}} + dEdt$$



**Flux Due to Reactions  
Background Flux Method without Storage:**

$$E_{\text{Rxn}} := \frac{-E_{\text{inzcond}} + E_{\text{outzcond}}}{L \cdot w}$$



## Loss Rate:

### Glucose Properties:

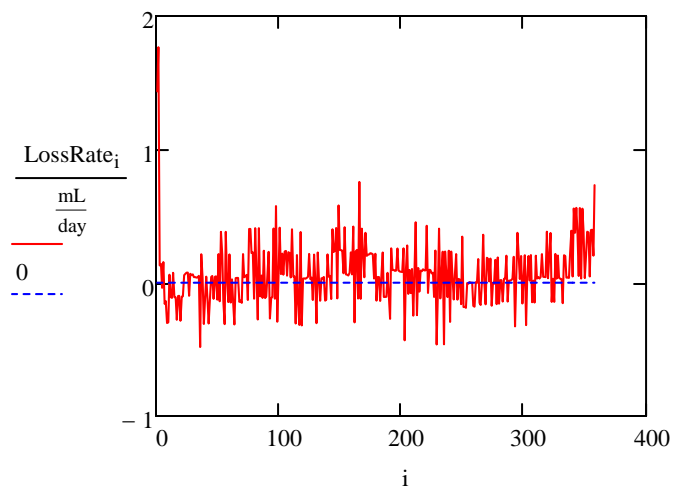
$$\Delta G_{\text{rglucose}} := -2878780 \frac{\text{J}}{\text{mol}} \quad \Delta H_{\text{rglucose}} := -2802740 \frac{\text{J}}{\text{mol}}$$

$$\text{MW}_{\text{glucose}} := 180.16 \frac{\text{gm}}{\text{mol}}$$

$$\rho_{\text{glucose}} := 1.54 \frac{\text{gm}}{\text{cm}^3}$$

### Glucose Loss Rate:

$$\text{LossRate} := \frac{-E_{\text{RxnSto}}}{\Delta H_{\text{rglucose}}} \cdot \frac{\text{MW}_{\text{glucose}}}{\rho_{\text{glucose}}}$$



	1
1	1.434
2	1.766
3	0.13
4	0.142
5	-0.039
6	0.155
7	-0.159
8	-0.139
9	-0.303
10	-0.298
11	0.06
12	-0.108
13	-0.114
14	0.074
15	-0.108
16	...

LossRate =  $\frac{\text{mL}}{\text{day}}$

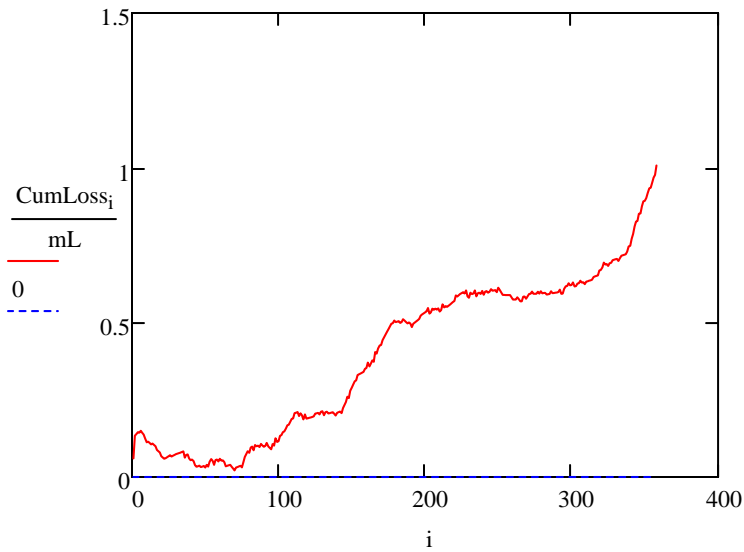
$$\text{AvgLossRate} := \frac{\sum_i \text{LossRate}_i}{N}$$

$$\text{AvgLossRate} = 0.067 \cdot \frac{\text{mL}}{\text{day}}$$

### Cumulative Losses:

$$\text{cumsum}(v) := \left| \begin{array}{l} w_{\text{ORIGIN}} \leftarrow v_{\text{ORIGIN}} \\ \text{for } k \in \text{ORIGIN} + 1 \dots \text{last}(v) \\ \quad w_k \leftarrow w_{k-1} + v_k \\ w \end{array} \right.$$

$$\text{CumLoss} := \text{cumsum}(\text{LossRate}) \cdot 1 \cdot \text{hr}$$



	1	
	0.06	
	0.133	
	0.139	
	0.145	
	0.143	
	0.149	
	0.143	
CumLoss =	0.137	· mL
	0.124	
	0.112	
	0.115	
	0.11	
	0.105	
	0.108	
	0.104	
	...	

## 9. APPENDIX B

### 9.1. Soil Core Thermal Properties

Table 21. Measured thermal properties of soil core from Kansas

Depth (ft)	Thermal Conductivity (W/mK)	Heat Capacity (MJ/m <sup>3</sup> K)	Diffusivity (mm <sup>2</sup> /s)	Comments
2	1.298	3.264	0.398	Top of Core
4	0.946	2.447	0.386	
6	1.227	2.844	0.431	
8	1.155	2.788	0.414	
9	1.022	1.986	0.515	Top of Core - material possibly slough
10	1.139	2.583	0.441	
11	0.946	1.778	0.532	
12	1.004	1.809	0.555	
13	0.627	1.382	0.453	Top of Core - material possibly slough
14	0.945	2.375	0.398	
15	0.797	1.502	0.531	
16	0.854	2.148	0.398	
17	0.969	2.394	0.405	Top of Core - material possibly slough
18	1.091	2.119	0.515	
19	1.273	2.829	0.45	
20	1.65	3.016	0.547	
21	1.517	2.816	0.539	Top of Core - material possibly slough
22	1.432	2.944	0.486	
23	0.906	1.488	0.609	Material is sand from here down
24	1.062	1.662	0.639	
25	1.327	3.149	0.421	Top of Core - material probably slough
26	1.892	2.225	0.85	
27	1.036	2.276	0.455	
28	1.015	1.778	0.571	
29	1.861	2.127	0.875	Top of Core - material probably slough
30	1.461	2.214	0.663	
31	1.502	1.994	0.753	
32	0.969	1.955	0.495	

## 9.2. Values Used in Thermodynamics Calculations

Table 22. Free energy and enthalpy of formation for species used in coupled oxidation-reduction reactions

Species	State	$\Delta G_f$ (kJ/mol)	Source	$\Delta H_f$ (kJ/mol)	Source
Decane	l	17.5	Dean (1999)	-300.9	Dean (1999)
Decane	aq	54.34	Plyasunov and Shock (2000)	-296.97	Plyasunov and Shock (2000)
Glucose	c	-910.4	Dean (1999)	-1273.3	Dean (1999)
O <sub>2</sub>	g	0	Standard	0	Standard
O <sub>2</sub>	aq	16.527	Shock et al. (1989)	-12.134	Shock et al. (1989)
CO <sub>2</sub>	g	-394.39	Dean (1999)	-393.51	Dean (1999)
CO <sub>2</sub>	aq	-386	Dean (1999)	-413.26	Dean (1999)
H <sub>2</sub> O	l	-237.14	Dean (1999)	-285.83	Dean (1999)
H <sup>+</sup>	aq	0	Standard	0	Standard
N <sub>2</sub>	g	0	Standard	0	Standard
N <sub>2</sub>	aq	18.188	Shock et al. (1989)	-10.439	Shock et al. (1989)
NO <sub>3</sub> <sup>-</sup>	aq	-111.3	Dean (1999)	-206.85	Dean (1999)
MnO <sub>2</sub>	c	-465.2	Dean (1999)	-520.1	Dean (1999)
Mn <sup>2+</sup>	aq	-228.1	Dean (1999)	-220.75	Dean (1999)
Fe(OH) <sub>3</sub>	s	-705	Dean (1999)	-833	Dean (1999)
Fe <sup>2+</sup>	aq	-78.87	Dean (1999)	-89.1	Dean (1999)
SO <sub>4</sub> <sup>2-</sup>	aq	-744.5	Dean (1999)	-909.34	Dean (1999)
H <sub>2</sub> S	aq	-27.87	Dean (1999)	-38.6	Dean (1999)
CH <sub>4</sub>	g	-50.5	Dean (1999)	-74.6	Dean (1999)
CH <sub>4</sub>	aq	-34.12	Plyasunov and Shock (2000)	-87.58	Plyasunov and Shock (2000)

Notes:

l = liquid

aq = aqueous

c = crystalline solid

### 9.3. Gas Chromatography Calibration Curves

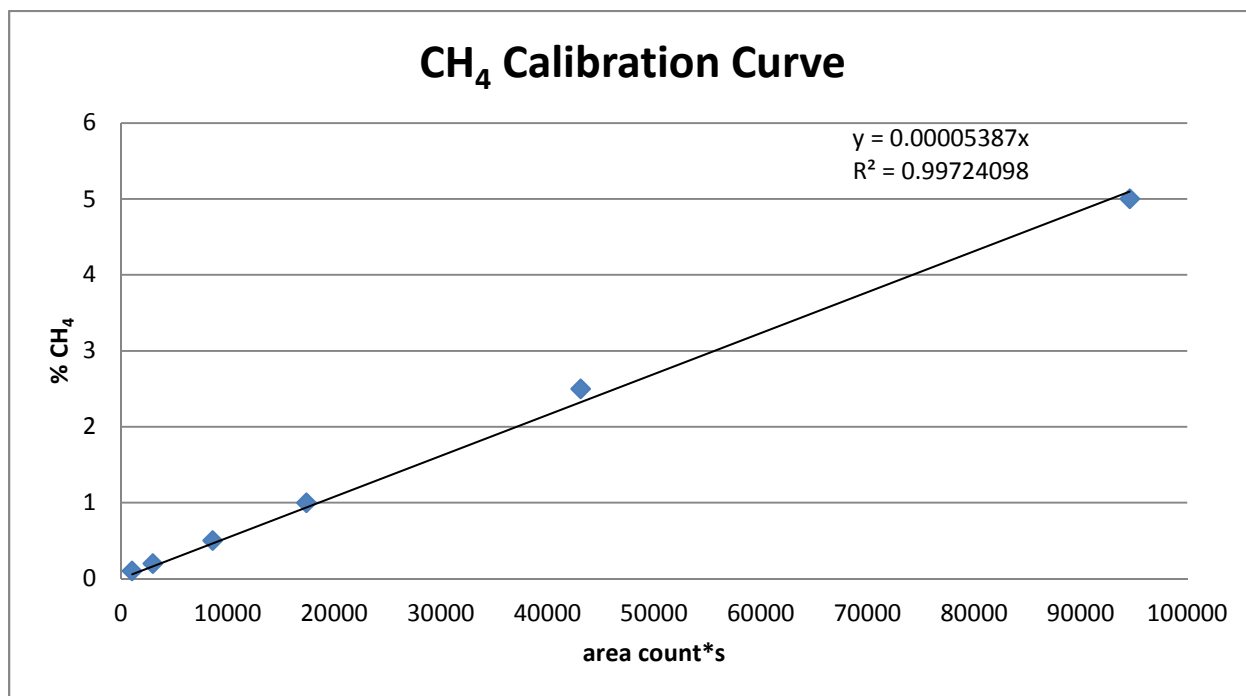


Figure 29. Calibration curve with equation used to determine methane percentage

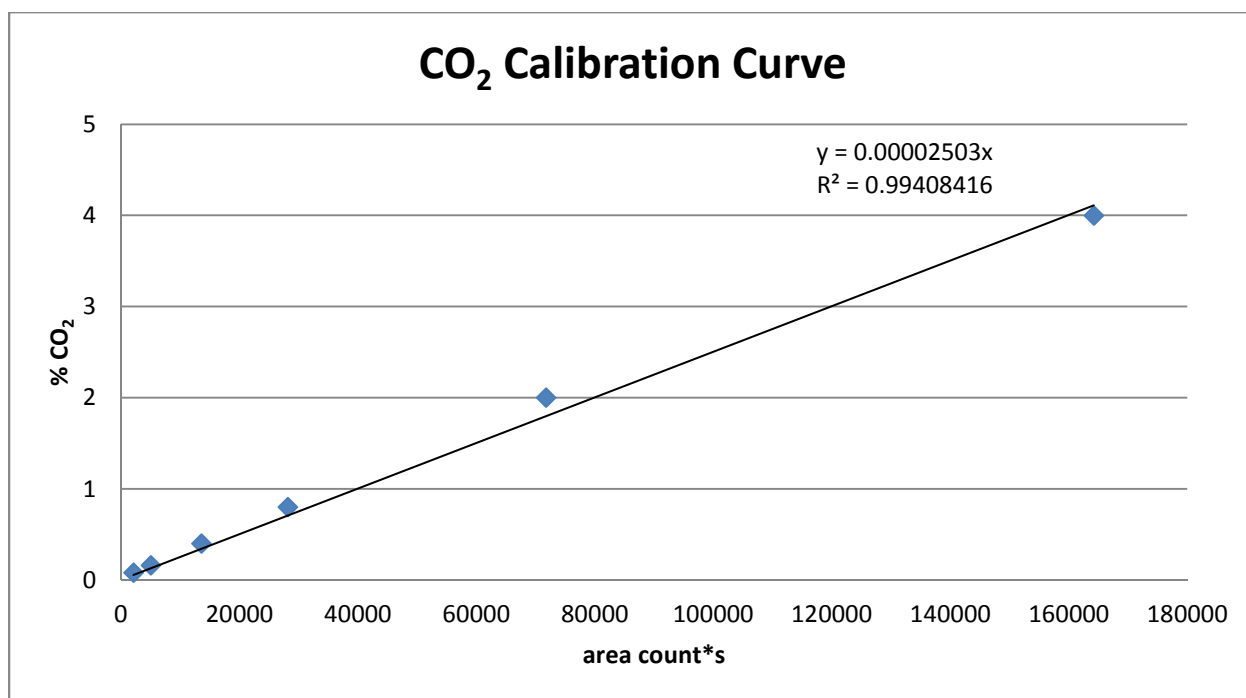


Figure 30. Calibration curve with equation used to determine carbon dioxide percentage